8-2016

Function And Mechanism Of Alkbh5 In N6-Methyl-Adenosine Rna Modification In Glioblastoma

Sicong Zhang

FUNCTION AND MECHANISM OF ALKBH5 IN N^6-METHYL-ADENOSINE RNA MODIFICATION IN GLIOBLASTOMA

By Sicong Zhang, B.S.

APPROVED:

_____

Suyun Huang, M.D., Ph.D., Advisory Professor

_____

Oliver Bogler, Ph.D.

_____

Richard R. Behringer, Ph.D.

_____

Sadhan Majumder, Ph.D.

_____

Xiaoping Sun, M.D., Ph.D.

_____

Zhen Fan. M.D.

APPROVED:

_____

Dean, The University of Texas

Graduate School of Biomedical Sciences at Houston

A

DISSERTATION

Presented to the Faculty of

The University of Texas

Health Science Center at Houston

and

The University of Texas

MD Anderson Cancer Center

Graduate School of Biomedical Sciences

in Partial Fulfillment

of the Requirements

for the Degree of

DOCTOR OF PHILOSOPHY

by

Sicong Zhang, B.S.

Houston, Texas

August, 2016

Dedicated to all those who have been afflicted by cancer.

ACKNOWLEDGEMENTS

First and foremost, I would like to thank all the GBM patients for their support to the research of this disease. All the biomaterials including the patient samples and stem-like GBM cell lines are contributed by the cancer patients and these resource from each of them becomes the foundation of this study.

I would like to thank my mentor, Dr Suyun Huang, for giving me the opportunity to perform basic research in her lab. I am truly grateful for her continuous support to my project and providing the best environment to pursue my degree.

I would like to thank my advisory committee members, Drs. Oliver Bogler, Richard R. Behringer, Sadhan Majumder, Zhen Fan, and defense committee member Dr. Xiaoping Sun, who dedicated their time and provided suggestion to progress my research.

I owe thanks to each of the members of Huang Lab. Dr. Aidong Zhou, thank you for bringing me to the non-coding RNA field and sharing your experience. Dr. Yaohui Chen, thank you for teaching me the calcium phosphate transfection and remembering that “someone” has the same birthday. Dr. Kangyu Lin, thank you for helping me with the flow cytometer and giving me a bottle of sleeping aids when I was struggling with my experiments and manuscript.

I would also like to thank Verlene Henry and Caroline Carrillo for their assistance in animal study.

Lastly, I would like to thank my parents for their unconditional support.

Function and Mechanism of ALKBH5 in N^6-methyl-adenosine RNA Modification in Glioblastoma

Sicong Zhang, B.S.

Advisory Professor: Suyun Huang, M.D.,Ph.D.

N^6-methyl-adenosine (m^6A) is the most prevalent internal chemical modification of mRNAs in eukaryotes. In mammals, m^6A installed by m^6A methyltransferases METTL3 and METTL14 is erased by two members of the AlkB family of nonheme Fe(II)/α-ketoglutarate (α-KG)-dependent dioxygenases, fat-mass and obesity associated protein (FTO) or ALKBH5. ALKBH5 affects nuclear RNA export and metabolism, gene expression and mouse fertility. To date, little is known about the biological significance of m^6A in human cancer. We found that ALKBH5 is highly expressed in human glioblastoma stem cells which are resistant to conventional therapy and give rise to glioblastoma recurrence by sustaining long-term tumor growth. Global manipulation of the m^6A modification by depleting ALKBH5 resulted in altered gene expression including subsets of genes enriched in “Cell Cycle”, “DNA Replication, Recombination, and Repair” and “Cellular Assembly and Organization”. Knockdown of ALKBH5 expression in human glioblastoma stem cells significantly reduced their self-renewal ability as a result of inhibition of cell cycle progression. Depleting ALKBH5 reduced expression of Nestin and SOX2, NANOG, OCT4, the core transcription factors that endow tumor cells with self-renewal capacity. This study demonstrated the important role of m^6A modification in human glioblastoma development.

TABLE OF CONTENTS

List of Figures

List of Tables

CHAPTER ONE: INTRODUCTION

m^6A RNA methylation

Introduction

The *N*^{6}-methyladenosine (m^6A) methylation (Figure 01) of ribosomal and transfer RNA from mammalian cells was discovered in 1960's (1, 2), but the m^6A methylation of messenger RNA was not determined until purification of polyadenylated RNA became possible. m^6A on mRNA was reported by a study to identify methylated nucleosides in mRNA from rat hepatoma cells in 1974 which estimated about 80% base methylation was m^6A (3). m^6A methylation occurs in the central adenosines in the GAC consensus sequence and in the less common AAC motifs sites (4, 5). The methylation sites can be extended to the $N_1(G/A)m^6ACN_2$ sequence where N_1 is predominantly a purine nucleotide and N_2 is rarely a G (6). Although these sequences are widespread in mRNA, the majority of these motifs lack m^6A modification. The methylation level varies considerably among different sites even with the same core sequence (7, 8). The highest m^6A levels are observed in the mouse brain, heart and kidney (9). During development, low levels of m^6A-containing mRNA increase in the fetal brain to a maximal level in the adult brain (9). With use of the methylated RNA immunoprecipitation followed by next-generation sequencing (MeRIP–Seq), m^6A residues are found to be enriched in the 3' untranslated regions (UTRs) and most abundant in vicinity of the stop codon (9, 10).

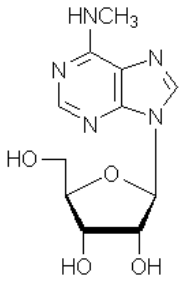

Figure 01. *N*^{6}-methyladenosine.

m^{6}A writer, eraser and reader

m^{6}A writer. In mammals, m^{6}A is installed by m^{6}A methyltransferases METTL3 and METTL14 and erased by two members of the AlkB family of nonheme Fe(II)/α-ketoglutarate (α-KG)-dependent dioxygenases, fat-mass and obesity associated protein (FTO) or ALKBH5 (11-15). The first m^{6}A methyltransferase ('writer') METTL3 was characterized from a ~200-kDa methyltransferase complex isolated from HeLa nuclear extracts (16). METTL3 has a classic the S-adenosyl-methionine-binding domain. Subsequent phylogenetic studies identified, METTL14, a homolog of METTL3, as a second methyltransferase (13, 14). Detecting m^{6}A levels in METTL3- or METTL14-depleted cells with siRNA or shRNA demonstrated a strong threshold dependence for both METTL3 and METTL14 (15). In addition, Wilms' tumor 1–associating protein (WTAP), a pre-mRNA splicing regulator can interact with the RNA-methylation complex (13, 17). WTAP lacks methyltransferase domains or activity, whereas it translocates the METTL3–METTL14 complex to nuclear speckles and affects this methylation. Knockdown of METTL3, METTL14 and WTAP causes ~30%, ~40% and ~50% global m^{6}A loss in mRNAs from Hela cells (13). WTAP depletion resulted in change of m^{6}A inversely correlated with mRNA stability at internal positions in transcripts but not at WTAP-independent sites at the first transcribed base as part of the cap structure (15).

m^{6}A eraser. The first enzyme to be identified as an m^{6}A demethylase ('eraser') is fat mass and obesity-associated protein (FTO) (11). FTO oxidizes m^{6}A in the presence of Fe(II) and α-ketoglutarate, generating N^6-hydroxymethyladenosine (hm^{6}A) as an intermediate modification and N^6-formyladenosine (f^{6}A) as a further oxidized product

(18). Overexpression of FTO in HeLa cells showed a decrease of m^6A by ~18%, whereas FTO knockdown increased m^6A levels by 23% in HeLa cells and 42% in 293FT cells (11). ALKBH5 (α-ketoglutarate-dependent dioxygenase alkB homologue 5), the second m^6A eraser to be discovered, is an FTO homologue of the AlkB family. ALKBH5 is most highly expressed in testis but low in heart and brain. ALKBH5 affects nuclear RNA export and metabolism, gene expression and mouse fertility (12). ALKBH5 knockdown increased m^6A levels in HeLa cells by ~9%, whereas overexpression of ALKBH5 decreased the m^6A level in total mRNA by ~29% (12).

m^6A reader. In mammalian cells, YTH-domain proteins are found to be m^6A-binding proteins, so-called m^6A 'readers'. m^6A can be directly recognized by these readers, which include cytoplasmic YTHDF1–3, and YTHDC1 and YTHDC2, which are localized in the nucleus (19-21). YTHDF2 recognizes over 3,000 cellular RNA targets, including mRNAs and non-coding RNAs. YTHDF2 recruits mRNA targets from the translatable pool to processing bodies and promotes mRNA degradation (19). YTHDF1, in contrast, actively promotes protein synthesis by interacting with translation initiation factors (21). YTHDF1 and YTHDF2 share ~50% common target transcripts. It has been shown that YTHDF1 knockdown decreased the translation efficiency of shared targets with no change of the average lifetime, whereas knockdown of YTHDF2 substantially increased the lifetime of the shared targets but only resulted in a slight difference in the translation efficiency (21). YTHDC1 has been shown to regulate mRNA splicing through recruiting and modulating pre-mRNA splicing factors for their access to the binding regions of targeted mRNAs (22). The YTH domain of YTHDC1 recognizes RNA in an m^6A-dependent manner and preferentially binds the GG(m6A)C sequence (20). Recent study shows that apart from acting as m^6A writer, METTL3 can function as a m^6A reader (23).

In the cytoplasm, METTL3 associates with ribosomes and promotes mRNA translation through interaction with the translation initiation machinery independent of methyltransferases catalytic ability (23).

Molecular function of m^{6}A modification

mRNA splicing. Transcriptomic analyses upon knockdown of WTAP and FTO suggests that m^{6}A regulates isoform diversity by alternative splicing (17, 24). By comparing the isoform changes upon knockdown of FTO and METTL3 in adipocytes, an inverse expression pattern was observed in 1491 isoforms of 1335 genes. 452 of these genes (522 isoforms) showed increased m^{6}A levels following knockdown of FTO, supporting the proposed roles for m^{6}A as a regulator of splicing (24). FTO knockdown led to increased inclusion of target exons by promoting the RNA binding ability of SRSF1 (Serine/Arginine-Rich Splicing Factor 1) and SRSF2 which binds to m^{6}A motifs (SRSF1- UGGAC; AGGACCU and 2- UGGAC; AAGGACC) (24). YTHDC1 directly regulates mRNA splicing through (1) recruiting pre-mRNA splicing factors SRSF3 but repelling SRSF10 and (2) facilitating SRSF3 but repressing SRSF10 in their nuclear speckle localization, RNA-binding affinity, and associated splicing events (22).

mRNA translation. YTHDF1 binds to m^{6}A-containing mRNA and promotes ribosome occupancy of its target mRNA to enhance mRNA translation through interacting with translation initiation factor complex 3 (eIF3). Epitope-tagged YTHDF1 expression with protein mass spectrometry also identified several other RNA-binding proteins including YBX1, IGF2BP1, G3BP1, and PCBP2, which are known to have roles in translational control (21). Whereas m^{6}A in the 3' UTR can be recognized by YTHDF1, YTHDF1 might also be able to recruit m^{6}A at coding regions or 5'UTR. Two recent

studies have indicated that m^{6}A in the 5'UTR promotes cap-independent translation (25, 26). A single m^{6}A in the 5'UTR is sufficient to induce cap-independent translation through interaction with the eIF3. eIF3 selectively binds m^{6}A modified GAC-containing RNA independent of RNA context and YTHDF1 (25). This effect of m^{6}A on cap-independent translation is more apparent in response to the heat-shock stress, when YTHDF2 translocates into nucleus and preserves 5'UTR methylation of stress-induced transcripts by limiting the FTO from demethylation (26). As mentioned earlier, METTL3 was found in the cytoplasm to associate with ribosomes and promotes translation in dependent of its catalytic activity. METTL3 promotes translation of certain mRNAs including epidermal growth factor receptor (EGFR) and the Hippo pathway effector TAZ by recruiting eIF3 to the translation initiation complex (23).

mRNA decay. Apart from direct recruitment of many inactively translated m^{6}A-containing mRNAs by YTHDF2 to cytoplasmic processing (P) bodies for degradation, m^{6}A indirectly hinders RNA binding protein HuR interaction with nearby sequences. Loss of HuR interaction exposes the miRNA binding sites in 3' UTR for RNA decay therefore leading to decreased RNA stability (14).

m^{6}A switches. 'm^{6}A switch' is proposed to describe the m^{6}A-dependent RNA structural remodeling which modulates RNA-protein interactions (27). Recent study shows that m^{6}A can alter local RNA structure in mRNA and non-coding RNAs thereby enhancing the accessibility of RNA-binding motifs to HNRNPC (Heterogeneous Nuclear Ribonucleoprotein C). HNRNPC, a member of the large family of heterogeneous nuclear ribonucleoproteins, is abundant in the nucleus and preferentially binds to U-tract motifs in nascent RNA. U-tract motifs are inaccessible by HNRNPC when buried within local

RNA structures. However, some U-tract motifs located in the stems of RNA stem-loop structures are found to base-pair with the m^6A consensus motif, methylation of which destabilizes the stem structure, and enables the U-tract motif to be exposed as single-strand for HNRNPC binding (27).

miRNA maturation. m^6A has also been shown to affect miRNA biogenesis (28). METTL3 methylates pri-miRNAs, enabling them to be recognized and processed by DGCR8, an RNA-binding protein of the microprocessor complex (28). Global m^6A reduction by depletion of METTL3 reduced the binding of DGCR8 to pri-miRNAs and resulted in the global decrease in mature miRNAs. This effect is mediated by HNRNPA2B1, another member of the nuclear HNRNP protein family (29). HNRNPA2B1 recognizes m^6A marks in a subset of primary miRNA transcripts and recruits DGCR8 protein complexes to promote primary miRNA processing.

mRNA nuclear export. Although global inhibition of mRNA methylation by S-tubercidinylhomocysteine (STH), a structural analog of S-adenosylhomocysteine, did not cause change in the half-life of total undermethylated mRNA, STH caused a significant delay in the time of cytoplasmic appearance of the polyadenylated RNA (30). In contrast, knockdown of the m^6A eraser ALKBH5 resulted in increased cytoplasmic accumulation of polyadenylated RNA possibly by accelerated nuclear export (12). ALKBH5 colocalizes with SRSF1 in nuclear speckles. Knockdown of ALKBH5 gave rise to relocalized SRPK1, one of the main kinases responsible for the phosphorylation of SRSF1, from nucleic locations to dot-like cytoplasmic and decreased level of phosphorylated SRSF1 (12).

Biological consequences of m^{6}A modification

stem cell fate. Transcriptome-wide m^{6}A profiling in murine embryonic stem cells (ESCs) showed that mRNAs encoding the core pluripotency regulators including Nanog, Klf4, Myc, Lin28, Med1, Jarid2, and Eed, have m^{6}A modifications (31). Both of Mettl3 and Mettl14 are shown to deposit m^{6}A onto these transcripts in mESCs (14, 31). However, contradicting results were observed when Mettl3 or Mettl14 was depleted in mESCs. Wang et al. (14) reported that knockdown of Mettl3 or Mettl14 in mESCs led to decreased m^{6}A levels and reduced self-renewal capability. A later study by Batista et al. reported that Mettl3 knockout decreased m^{6}A and promotes ESC self-renewal. Mettl3 knockout blocked mESC differentiation and displayed persistence of a stem-like, highly proliferative state. When injected into immunodeficient mice, Mettl3 knockout mESCs formed larger and poorly differentiated teratomas with very high mitotic indices and numerous apoptotic bodies. Similarly, knockdown of METTL3 in human ESC led to a profound block in endodermal differentiation at day 2 and day 4 (31). The confusing role of m^{6}A was explained by a more recent study (32). Unlike the pluripotent mESCs characterized by a “naïve” molecular state close to the pre-implantation inner-cell-mass (ICM), epiblast stem cells (EpiSCs) derived from the post-implantation epiblast, reside in an advanced developmental stage and are already “primed” for differentiation. Mettl3 knockout mESCs displayed decreased m^{6}A, preserved naïve pluripotentcy and block to proceed into the primed EpiSC-like state. However, Mettl3 knockdown in mEpiSCs boosted the highly expressed lineage commitment markers and resulted in an enhanced tendency to lineage priming. Thus, m^{6}A modification which functions naïve and primed pluripotency in an opposing manner, plays a key role in facilitating transition of mESCs from the naïve pluripotency toward the primed state upon differentiation.

circadian clock. While about 10% of genes are rhythmic in the liver, only about a fifth is driven by de novo transcription. The important physiological function of m^6A methylation in setting the speed of the circadian clock was demonstrated in a recent work which showed that a subset of clock gene transcripts bear m^6A modifications (33). Inhibition of m^6A formation by transmethylation inhibitor or by silencing METTL3 caused an mRNA processing delay and circadian period elongation. Despite a decrease in steady-state pre-mRNA and in cytoplasmic mRNA, loss of m^6A prolongs nuclear retention of mature mRNAs of the clock genes Per2 and Arntl.

m^6A modification in human disease

FTO and obesity. Variants in introns 1 and 2 of the gene *FTO* have the strongest genetic association with body mass index (34, 35). Gain or loss of *FTO* resulted in reduced or increased body weight and fat mass, respectively (36, 37). Recent study suggests that FTO controls exonic splicing of adipogenic regulatory factor RUNX1T1 and is required for adipogenesis (24). However, the variation of single nucleotide polymorphisms in *FTO* intron regions makes the *FTO* locus a super-enhancer for *IRX3* and *IRX5* gene expression but does alter *FTO* demethylase expression or function, suggesting that the structural basis rather than its enzyme activity has a clinical significance in obesity (38, 39).

m^6A and cancer. The first evidence to show the function of m^6A in cancer derived from a very recent study that demonstrated the dependence of breast cancer cells on ALKBH5 to acquire cancer stem cell phenotype during hypoxia (40). Exposure of breast cancer cells to hypoxia induced hypoxia-inducible factor (HIF)-1α- and HIF-2α-dependent expression of ALKBH5, which increased NANOG mRNA and protein

expression through demethylation of NANOG mRNA at an m^{6}A residue in the 3' UTR. Knockdown of ALKBH5 in MDA-MB-231 human breast cancer cells significantly reduced their tumor-initiating potential *in vivo*. Overexpression of ALKBH5 was sufficient to stimulate NANOG expression and induce cancer stem cell phenotype. The effect of ALKBH5 on global transcriptome in cancer cells remains unclear. Previous study identified ALKBH5 to be a direct transcription target of HIF-1α but not HIF-2α in breast cancer cells (41). However, the more recent study suggested that ALKBH5 is also regulated by HIF-2α (40), the expression of which is known to be restricted to cancer stem cell population (42).

The second evidence linking m^{6}A to cancer is the observation that the expression of METTL3 in the Cancer Genome Atlas (TCGA) datasets is significantly elevated in lung adenocarcinoma (LUAD) and colon adenocarcinoma compared with the normal tissues (23). The expression of METTL3 is also found to be elevated in lung adenocarcinoma cancer cell lines compared to the non-transformed human fibroblasts cell lines. Knockdown of METTL3 in lung cancer cells reduced expression of EGFR, TAZ, MAPKAPK2 (MK2), and DNMT3A, accompanied with inhibited cell growth, increased cell apoptosis, and decreased the invasion *in vitro,* whereas METTL3 overexpression in human fibroblasts promoted cell invasion. These findings suggest a potential role of METTL3 in lung cancer, but whether METTL3 acts as the m^{6}A reader or writer to promote the malignancy of tumor cells is unknown in this study.

Glioblastoma Multiforme (GBM)

Introduction

Gliomas represent approximately 30% of all tumors from central nervous system (43). In the World Health Organization (WHO) system, gliomas are named and classified after their histopathological appearance (44). GBM is classified as WHO grade IV tumors for the presence of necrosis or microvascular proliferation. GBM is the most common malignant type of brain tumor which accounts for 15.1% of all primary brain tumors and 46.1% of primary malignant brain tumors (45). While 90%–95% of glioblastomas are diagnosed as ‘‘primary’’ for lacking history of a precursor lesion, 5%–10% progress from lower grade gliomas and are termed ‘‘secondary’’ (46, 47). Even with standard treatment including surgical resection followed by chemotherapy and radiotherapy, GBM patients have a median survival of only 14 months (48). Recurrence is common and may be treated with repeat surgery and inhibitors of angiogenesis such as bevacizumab (49).

Molecular basis of GBM

Extensive research in the past two decades to describe genomic alterations in GBM has helped to illuminate common pathways on the basis of the characterization the genome and transcriptome of the disease. Among these is The Cancer Genome Atlas (TCGA) project with integrated multiplatform data analysis including microRNA, messenger RNA, single-nucleotide polymorphism, and exome sequencing data for more than 520 GBM samples (50). As the first type of cancer characterized by TCGA, GBM was found to be a heterogeneous collection of distinct diseases with multiple structural and expression alterations.

EGFR/ EGFRvIII*.* Receptor tyrosine kinases (RTKs) initiate signal transduction events and play important roles in tumor development. RTK members include EGFR, platelet-derived growth factor receptor (PDGFR), vascular endothelial growth factor receptor (VEGFR), and MET, mutations of which often act to relieve auto-inhibition or to prevent degradation (51). In-frame deletion of exons 2 to 7 of EGFR, which encode part of the extracellular domain, results in a constitutively active, ligand-independent mutant called EGFRvIII (52). Approximately 50% of primary GBM samples harbor EGFR amplification with or without EGFRvIII expression and is associated with poor prognosis (53). Overexpression EGFR and EGFRvIII enhance GBM cell survival through several mechanisms, including activation of growth signaling, such as RAS/RAF/ mitogen-activated protein kinase kinase (MEK) / (mitogen-activated protein) MAP and mammalian target of rapamycin (mTOR) pathways, suppression of cell cycle inhibitor proteins such as p27, and development of apoptotic resistance through the modulation of B cell lymphoma extra large (Bcl-X_L) expression (54, 55). The interplay of EGFR and EGFRvIII was characterized in two observations representing different functional models: A paracrine fashion composed of heterogeneous expression of wild-type EGFR and EGFRvIII in adjacent cells in which a minority of EGFRvIII-expressing cells drive the proliferation of both wild-type and EGFRvIII-expressing cells through the cytokine coreceptor gp130 (56). The other model involves co-expression of EGFR and EGFRvIII in the same tumor cells that drives transformation and tumorigenesis in a cell-intrinsic manner. EGFR catalyzed phosphorylation of EGFRvIII, enhancing the nuclear entry of EGFRvIII and formation of an EGFRvIII-STAT3/5 (Signal Transducer and Activator of Transcription) nuclear complex (57).

Ligand-independent activation of the RTK c-MET by increased levels of EGFR/EGFRvIII (58, 59) and transcriptional activation of EGFR ligands by hepatocyte

growth factor (HGF) (60) suggest that the crosstalk between c-MET and EGFR/EGFRvIII signaling pathways is employed by the GBM cells to be less dependent on either RTK and to develop treatment resistance.

PDGFR/VEGFR. PDGFRA amplification is found in approximately 15% of GBMs and is enriched in the TCGA proneural subtype (48). Two mutant forms of PDGFRA have been reported to be constitutively active and transforming. The intragenic deletion PDGFRα (Δ8,9) features an in-frame deletion of 243 base pairs (bp) of exons 8 and 9, generating a truncated extracellular domain (61, 62). Overexpressed PDGFRα (Δ8,9) in GBM has been suggested to be associated with enhanced downstream c-Jun phosphorylation independent of ligand activation. The other mutant (KDR-PDGFRA) with in-frame gene fusion of the extracellular domain of KDR/VEGFR-2 and the intracellular domains of PDGFRA displays elevated tyrosine kinase activity (63). Not only PDGFRA is amplified in GBMs, the PDGF ligands are also amplified and overexpressed. These aberration leads to subsequent activation of intracellular signaling pathways, such as The Phosphoinositide 3-Kinase (PI3K) /AKT (Protein kinase B) and RAS/MAPK, which promote tumor growth (64).

PI3K/AKT/PTEN/mTOR. The signal transduction initiated by activated RTKs is relayed and amplified by the PI3K/AKT/ phosphatase and tensin homolog (PTEN) /mTOR pathway to enhance GBM growth. This pathway regulates cell division, proliferation, differentiation, metabolism, and survival and is hyperactivated in cancer cells (65). The aberrant activation of the PI3K/AKT/PTEN/mTOR pathway is not only caused by the amplification/mutation of EGFR, other genetic alterations such as frequent mutations in PIK3R1/PIK3CA, AKT, PTEN all give rise to the hyperactivation of this

pathway (66). This activation is antagonized by the powerful inhibitor of the oncogenic AKT pathway, the PtdIns(3,4,5)P_3 phosphatase PTEN. *PTEN* is a major glioma tumor suppressor and is mutated or deleted in 30-44% of GBMs, which fails to block the activation of this pathway (67-69). In one report, PTEN inactivation was shown to specifically raise EGFR activity by limiting the ligand-induced ubiquitylation and degradation (70). The expression of PTEN may also be regulated post-translationally by the HECT domain ubiquitin ligase NEDD4-1 (71). The proto-oncogenic ubiquitin ligase NEDD4-1 suppresses PTEN function by targeting it for proteasomal degradation. NEDD4-1 upregulation associated with overexpression of the Forkhead box protein M1 transcription factor in gliomas led to dysfunction even in cells with intact function of *PTEN* (72). mTOR is a protein kinase comprising two different complexes (mammalian target of rapamycin complex 1 [mTORC1] and mTORC2). mTOR can be activated by PI3K and also acts upstream as a regulator of PI3K (73). mTOR regulates different cellular processes such as gene transcription and protein synthesis and contributes to cancer development through its effect on cell cycle progression and anti-apoptotic activity (73).

RAS/RAF/ERK kinase (MEK)/extracellular-signal-regulated kinase (ERK)/NF-1. Activation of the RAS/RAF/MEK/ERK pathway by RTKs such as EGFR and PDGFR and mediated by growth factor receptor–bound protein 2 (GRB2) and son of sevenless (SOS) transmits signals to transcription factors, which regulate gene expression responsible for growth, migration, apoptosis, proliferation, differentiation, and cell survival. Disregulation of this signal cascade can cause malignant transformation (74). RAS signaling could be terminated through Neurofibromin, encoded by the *NF1* gene, which is a powerful tumor suppressor that negatively regulates RAS and mTOR

signaling in astrocytes (75). NF1 can be inactivated by genetic loss or mutation or by increased proteasomal degradation, which may be mediated by hyperactivation of protein kinase C (76). *NF1* mutations defines the mesenchymal GBM subtype with poor patient survival (48).

p53/RB/CDKN2A. The well-known tumor suppressor p53 was found to be mutated in 37.5% untreated and 58% of treated GBMs, respectively (50). p53 is a transcription factor that regulates expression of genes involved in processes such as apoptosis and DNA repair. Disruptions of the p53 pathway arise from mutations of *p53* itself and dysregulation in its upstream genes such as MDM2/4 and ARF, which are mutated in approximately 70% of GBM samples (50). The MDM2-MDM4 heterocomplex is an E-3 ubiquitin ligase complex for degradative control of p53. Amplification and overexpression of MDM2/MDM4 may represent an alternative mechanism by which the GBM escapes from p53-regulated growth control (77). Inactivation of CDKN2A also causes the misregulation of p53 signaling. Deleted in approximately 55% of GBMs, CDKN2A encodes p16INK4a and p14ARF, two distinct tumor suppressors that negatively regulates the cell cycle (50, 78). p14ARF stabilizes and upregulates p53 through promoting the degradation of MDM2, thus restraining cell growth. p16INK4A inhibits the CDK4/6 (cyclin-dependent kinase) interaction with cyclin D, which is required for G1/S transition (79-81). The CDK4,6/cyclin D complex phosphorylates the tumor suppressor retinoblastoma protein (pRB), leading to the release of bound E2F and enabling cell cycle progression. p16INK4a deletion therefore, enables the association CDK4/6 and cyclin D, subsequently promoting the G1/S transition.

Glioma stem cells

Glioma stem cells (GSCs) represent the cancer stem cells (CSCs) within GBM. CSCs are a subpopulation of cells with self-renewal capacity in the tumor that can give rise to heterogeneous cancer cells that recapitulate the tumor (82). GSCs were one of the first CSCs isolated from solid tumors (83). Only 100 GSCs reportedly gave rise to tumors that resembled the parental tumors when implanted in immunodeficient mice (83). GSCs are often cultured as sphere suspension in serum-free medium containing EGF and FGF (83, 84). The expression of transcription factors or structural proteins (sex determining region Y)-box 2 (SOX2), Nanog homeobox (NANOG), oligodendrocyte lineage transcription factor 2 (OLIG2), v-myc avian myelocytomatosis viral oncogene homolog (MYC), Musashi RNA Binding Protein 1 (MUSASHI1), BMI1 proto-oncogene (BMI1), NESTIN that are essential for normal neural stem/progenitor cell function are also found in GSCs. Another similarity to normal neural stem cells (NSCs) is that these GSCs could be differentiated to more linage-committed tumor cells that express neuronal or glial markers upon induction (84).

transcriptional regulation and chromatin modification. Maintenance of the CSC state involves an array of transcription factors, including MYC, STAT3, SOX2, FOXM1, Forkhead Box G1(FOXG1), GLI Family Zinc Finger 1 (GLI1), Achaete-scute homolog 1 (ASCL1), zinc finger protein, X-linked (ZFX), NANOG, and Zinc Finger Homeobox 4 (ZFHX4), which recruit necessary chromatin remodeling factors to main the glioma CSC state (85). A core set of four master transcription factors POU3F2, SOX2, SALL2, and OLIG2 coordinately bind and activate GSC-specific regulatory elements and have been shown to be sufficient to induce differentiated GBM cells to GSCs (86). Additional epigenetic regulator such as the mixed lineage leukemia 1 (MLL1) protein is also required to maintain the CSC state through activation of Homeobox A10 (HOXA10) (87).

The mixed lineage leukemia 5 (MLL5) suppresses histone 3 variant H3.3 to maintain the self-renewal hierarchies (88). Enhancer of zeste 2 polycomb repressive complex 2 subunit (EZH2) is important for CSC maintenance through regulation of both Polycomb-repressive domains and STAT3 activity (89).

metabolic stress. The tumor microenvironments around GSCs are often limited with glucose and oxygen, forcing the GSCs to shift toward aerobic glycolysis. Under such conditions, GSCs up-regulate the high-affinity glucose transporter 3 (GLUT3) for glucose uptake to outcompete neighboring non-GSC tumor cells. Similarly, GSCs preferentially up-regulate HIF-2α compared with non-GSC tumor cells and normal progenitors to maintain the self-renewal, proliferation, and survival (90, 91). GSCs also increase mitochondrial fission by dynamin-related protein 1 (DRP1) to suppress apoptosis and promote tumor growth. DRP1 is activated upon phosphorylation by cyclin-dependent kinase 5 (CDK5) in GSCs and inhibited by Ca^{2+}-calmodulin-dependent protein kinase 2 (CAMK2) in non-GSC tumor cells (92). In addition, GSCs can provide vascular structure through transdifferentiation into endothelial cells and vascular pericytes to promote tumor growth (93-95).

developmental signaling. GSCs can hijack normal developmental programs to maintain an undifferentiated state. These pathways include Notch, bone morphogenetic protein (BMP), nuclear factor κB (NF-κB), and Wnt signaling. Wnt signaling is highly active in GSCs and is required for the maintenance of CSC phenotype. Enhanced PLAGL2 expression impeded GSC differentiation through modulation of Wnt/β-catenin signaling (96). Inhibition of β-catenin substantially reduced the self-renewal and tumorigenesis of GSCs (97). In addition, canonical growth factor signaling pathways also

contribute to maintenance and proliferation of GSCs. PDGFR signaling promotes GSC proliferation, self-renewal, and tumor growth through activation of STAT3 (98, 99).

therapeutic resistance. Targeting the GSCs subpopulations might provide effective therapeutic strategies with the concept that these self-renewing tumor cells are resistant to conventional therapy and give rise to tumor recurrence by sustaining long-term tumor growth (100, 101). GSCs contribute to radiation resistance by activation the DNA damage checkpoint response an increase in DNA repair capacity (100). Using a genetically engineered mouse model of glioma, the nestin positive glioma cells resembling human GSCs have been characterized to be the source of tumor recurrence after temozolomide (TMZ) treatment through the production of transient populations of highly proliferative cells (101).

Forkhead box protein M1

Introduction

Forkhead box protein M1 (FOXM1) is also known in the literature as HFH-11, MPP-2, WIN, and Trident. FOXM1 belongs to the Forkhead superfamily which comprises a large number of transcription factors sharing a conserved DNA binding domain called Forkhead or winged-helix domain. FoxM1 binds to the consensus sequence, TAAACA in DNA in vitro. The human *FOXM1* gene, spanning approximately 25 kb on the 12p13-3 chromosomal band, consists of 10 exons, including exon Va (A1) and exon VIIa (A2) that are alternatively spliced and give rise to three classes of transcripts (102). The FOXM1A isoform containing both alternative exons is transcriptionally inactive. Inclusion of exon VIIa disrupts the transactivation domain in the C-terminal, leading to transcriptional inactivation and function as a dominant-negative variant due to retained normal DNA binding activity (103). FOXM1B contains neither of the alternative exons, and FOXM1C has the Va exon only. Both FOXM1B and FOXM1C are transcriptionally active and can stimulate cellular proliferation.

FoxM1 exhibits a wide cellular expression pattern in mouse embryo and is expressed in particular in proliferating epithelial and mesenchymal cells. In adult tissues, FoxM1 is restricted in epithelial cells of Lieberkuhn's crypts of the intestine, the spermatocytes and spermatids of the testis, and the thymus and colon. FoxM1 is absent in adult hepatocytes but is reactivated by proliferative signals or oxidative stress (103).

FOXM1 and proliferation. Loss of FOXM1 resulted in cell cycle defects, premature cellular senescence and cell death. FOXM1 is required for G1/S and G2/M transition, and M phase progression. Low at G0-phase, FOXM1 expression increases to a maximal level in late G1 or early S-phase and maintains until the end of G2–phase when it rapidly

decreases during the mitosis (104). FOXM1 regulates G1/S transition and DNA replication through control of the transcription of cyclin A2, JNK1, ATF2, Cdc25A phosphatase and enhancing the ubiquitinylation and degradation of the cyclin-dependent kinase inhibitors (CKIs), p21Waf1/Cip1 and p27Kip1 by stimulating the expression of the Skp2 and Cks1 subunits of Skp1/cullin/F-box protein (SCF) complex (105). FOXM1-deficient cells have been also shown to fail to accumulate Cdc25B, cyclin B, Aurora B kinase, survivin, polo-like kinase 1 (PLK1) and centromere protein A (CENPA), CENPB and CENPF, which led to prolonged G2-arrest, mitotic spindle defects, chromosome missegregation, mitotic spindle checkpoint dysfunction, centrosome amplification and overt polyploidization. The *CENP-F* gene, as a kinetochore binding protein in the mitotic checkpoint machinery, is a direct target of FOXM1, and is required for proper chromosome segregation (105-107). Therefore, in addition to promote cell cycle progression, FOXM1 is also crucial to chromosomal stability.

FOXM1 in GBM

FOXM1 is a human proto-oncogene, overexpression of which has been reported in an array of tumor types, including tumors from skin, liver, breast, lung, prostate, colon, pancreas, ovarian and brain (108). FOXM1 expression is absent in normal brain tissues and arises in brain tumor samples. In low-grade astrocytomas, FOXM1 was found to be high in 4% tumors, low in 4% tumors and absent in 92% tumors. In the grade III anaplastic astrocytomas, 14.7% and 26.5% were high and low, respectively. However, high FOXM1 expression was found in 36% GBMs and another 36% tumors expressed low levels of FOXM1. Overexpression of FOXM1 and its associated transcription targets such as AURKB, CCNB1, CDC25B, Skp2 and PLK1, was frequently detected in GBMs (109). FOXM1 has been shown to inform poor overall survival of glioma patients. Apart

from its contribution to control of cell cycle progression and chromosomal stability, FOXM1 regulates tumorigenesis of GBM in many aspects, including promotion of angiogenesis, invasion, transformation, and de-differentiation.

FOXM1, invasion and angiogenesis. FOXM1 can directly bind to the promoter of *VEGF* and *matrix metalloproteinase (MMP)-2* and activate VEGF and MMP2 transcription. MMP-2 promotes GBM invasion through basement membrane degradation. Epitopic overexpression of FOXM1 in human anaplastic astrocytoma cells led to the formation of highly angiogenic and invasive glioblastoma associated with VEGF and MMP2 upregulation in nude mice. These regulatory interactions were also identified in human GBM samples (110, 111).

FOXM1 and transformation. FOXM1 not only promotes glioma malignant progression, it can also transform the normal human astrocytes (NHA) incorporated with p53 and pRB inhibition, giving rise to tumor resembling human GBM in nude mice. FOXM1, importantly functional in the early development of glioma, stimulated the expression of survivin, cyclin D1, cyclin E and NEDD4-1, an E3 ligase that mediates the degradation and downregulation of PTEN. Decreased PTEN resulted in the hyperactivation of PI3K pathway with cytoplasmic accumulation of FoxO3a. This effect was reversed when using the phosphoinositide 3-kinase/Akt inhibitors, which blocked Akt activation and inhibited the FOXM1-induced transformation of immortalized NHAs (72).

FOXM1 and stress. FOXM1 is induced by heat shock in a heat shock factor 1 (HSF1)-dependent manner. In response to heat shock, HSF1 directly bound to *FOXM1*

promoter in GBM cells and activated FOXM1 expression, which subsequently induced expression of Cdc2, Cdc20, and Cdc25B the G2-M phase progression. FOXM1 is required for the cell survival under lethal heat shock stress condition (112). In another research to characterize the mechanism underlying resistance of recurrent GBM to alkylator temozolomide (TMZ), FOXM1 was found to be elevated in recurrent and TMZ resistant GBM samples compared to primary tumors. In the course of a 5-day *in vitro* treatment of TMZ, Rad51, a central component of the DNA double-strand break repair machinery, sequentially increased in expression level with FOXM1. FOXM1 directly bound to *Rad51* promoter in GBM cells and activated Rad51 expression. Knockdown of FOXM1 sensitized the TMZ-resistant GBM cells, which was partially reversed by Rad51 reexpression (113).

FOXM1 and nuclear localization of GLI1 and β–catenin. FOXM1 directly binds to the *importin-7 (IPO7)* promoter and activates IPO7 expression in GBM cells (114). IPO7 interacts with glioma-associated oncogene homolog 1 (GLI1) to facilitate its nuclear translocation, which mediates the HEDGEHOG (HH)-GLI signaling in regulation of glioma growth and survival and maintenance of stemness signature of GSCs (115). FOXM1 can induce nuclear import of GLI1 through activation of IPO7 expression. FOXM1 also directly binds to β–catenin through its forkhead box domain. This interaction is required for β–catenin translocation into nucleus where it forms the TCF transcription activation complex with FOXM1 and subsequently activates Wnt target genes (97).

FOXM1 and GSC. The earliest study linking FOXM1 to GSCs identified a Wnt-FOXM1-β–catenin signal pathway in which Wnt triggers the accumulation and nuclear translocation of FOXM1 and β–catenin (97). The β–catenin/FOXM1 complex formed in the cytoplasm enters nucleus under Wnt signal and associates with TCF4 at the promoters of Wnt-responsive genes such as *Axin2, LEF-1, c-Myc*, and *cyclin D1*. Interacting with FOXM1 appears to be required for the localization and function of β–catenin, whereas the DNA binding ability of FOXM1 is not essential to induce the expression of these genes. Disruption of either FOXM1 or β–catenin substantially abolished the self-renewal capacity of GSCs, with FOXM1-depleted GSCs displaying more severe phenotypes that tumorigenesis was completely abrogated in nude mice. Subsequent study found that the FOXM1-β–catenin also control the expression level of STAT3, a transcription factor downstream of interleukin 6 (IL6), erythropoietin receptor (EPOR), PDGFR and EGFR which is essential to maintain survival and self-renewal of GSCs (98, 99, 116-118). Apart from transcription regulation of STAT3, FOXM1 binds to the promoter of *PDGFA*, leading to the active expression of PDGFA and STAT3 phosphorylation (99). Therefore, FOXM1 drives a feed-forward STAT3-activation signaling loop that promotes the self-renewal and tumorigenicity of GSCs. The critical role of FOXM1-STAT3 regulatory axis was highlighted in a more recent study which showed that FOXM1 mediates the iron-regulated mitotic progression of GSCs (119). Knockdown of transferrin receptor and ferritin, two core iron regulators, reduced FOXM1 expression and abrogated the proliferation and tumorigenesis of GSCs. Overexpression of FOXM1, however, was sufficient to rescue the growth inhibition by loss of either iron regulator. On the other hand, overexpressing FOXM1 in non-GSC glioma cells

reprogramed the tumor cells to GSC-like GBM cells with a more de-differentiated state characterized by enhanced self-renewal and tumorigenesis *in vitro* and *in vivo* (97, 99).

FOXM1 has been shown by another study (120) as a substrate for the mitotic kinase MELK in GSCs. MELK cooperates with PLK1 to phosphorylates and activates FOXM1, which lead to increased expression of mitotic regulatory genes in GSCs. Further study revealed that the catalytic subunit of Polycomb repressive complex 2, EZH2, is a direct target of the MELK-FOXM1 complex (121). EZH2 and MELK are co-expressed in GBM, substantially induced by radiation and inversely correlated with patient prognosis. FOXM1 overexpression enabled resistance to irradiation-induced apoptosis by regulation of EZH2.

SUMMARY

N^6-methyl-adenosine (m^6A) is the most prevalent chemical modification of mRNAs in eukaryotes (3, 9, 10). In mammals, m^6A installed by m^6A methyltransferases METTL3 and METTL14 is erased by two members of the AlkB family of nonheme Fe(II)/α-ketoglutarate (α -KG)-dependent dioxygenases, fat-mass and obesity associated protein (FTO) or ALKBH5 (11-15). Different influences of mRNA m^6A modification on cellular process include alterations in RNA stability (14, 15, 19), translation efficiency (21, 25, 122), secondary structure (27), subcellular localization (12, 33, 123) and alternative splicing (10, 17, 24). m^6A methyltransferases are crucial for the differentiation of mouse embryonic stem cells (14, 31, 32). FTO is known to regulate adipogenesis and energy homeostasis (24, 36). ALKBH5 is most highly expressed in testis but low in heart and brain. ALKBH5 affects nuclear RNA export and metabolism, gene expression and mouse fertility (12). To date, the biological significance of these m^6A modification enzymes is little studied in human diseases.

Glioblastoma (GBM; World Health Organization [WHO] grade IV glioma) is the most common and devastating primary malignant brain tumor. Even with surgical resection and the use of highly aggressive therapies, recurrence is inevitable and the median survival of GBM patients is only one year (48). GBMs are characterized by marked intra- and intertumoral heterogeneity and contain cells featuring stem-like properties at the apex of cellular hierarchies (85, 124). Targeting the glioblastoma stem-like cells (GSCs) subpopulations might provide effective therapeutic strategies with the concept that these self-renewing tumor cells are resistant to conventional therapy and give rise to tumor recurrence by sustaining long-term tumor growth (100, 101). Recent studies have shown that the transcription factor FOXM1 plays a pivotal role in regulating GSC self-renewal and proliferation (119, 121, 125). Being overexpressed in GBM (109, 126, 127), FOXM1

interacts with β-catenin (97) and MELK (120), induces SOX2 (128), and activates STAT3 (99) in GSCs. However, the molecular mechanism underlying FOXM1 upregulation in GSCs has not been identified.

Dysregulated DNA methylation by cancer epigenetic regulators is a hallmark of GBM (88, 129). The lack of study for m^6A mRNA modification in human disease prompted us to investigate the possible relationship between m^6A and cancer.

CHAPTER 2: MATERIALS AND METHODS

Cell Lines and Culture Conditions

Human glioma Hs683 and SW1783 cell lines, and GBM LN229 and U-87 MG cell lines were from the American Type Culture Collection. Immortalized normal human astrocyte line NHA-E6/E7/hTERT is previously described (130). The above cell lines were cultured in DMEM with 10% FBS. Glioma stem-like cell lines isolated from fresh surgical specimens of human GBM and cultured as GBM tumorspheres in neurosphere medium (NM) containing DMEM/F12 medium supplemented with B27 supplement (Life Technologies) and bFGF and EGF (20 ng/ml each) as described previously (99). Only early-passage cell lines were used for the study.

Immunofluorescence, Immunohistochemistry, Immunoprecipitation, and Immunoblot Analysis

For immunofluorescence (IF) analysis, GSCs were fixed with 4% formaldehyde (Fisher) for 15 min and then blocked with 5% normal goat serum (Vector) with or without 0.1% Triton X-100 in PBS for 60 min at room temperature. Immunostaining was performed using the appropriate primary and secondary antibodies. Nuclei were counterstained with Hoechst. Images were taken with a ZEISS Axio Scope.A1 Upright Microscope. For immunohistochemical (IHC) analysis, GBM xenografts or surgical specimens tissue slides were deparaffinized, rehydrated through an alcohol series. IHC staining was performed with appropriate antibodies using DAB detection. Immunoblotting and immunoprecipitation were done as described (97).

Specific antibodies against FOXM1 (K19), Nestin, HuR, GFAP, Tuj-1, SSEA-1, SOX2 (E4, IF), Nanog, YTHDF3, β-actin from Santa Cruz; α-Tubulin, SOX2 (D6D9, immunoblotting), OCT4, Histone 3, CD133 from Cell Signaling; U1-70K, ALKBH5 (ABE547, immunoblotting) from Millipore; FLAG, ALKBH5 (HPA007196) from Sigma; and FOXM1 (M02, IF) from Abnova were used for the IF, IHC, or immunoblot analyses.

RNA Pull-down Assay and RNA Immunoprecipitation

The mix of six 90- to 120-nucleotide probes antisense to *FOXM1-AS* sequence was designed to capture *FOXM1-AS.* Antisense probes to the capture probe set omitted the *FOXM1* - *FOXM1-AS* overlapping region and were generated as negative control. 50 pmole RNA probes were *in vitro* transcribed with the MEGAscript® T7 Transcription Kit and labeled with Pierce RNA 3' End Biotinylation Kit (Life Technologies), treated with TURBO DNase (Life technologies) and purified with RNeasy Mini Kit (QIAGEN). Next, RNA pull-down was performed as previously described (131) with 30ul Dynabeads MyOne Streptavidin C1 using GSC17 nuclear extracts. Associated proteins were detected by Western blotting. RNA immunoprecipitation was performed with Magna RIP™ RNA-Binding Protein Immunoprecipitation Kit (Millipore) following manufacturer's instruction. Briefly, magnetic beads coated with 3µg normal Immunoglobulin G (IgG, Millipore), HuR (Santa Cruz), or FLAG (Sigma Aldrich) antibody were incubated with pre-frozen cell lysates or nuclear extracts overnight at 4^{o}C. Associated RNA-protein complexes were collected and washed for six times, followed by proteinase K digestion and RNA extraction by TRIzol. Relative interaction was determined by qPCR using IgG as negative control.

AMT Crosslink Assay

GSCs were suspended in PBS with or without 0.5 mg/mL AMT (4′-Aminomethyltrioxsalen hydrochloride, Sigma) at a concentration of $2x10^7$ cells/ml in 6-well tissue culture plates and incubated on ice for 15min. Then the plates were covered with a 2-mm-thick glass plate without lid. The cells were irradiated for 15min from a distance of 2.5cm with a handheld 365-nm UV light and mixed every 5min. After cross-linking, cells were pelleted in 1.5ml microcentrifuge tubes for RNA isolation by TRIzol. RNA yield was determined with a NanoDrop spectrophotometer. To pull-down the target RNAs, 25 pmole *in vitro* transcribed and biotin labeled RNA probes were denatured to 90°C for 2 minutes, transferred immediately on ice. Then probes and 10ug RNA were mixed in binding buffer (50mM Tris-HCl pH 7.5, 150 mM NaCl, 0.5% NP40 and 1mM ribonucleoside vanadyl complexes) and transferred to a 37°C Thermomixer, shaking at 1,200 r.p.m. After 2 hours, 30µl washed Dynabeads MyOne Streptavidin C1 were added and incubated for 2 hours at room temperature. After six washes, precipitated RNAs were extracted by TRIzol.

RNA Isolation, cDNA synthesis and Quantitative Real Time PCR

RNA was isolated using TRIzol (Life Technologies) following the manufacturer's protocol. cDNA was generated using the iScript cDNA Synthesis Kit (BioRad). Quantitative real-time PCR using Powerup SYBR Green PCR Master Mix (Life Technologies) was performed on a 7500 Fast Real-time PCR System (Applied Biosystems). For RNA stability assay, GSCs were plated in a poly-lysine coated 6-cm dish and incubated with actinomycin D (Santa Cruz) at 5 µg/ml for indicated time. Total RNA was isolated for qPCR.

Quantitative PCR primers:

FOXM1-AS	forward: 5′-AAGGCTGGATTTCTTCCTC-3′
	reverse: 5′-TCACCTTATCTCTGTTTCCC-3′

FOXM1 pre-mRNA	forward: 5′-CATAGCAAGCGAGTCCGCAT-3′
	reverse: 5′-TGCAAGCTGAAGGTCCAACA-3′
FOXM1	forward: 5′-TGCAGCTAGGGATGTGAATCTTC-3′
	reverse: 5′-GGAGCCCAGTCCATCAGAACT-3′
FOXM1A	forward: 5′-TGGGGAACAGGTGGTGTTTGG-3′
	reverse: 5′-GCTAGCAGCACTGATAAACAAAG-3′
FOXM1B	forward: 5′-CCAGGTGTTTAAGCAGCAGA-3′
	reverse: 5′-TCCTCAGCTAGCAGCACCTTG-3′
FOXM1C	forward: 5′-CAATTGCCCGAGCACTTGGAATCA-3′
	reverse: 5′-TCCTCAGCTAGCAGCACCTTG-3′
ALKBH5	forward: 5′-ATCCTCAGGAAGACAAGATTAG-3′
	reverse: 5′-TTCTCTTCCTTGTCCATCTC-3′
MALAT1	forward: 5′-CATTCGCTTAGTTGGTCTAC-3′
	reverse: 5′-TTCTACCGTTTTTAGCTTC-3′
GAPDH	forward: 5′-TGCACCACCAACTGCTTAGC-3′
	reverse: 5′-GGCATGGACTGTGGTCATGAG-3′
CENPE	forward: 5′-CTCTTACGTGTATCTTACATGG-3′
	reverse: 5′-CAACTTCTTCTGTGAGATCAG-3′
CENPF	forward: 5′-ACTCACATCAGTAAAGCAAC-3′
	reverse: 5′-TCATTCTCCTTGATCTGACTC-3′
PLK1	forward: 5′-ATTTCCGCAATTACATGAGC-3′

	reverse: 5′-TCCTGGAAGAAGTTGATCTG-3′
AURKA	forward: 5′-CGGCATCCTAATATTCTTAGAC-3′
	reverse: 5′-ATAAACTGTTCCAAGTGGTG-3′
PRC1	forward: 5′-ACTACACAGAAAGTCTGCTC-3′
	reverse: 5′-CTCTCAAACTCTAAGAAAAGCC-3′
CCNB2	forward: 5′-ATTTTTACAGGTTCAGCCAG-3′
	reverse: 5′-ATCTCCTCATACTTGGAAGC-3′
MELK	forward: 5′-AGGGTAACAAGGATTACCATC-3′
	reverse: 5′-CTGATCCAAGATATGATTTGCC-3′
PLK4	forward: 5′-GTGGTGAGCATACTTGATTC-3′
	reverse: 5′-GTCTATCAGCAAGAGGAAAAC-3′
AURKB	forward: 5′-ATTGGAGTGCTTTGCTATG-3′
	reverse: 5′-TTTAGGTCCACCTTGACG-3′

Subcellular Fractionation Assay

The method for subcellular fractionation assay was adapted from Wuarin and Schibler (132). Briefly, GSCs were collected by centrifugation and washed with PBS. Cell pellets were resuspended in cold NP-40 lysis buffer (10 mM Tris-HCl pH 7.5, 0.15% NP40, 150 mM NaCl) for 5 min. The lysate was then transferred onto 2.5 volumes of a chilled sucrose cushion (ice cold sucrose buffer (10 mM Tris-HCl pH 7.5, 150 mM NaCl, 24%

sucrose), and centrifuged at 13,000 rpm and 4°C for 10 min. The supernatant (cytoplasmic fraction) was collected for immunoblotting analysis or RNA extraction by TRIzol. The nuclear pellet was resuspended in cytoplasmic lysis buffer without NP40, and passed through sucrose buffer again. Washed nuclei pellet was resuspended in an ice cold glycerol buffer (20 mM Tris pH7.9, 75 mM NaCl, 0.5 mM EDTA, 50% glycerol) and then mixed with an equal volume of cold nuclei lysis buffer (10 mM HEPES pH 7.6, 1 mM DTT, 7.5 mM MgCl2, 0.2 mM EDTA, 0.3 M NaCl, 1 M UREA, 1% NP-40) by vortex for 2X5 seconds. After incubation for 2 min on ice, the supernatant (nucleoplasm fraction) was collected for immunoblot analysis or TRIzol RNA extraction by centrifuge at 13,000 rpm and 4°C for 2 min. The chromatin pellet was washed with cold PBS and then dissolved in TRIzol or saved for immunoblotting analysis.

m^{6}A Dot Blotting

The m^{6}A dot blot using total cellular RNA or mRNA purified by Dynabeads® purification kit (Ambion) was performed on a Bio-Dot Apparatus (Bio-Rad). RNA (10µl) in 1 M NaCl/10 mM NaOH was applied to the BrightStar®-Plus membranes (Ambion) and autocross-linked by UV (Stratalinker® 1800). The membrane was blocked with 5% non-fat milk for 30 minutes, incubated with the m^{6}A primary antibody (Synaptic Systems, 202003, 1:500) followed by anti-rabbit-HRP secondary antibody and exposed to an autoradiographic film.

Plasmids and RNA knockdown

ALKBH5 expression plasmid was generated by cloning the full-length ORF of human ALKBH5 gene (NM_017758.3) into pcDNA3.1-DYK vector (GenScript).

siRNA oligonucleotides were synthesized by Sigma Aldrich except the siRNA pools for YTHDF3, which were purchased from Dharmacon and used with the ON-TARGETplus Non-targeting pool from the same manufacturer.

RNAi oligonucleotides sequences are listed below:

	siRNA Oligonucleotides
Non-targeting control	5′-GAAUACGUACCCCAUUAUA-3′
ALKBH5 pool	5′-ACAAGUACUUCUUCGGCGA-3′
	5′-GCGCCGUCAUCAACGACUA-3′
	5′-CUGAGAACUACUGGCGCAA-3′
FOXM1-AS#1	5′-GCGAUGACAUUUACACAUA-3′
FOXM1-AS#2	5′-GGGUUCUGAUCCUCUUUGUGU-3′
FOXM1-AS#3	5′-CCUUCCUGUUGUACUUUCAGCUUCC-3′
FOXM1-AS#4	5′-CAUUUACACAUAGGUCACUAUGGAG-3′
FOXM1-AS#5	5′-CAGAGAUAAGGUGAACCAACGGUCA-3′
YTHDF3 pool	5′-UGGUUUACAUGUCGACUAA-3′
(SMARTpool ON-TARGET plus)	5′-UGGUUUACAUGUUGUGUGA-3′
	5′-UGGUUUACAUGUUUUCUGA-3′
	5′-UGGUUUACAUGUUUUCCUA-3′

Transfections were performed using X-tremeGENE HP DNA Transfection Reagent for plasmid and X-tremeGENE siRNA Transfection Reagent (Roche) for siRNA following the manufacturer’s protocols.

Lentiviral Transduction and Establishment of Stable Cell Lines

Lentiviral vectors expressing non-targeting control shRNA (SCH002), and two shRNA constructs targeting ALKBH5 (NM_017758), shRNA1 (TRCN0000064783) and shRNA2 (TRCN0000064787) were obtained from Sigma. The lentiviral vectors were co-transfected with packaging vectors psPAX2 and pMD2G (Addgene) into 293FT cells for lentivirus production. To establish stable cell lines, GSC cells were transduced by using the above lentiviruses with polybrene (6 μg/ml, Sigma). After 72 hr of transduction, cells were selected with 2 μg/ml puromycin for 4 days. For the ALKBH5 rescue experiment, shRNA targeting 3'UTR of ALKBH5 (TRCN0000307780) was used for knockdown.

Limiting Dilution Assay

In vitro limiting dilution assay (LDA) was performed as described previously (119). Briefly, dissociated GSC cells were seeded in 96-well plates at density of 5, 10, 20, 50, 100 or 200 cells per well and each well was examined for formation of tumorspheres after 7 days. Stem cell frequency was calculated using extreme limiting dilution analysis (http://bioinf.wehi.edu.au/software/elda/).

Microarray Analysis

RNA from GSC11 cells with shControl or shALKBH5-2, GSC17 cells with shControl or shALKBH5-1 was collected on day 7 after transduction for microarray analysis at MD Anderson DNA Core Facility using Affymetrix Human Gene 2.0 ST array, Expression Console Software and Transcriptome Analysis Console v3.0 (Affymetrix). The genes showing altered expression (fold change > 2) compared with the control shRNA in both

cell lines were selected and analyzed using Ingenuity Pathway Analysis (IPA, Ingenuity Systems).

BrdU Incorperation Assay and Cell-Cycle Analysis

For BrdU incorperation assay, cells were cultured with BrdU labeling reagent (Life Technologies) overnight and stained with BrdU antibody (Cell Signaling) according to manufacturer's instructions. Five field of view per slide were examined for BrdU positive cells. For cell-cycle analysis, cells were fixed, stained with PI/RNase Staining Buffer (BD Pharmingen) for 15 min at room temperature. Samples were acquired with FACScan (BD Biosciences).

Luciferase Reporter Assay

Cells seeded in 12-well plates were transfected with the pMIR-REPORT luciferase vector fused with or without FOXM1-3'UTR. Transfection efficiency was quantified by co-transfection with a Renilla luciferase reporter. The activities of firefly luciferase and Renilla luciferase in each well were calculated by dual-luciferase reporter assay system (Promega). The values of FOXM1-3'UTR luciferase activities were further normalized by the pMIR-REPORT vector activities under the same treatment.

Intracranial Tumor Assay

All mouse experiments were approved by the Institutional Animal Care and Use Committee of MD Anderson. For FOXM1 rescue studies, GSCs with ALKBH5 or FOXM1-AS shRNA knockdown were transfected with a pcDNA3.1-FOXM1 expression plasmid. A total of 50,000 GSCs (n = 5 mice per group) were intracranially injected into male athymic nude mice 4–6 weeks of age. Mice were sacrificed and brains were

harvested 30 days post-injection of GSC11 and 20 days post-injection of GSC17. Each mouse brain was fixed in 4% formaldehyde, embedded in paraffin, and examined for tumor formation by histologic analysis of hematoxylin- and eosin-stained sections. Tumor volume was calculated by the formula $V = ab^2/2$, where a and b are the tumor's length and width, respectively.

Statistical Analysis

Data are presented as mean ± S.E.M. The significance of mean values between two groups was analyzed with two-tailed Student's t test using GraphPad Prism 6.0. Kaplan-Meier survival data were analyzed using the log-rank test. $p \leq 0.05$ was considered statistically significant. Correlation studies were analyzed with Pearson correlation.

CHAPTER 3: RESULTS

ALKBH5 Is Elevated in GSCs and Informs Poor Survival of GBM Patients

Our initial studies focused on the m^{6}A modifier that may result in poor clinical outcome in GBM patients. We queried the TCGA (133), R2 database (http://hgserver1.amc.nl/cgi-bin/r2/main.cgi), Freije, Phillips and the Repository for Molecular Brain Neoplastic Data (REMBRANDT) data sets. In all data sets, expression of ALKBH5 rather than the methyltransferases and the alternative demethylase FTO informed poor patient survival (Figures 1-2).

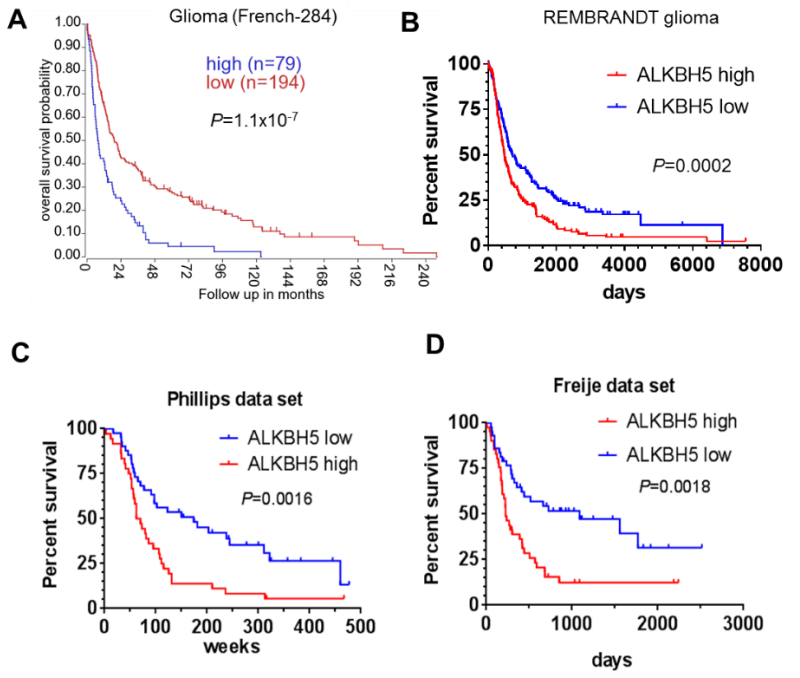

Figure 1. ALKBH5 informs poor glioma patients survival. (A) Analysis of correlation between *ALKBH5* mRNA expression (high versus low expression; Kaplan-Meyer scanner) and glioma patient overall survival of 284 glioma patients of different histopatological grade in the R2 database (http://hgserver1.amc.nl/cgi-bin/r2/main.cgi) with log rank analysis. (B-D) Analysis of correlation between *ALKBH5* mRNA expression (high versus low expression; median cut) and glioma patient overall survival in (B) REMBRANDT data set (329 glioma), (C) Phillips Brain (100 high grade gliomas) and (D) Freije Brain (85 high grade gliomas) Oncomine data set by Kaplan-Meier survival curve with log rank analysis.

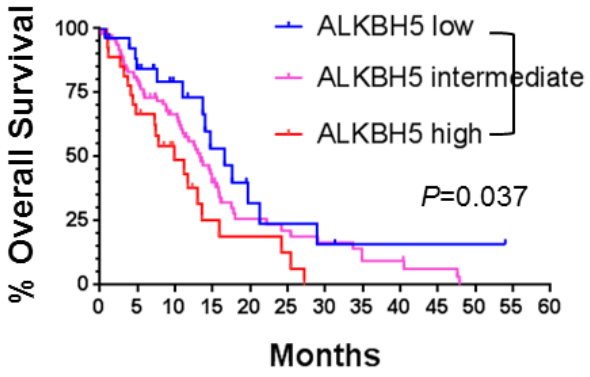

Figure 2. ALKBH5 informs poor patients survival in TCGA GBM. Analysis of correlation between *ALKBH5* mRNA expression and GBM patient survival in TCGA data set (http://www.cbioportal.org). Overall patient survival in groups of high, intermediate and low expression was analyzed by Kaplan-Meier survival curve. High expression (overall median survival=9.9 months) versus low expression (overall median survival=16.6 months) with log rank analysis (p=0.037).

We then examined ALKBH5 expression in established and primary glioma cell lines representing different stages of tumor progression. Although ALKBH5 was weakly or moderately expressed in NHA (immortalized normal human astrocytes), Hs683, SW1783 (WHO lower grade glioma), U87MG, LN229 (GBM, WHO grade IV), it was highly expressed in U251MG (GBM, WHO grade IV) and particularly patient-derived GBM primary cultures that enrich for cells with self-renewal and tumor propagation potential (GSCs) (Figure 3) (97, 134). The elevated ALKBH5 expression in the GSC cell lines led us to hypothesize that ALKBH5 may be associated with cancer stem cell (CSC) niches. Thus, we first examined the expression of ALKBH5 protein in 30 GBM patient samples using immunohistochemical analysis. We found extensive inter- and intra-tumoral heterogeneity of ALKBH5 expression in primary bulk GBM samples, with some tumor

niches being highly positive for nuclear ALKBH5 and others with low levels (Figure 4, images representative of three tumors). Then with use of immuneflorescent analysis, we found that indeed, co-localized expression of ALKBH5 with Sox2, a transcription factor indicative of CSC self-renewal and Nestin, an intermediate filament protein recognized as the marker of neural stem cells (NSC) was detected in bulk GBM samples (Figures 5-6). Gene-expression analysis further indicated a positive correlation between ALKBH5 and Sox2 or Nestin expression in The Cancer Genome Atlas (TCGA) GBM data set (Figures 5-6). ALKBH5 expression is not restricted to GSCs; however, high ALKBH5 expression in the subpopulation characterized by CSC niche suggests more important ALKBH5 dependence of the GSC within bulk tumor, which became the focus of our investigations.

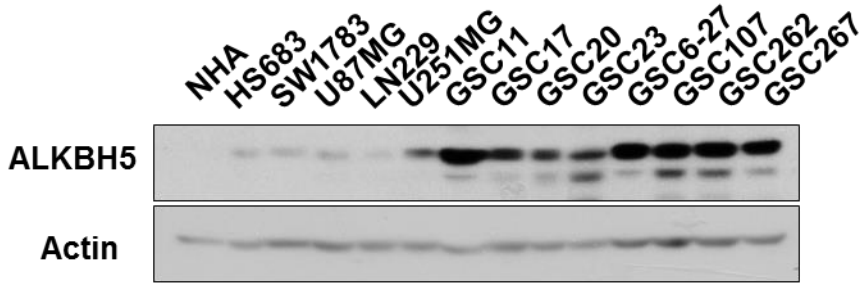

Figure 3. ALKBH5 expression in cell lines. Western blotting of ALKBH5 in NHA, glioma and GSC cells. Actin served as a loading control.

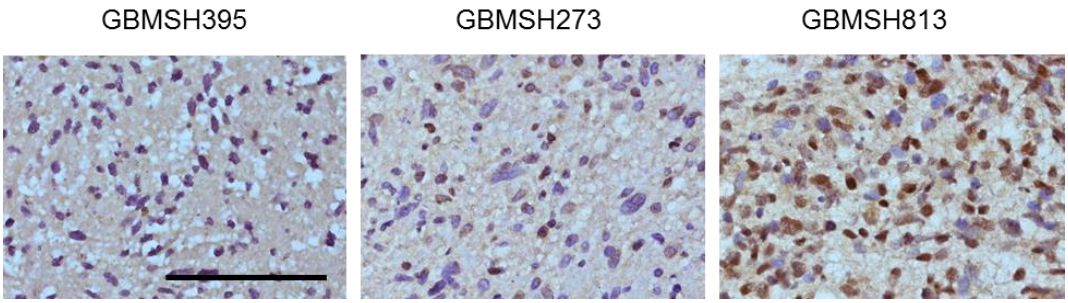

Figure 4. ALKBH5 expression in patient samples. Representative images of IHC analysis of ALKBH5 protein expression in human GBM specimens. Scale bar, 100 μm.

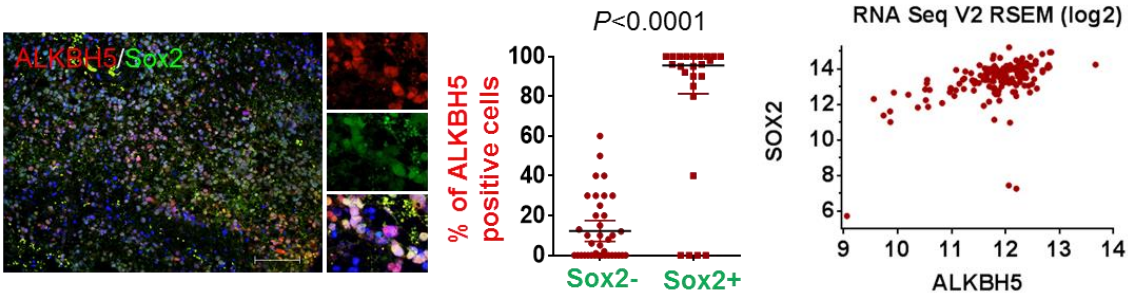

Figure 5. ALKBH5 correlates with SOX2 expression in patient samples. Correlation between ALKBH5 and Sox2 protein expression in GBM specimens. Tumor sections from 15 GBM specimens were immunofluorescence (IF)-stained with anti-ALKBH5 and anti-Sox2 antibodies. Left, representative images are shown. Scale bar, 100 μm. Middle, two different microscope fields of each tumor were quantified for positive expression of the proteins. Percentages of tumor cells expressing ALKBH5 in Sox2 positive versus negative cells are shown with t-test. Right, Analysis of correlation between ALKBH5 and Sox2 mRNA expression in the TCGA GBM data set with Pearson's test (r=0.511, P=1.3e-11).

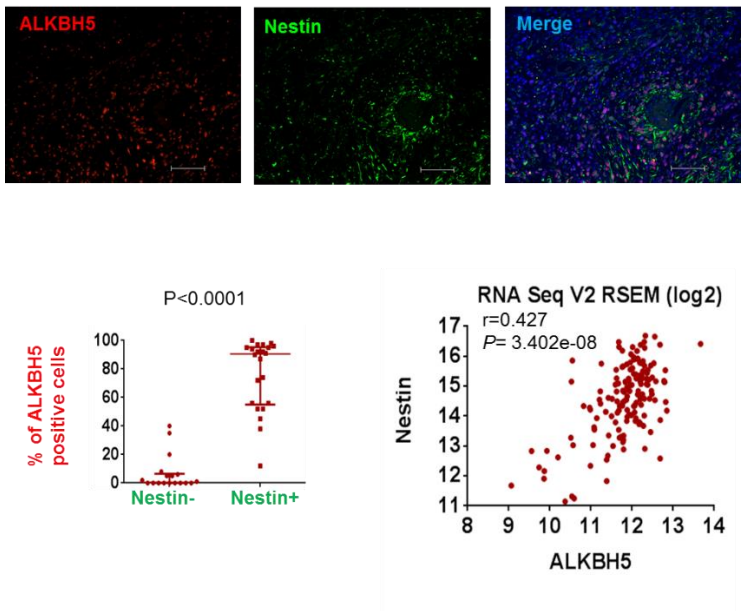

Figure 6. ALKBH5 correlates with Nestin expression in patient samples. Analysis of correlation between ALKBH5 and Nestin protein expression in 10 GBM specimens. Tumor sections from GBM specimens were IF-stained with anti-ALKBH5 and anti-Nestin antibodies. Representative images are shown in top panel. Scale bar, 100 μm. Two different microscope fields of each tumor were quantified for positive expression of the proteins. Percentages of tumor cells expressing ALKBH5 in Nestin positive or negative cells are shown in bottom left with t-test. Bottom right, correlation between ALKBH5 and Nestin mRNA expression in the TCGA GBM data set. Pearson's r and P-value are shown.

Targeting ALKBH5 Expression Impairs GSC Self-renewal

To determine if ALKBH5 is important to GSC self-renewal, we used two distinct short hairpin RNAs (shRNA1 and shRNA2) to ablate ALKBH5 expression (referred to hereafter as shALKBH5). Each shALKBH5 significantly reduced ALKBH5 protein expression compared to a non-targeting shRNA control that does not target any mammalian sequence (referred to as shCtrl). Expression of ALKBH5-directed shRNAs resulted in a decrease in the tumorsphere formation frequency of recurrent GBM-derived

GSC11, GSC17 and GSC23 by *in vitro* limiting dilution assays, a method widely used to determine self-renewal capacity (Figure 7). To confirm the impact of ALKBH5 on GSC self-renewal, tumorspheres were dissociated for immunofluorescence analysis or Western blotting. Depleting ALKBH5 reduced expression of Nestin and Sox2, Nanog, Oct4, the core transcription factors that endow tumor cells with self-renewal ability (Figures 8-9).

GSCs are characterized by multipotency (84). Addition of serum deprives the self-renewal ability of GSCs and induces astrocytic or neuronal commitment featured by GFAP and Tuj-1 expression (99). Depleting ALKBH5 increased GFAP or Tuj-1 positive population when cultured with serum for a short term (3 days) (Figures 8). Taken together, these data suggest that targeting ALKBH5 in the GSCs tips the balance toward a more differentiated state.

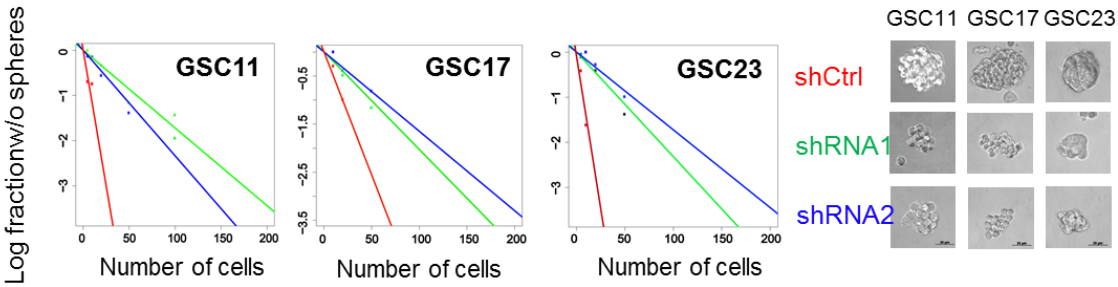

Stem Cell Frequency	GSC11			GSC17			GSC23		
	shCtrl	shRNA1	shRNA2	shCtrl	shRNA1	shRNA2	shCtrl	shRNA1	shRNA2
Lower	11.7	79.5	58.5	29.1	74.7	91.6	10.9	64.3	86.7
Estimate	8.33	58.12	42.79	19.6	49.3	60.5	7.34	43.16	57.98
Upper	5.94	42.5	31.29	13.2	32.6	40	4.96	28.98	38.78

Figure 7. *In vitro* limiting dilution assays of GSCs with or without ALKBH5 knockdown. Steeper slopes (top left panel) indicate higher frequencies of colony-forming cells. Stem cell frequencies calculated by ELDA are shown in bottom panel. Representative tumorsphere formation in dose of 100 cells/well were shown in top right panel. Scale bar, 20 μm.

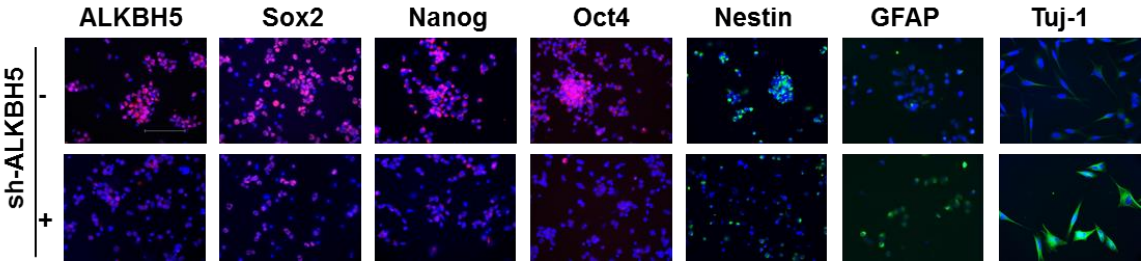

Figure 8. GSC marker expression following knockdown of ALKBH5. Representative images of IF staining of ALKBH5, self-renewal and lineage differentiation markers in GSC11 with or without ALKBH5 knockdown. Scale bar, 100 μm.

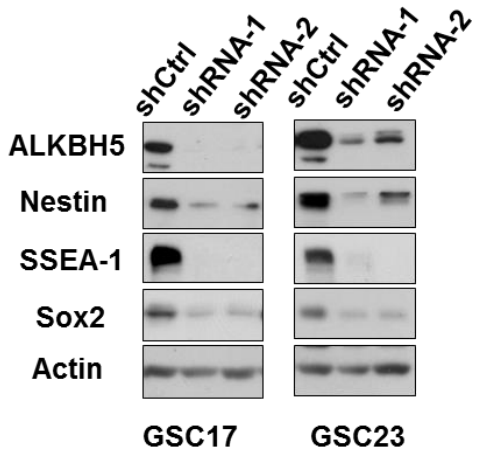

Figure 9. GSC marker expression following knockdown of ALKBH5. Western blotting of indicated proteins in GSC17 and GSC23 transduced with shRNAs for control or ALKBH5.

ALKBH5 Inhibition Decreases GSC Proliferation

Because cell proliferation is ultimately required, although not sufficient, for the self-renewal of GSCs, we examined the effects of ALKBH5 knockdown on GSC proliferation. Loss of ALKBH5 resulted in compromised GSC cell growth (Figure 10), and decrease in DNA replication determined by BrdU (5-bromo-2'-deoxyuridine) incorporation assay (Figure 11). However, depletion of ALKBH5 had no effect on the cell growth of SW1783 non-CSC glioma cells (Figure 12). Moreover, cell cycle analysis showed knockdown of ALKBH5 in GSC cells increased the proportions of cells in G0/G1 phase and decreased the S and G2/M proportions of ALKBH5-depleted GSCs (Figure 13). Collectively, these results suggest that ALKBH5 critically regulates cell proliferation in GSCs.

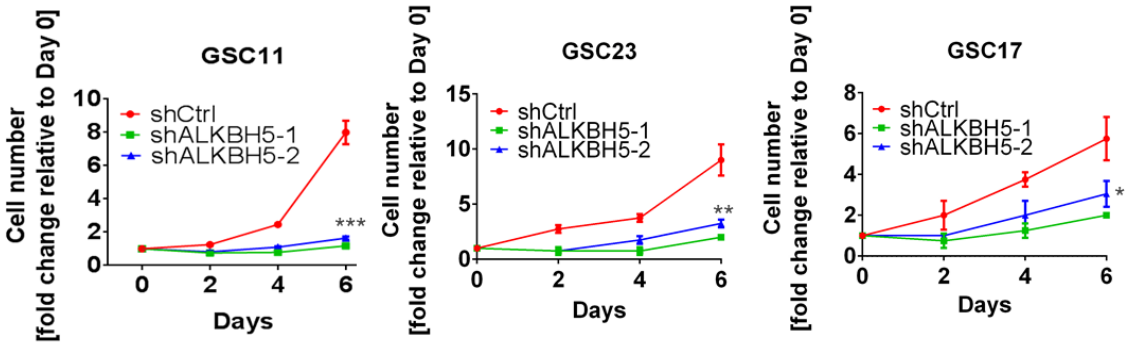

Figure 10. Proliferation of GSCs with or without ALKBH5 knockdown determined by cell counting. Error bars: ±SEM of triplicates. *p<0.05, **p<0.01, ***p<0.001.

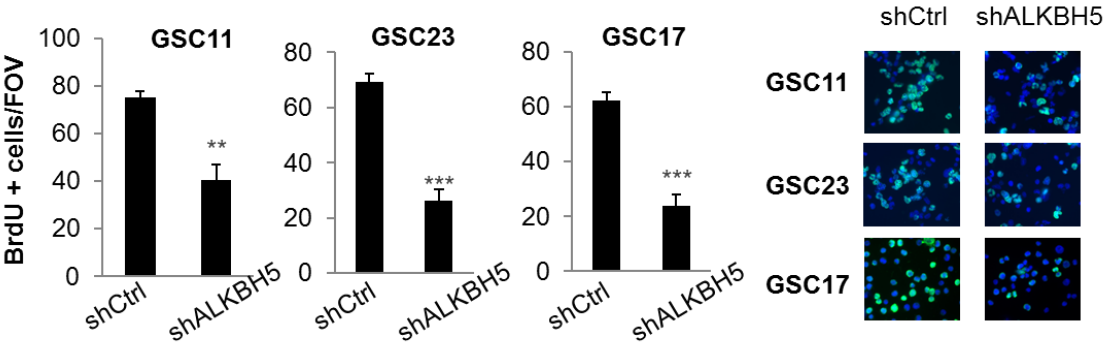

Figure 11. Proliferation of GSCs with or without ALKBH5 knockdown. Analysis of GSC proliferation by 5-Bromo-2'-deoxyuridine (BrdU) incorporation assay. The number of BrdU-positive-stained cells in GSCs with or without ALKBH5 knockdown per field of view (FOV) are means ± SEM, n=5.

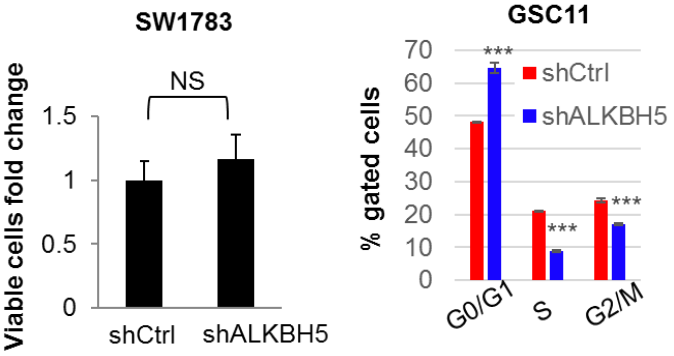

Figure 12. Proliferation of SW1783 with or without ALKBH5 knockdown calculated three days after seeding cells. Error bars: ±SEM of triplicates. Cell-cycle analysis of GSC 11 with or without ALKBH5 knockdown. Error bars: ±SEM of triplicates. ***p<0.001.

Figure 13. Cell-cycle analysis of GSC 11 with or without ALKBH5 knockdown. Error bars: ±SEM of triplicates. ***p<0.001.

Knocking down ALKBH5 could increase global m^6A level and subsequently affect mRNA export, RNA metabolism and RNA splicing (12). We asked whether higher ALKBH5 levels would give rise to reduced m^6A levels in GSCs which might contribute to GSC proliferation. To test this, we used the anti-m^6A antibody to probe m^6A modification in the mRNA of HEK293T, NHA and six glioma cell lines. Although cellular m^6A levels increased following ALKBH5 knockdown (Figure 14), global detection of m^6A mRNA levels in the cell lines showed no significant correlation with ALKBH5 expression or GSC phenotype (Figure 15), which suggests the global m^6A level can neither explain the ALKBH5 function in GSCs nor define the GSC characteristic. In light of this, we hypothesized the existence of subset of genes that require ALKBH5 activity for sustained up- or down- regulation to promote GSC survival. To this end, the transcriptional profile analysis was employed to gain mechanistic insight into ALKBH5 function. First, microarray analysis was used to compare the gene expression profile following ALKBH5 knockdown by shALKBH5-1 and shALKBH5-2 in GSC11 and GSC17. 206 genes that were increased or decreased by at least 2-fold in both cell lines were selected for ingenuity pathway analysis (IPA) (Figure 16, Table 1). Notably, the largest subset of genes were enriched for genes involved with “Cell Cycle” (69 of 206 [33.5%]), “DNA Replication, Recombination, and Repair” (60 of 206 [29.1%]) and “Cellular Assembly and Organization” (62 of 206 [30.1%]). Next, ingenuity upstream regulator analysis was used to predict key regulatory molecules that most likely account for the observed changes of the gene expression profiles. Among the genes predicted to be activated or inhibited following ALKBH5 knockdown, the transcription factor FOXM1 has a high predicted activation Z-score (Figure 17). Moreover, among the predicted genes with high scores, only FOXM1 gene showed altered expression in our microarray data set, suggesting downregulation of FOXM1 might explain the loss of GSC proliferation

signature (Figure 2E, Table 2). Previous reports indicate that FOXM1 is a pivotal transcription factor in cell cycle and plays critical roles in self-renewal and tumorigenesis of GSCs (97, 99, 104, 119, 120). Searching the literature revealed a more extensive FOXM1 regulatory network in cancer cells than IPA predefined interaction (135). These FOXM1 transcription targets were all decreased following ALKBH5 knockdown in our microarray data set (Figure 18). Thus, FOXM1, an essential transcription factor to the stem-like proliferation of GBM, may be a direct and important downstream target of ALKBH5.

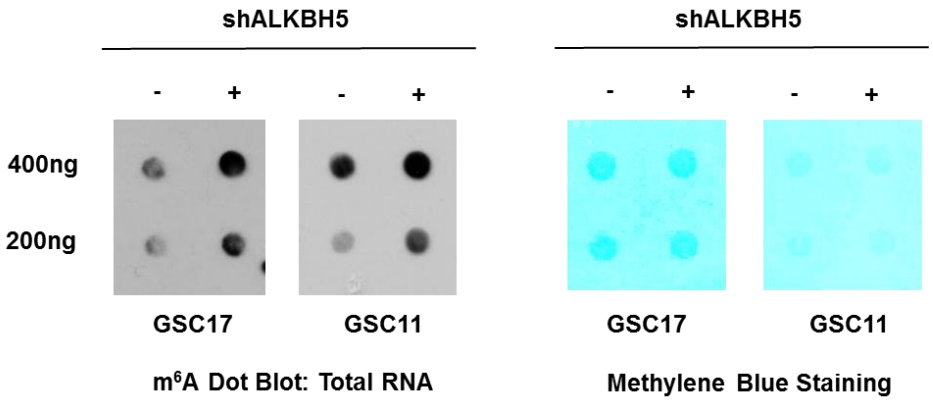

Figure 14. m^{6}A dot-blot of GSCs with or without ALKBH5 knockdown. Anti-m^{6}A dot-blot showing the amount of m^{6}A in total RNA from GSCs transduced with shRNAs for control or ALKBH5. Methylene blue staining showing equal mRNA loading in the samples shown in the left panel.

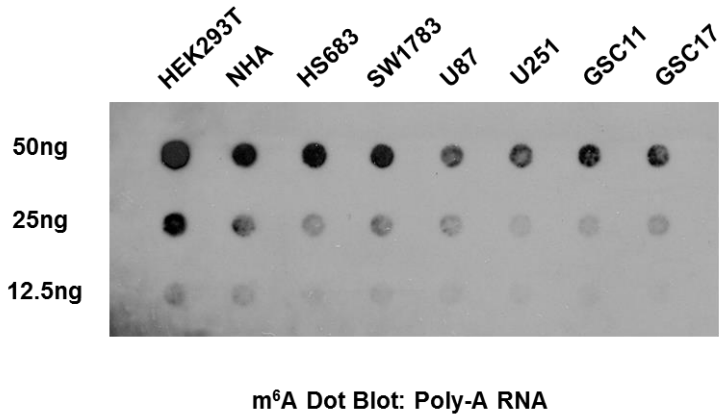

Figure 15. m^{6}A dot-blot of cell line mRNA. Anti-m^{6}A dot-blot showing the amount of m^{6}A in poly(A)-selected RNA from 8 cell lines.

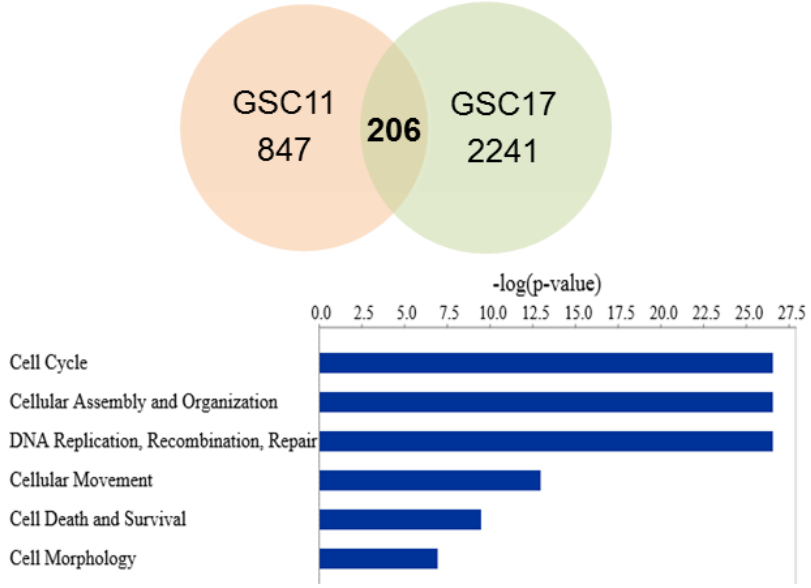

Figure 16. Microarray analysis in GSCs with or without ALKBH5 knockdown. Affymetrix HuGene 2.0 ST microarray analysis performed seven days after GSC11 and GSC17 transduced with shRNAs for control or ALKBH5. Enriched gene ontology processes of 206 genes changed > 2-fold were analyzed by IPA.

Upstream Regulator	Fold Change	Predicted State	Activation z-score	p-value
VEGF		Inhibited	-4.630	8.63E-13
RABL6		Inhibited	-4.123	1.37E-21
CCND1		Inhibited	-2.828	1.69E-23
EP400		Inhibited	-2.621	3.23E-08
CD24		Inhibited	-2.449	1.94E-04
PTGER2		Inhibited	-4.796	9.73E-28
MED1		Inhibited	-2.390	1.01E-03
CSF2		Inhibited	-5.098	2.35E-16
NKX2-3		Inhibited	-2.000	8.49E-02
FOXM1	-3.020	Inhibited	-3.065	1.41E-11
FOXO1		Inhibited	-3.138	6.57E-06
S100A6		Inhibited	-2.646	2.23E-09
MITF		Inhibited	-3.357	4.98E-10
YAP1		Inhibited	-2.000	1.27E-05
HGF		Inhibited	-4.640	1.98E-12
RARA		Inhibited	-3.464	1.21E-06
TBX2		Inhibited	-3.162	5.37E-10
ESR1		Inhibited	-4.955	3.07E-08
MYC		Inhibited	-2.923	2.57E-04

Figure 17. Ingenuity upstream analysis of pathways downregulated by ALKBH5 shRNA-derived gene expression data.

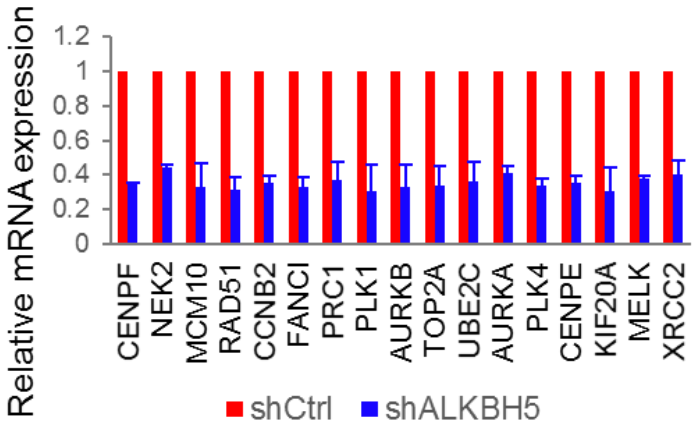

Figure 18. Gene expression of FOXM1 downstream targets in microarray data. The expression levels are the mean +SEM of expression levels in both GSC11 and GSC17 cells.

ALKBH5 Regulates FOXM1 Expression in GSCs

Because *FOXM1* mRNA could be a direct substrate for ALKBH5 due to multiple m^6A sites on FOXM1 RNA (9, 136, 137) and the above transcriptional profile analysis emphasized FOXM1 could be a driver for this altered proliferative gene profile, we were next interested in understanding the mechanism of ALKBH5 regulating *FOXM1* expression. We first measured total mRNA expression and different isoform levels of *FOXM1* by quantitative PCR (qPCR). Consistent with the gene expression data, both GSC cell lines expressing shALKBH5 displayed decreased expression of different *FOXM1* isoform by ~70-80% (Figure 19). We also measured the amount of FOXM1 protein following ALKBH5 knockdown by siRNA treatment or shRNA lentiviral transduction. Both transient and stable knockdown resulted in reduced FOXM1 protein abundance, whereas Sox2 expression was almost unaffected by siRNA treatment, suggesting loss of Sox2 expression in GSCs could be a chronic effect (Figure 20).

Next, we examined the correlation between ALKBH5 and FOXM1 in GBM patient samples. Immunofluorescence analysis revealed a spatial correlation of ALKBH5 and FOXM1 in primary bulk GBM samples (Figure 21). We further queried the TCGA data set, unraveling a positive correlation with high significance (Pearson's r=0.4723914, p= $6.197x10^{10}$) between ALKBH5 and FOXM1 expression (Figure 22). These results indicated FOXM1 as a direct downstream target of ALKBH5 in GBMs.

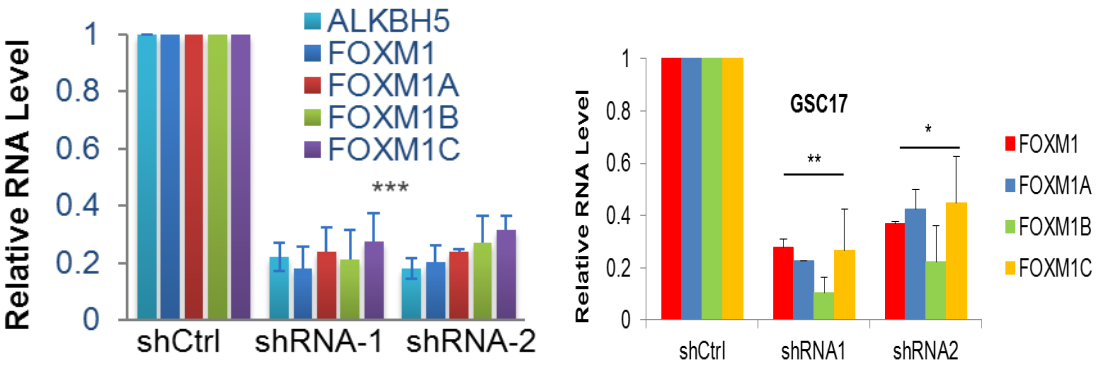

Figure 19. qPCR analysis for FOXM1 mRNA expression in GSC11 (left) and GSC17 (right) with or without ALKBH5 knockdown. Samples were normalized to GAPDH mRNA.

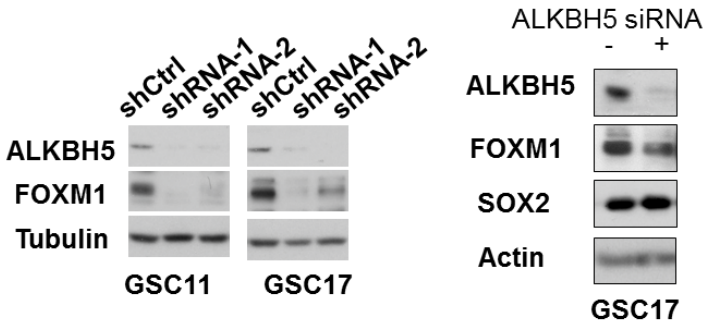

Figure 20. Western blotting of FOXM1 in GSCs with or without ALKBH5 knockdown. left panel, Western blotting of FOXM1 in GSCs transduced with shRNAs for control or ALKBH5. Right panel, Western blotting of FOXM1 in GSC17 treated with siRNAs for control or ALKBH5.

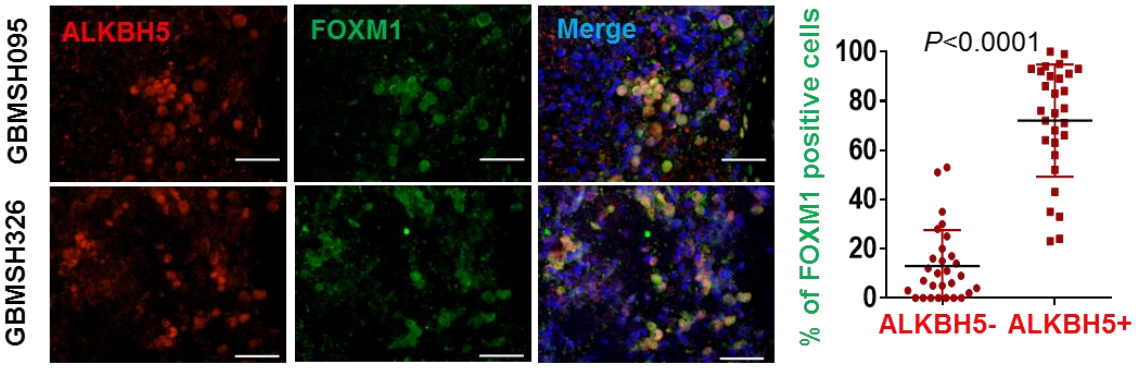

Figure 21. Correlation between ALKBH5 and FOXM1 protein expression in GBM specimens. Left, tumor sections from 15 GBM specimens were immunofluorescence (IF)-stained with anti-ALKBH5 and anti-FOXM1 antibodies. Representative fluorescence images are shown. Scale bar, 100 μm. Right, two different microscope fields of each tumor were quantified for positive expression of the proteins. Percentages of tumor cells expressing FOXM1 in ALKBH5positive versus negative cells are shown with t-test.

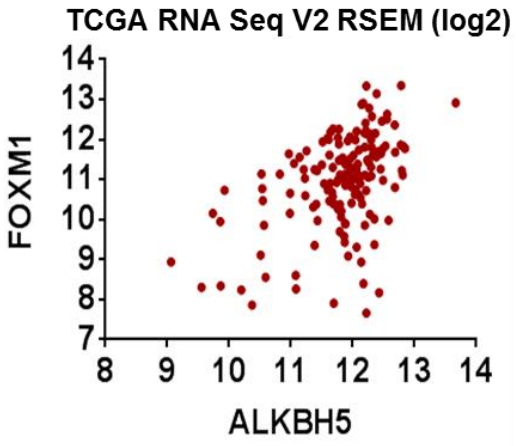

Figure 22. Correlation between FOXM1 and ALKBH5 mRNA expression in the TCGA GBM data set. Pearson's r and P-value are shown.

The reduced FOXM1 expression in ALKBH5 knockdown cells cannot be explained by RNA splicing, as knockdown of ALKBH5 in GSCs decreased the expression of all of FOXM1 major isoform. It was reported that methylation inhibition delayed RNA processing (123) and knockdown of ALKBH5 increased mRNA export and RNA metabolism (12). We therefore assessed the mRNA stability and subcellular localization of *FOXM1* mRNA. Surprisingly, measuring the loss of FOXM1 mRNA after blocking new RNA synthesis with Actinomycin D revealed similar *FOXM1* mRNA stability (Figure 23). On the other hand, knocking down ALKBH5 appeared not to affect *FOXM1* RNA nuclear retention or export (Figure 24), probably due to the abundant pre-existing cytoplasmic *FOXM1* mRNA overwhelming the small amount of increased export portion, which could not be distinguished by our experiments. Nonetheless, these observations raise the possibility that ALKBH5 deficiency resulted in *FOXM1* precursor mRNA decrease that would be detectable as changes in mature RNA or protein expression. Indeed, we found that *FOXM1* pre-mRNA expression was decreased by 40% following ALKBH5 siRNA treatment and further decreased in GSCs stably expressing shALKBH5 whereas *FOXM1* promoter activity was unaffected (Figures 25-26).

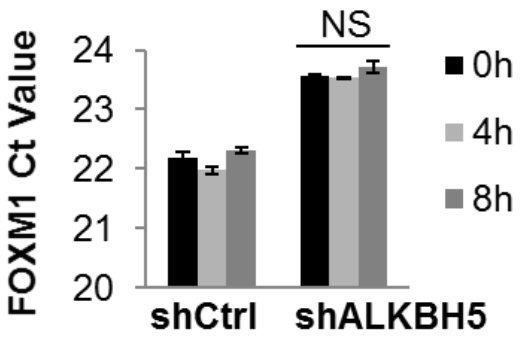

Figure 23. qPCR for FOXM1 mRNA stability in GSC17 with or without ALKBH5 knockdown. Same amount RNAs from cells treated with 5ug/ml actinomycin D for 4 and 8 hours were collected and measured by real-time PCR. Ct values were generated at default settings. Note that GSC17 transduced with shALKBH5 had less FOXM1 expression and higher Ct value compared with control at initial time points. Results from one representative experiments are shown. Error bars: ±SD of technical triplicates.

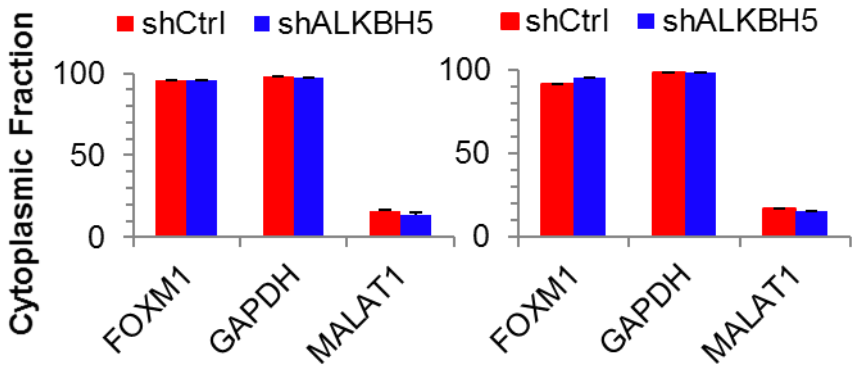

Figure 24. qPCR analysis for FOXM1, GAPDH mRNA and MALAT1 RNA distribution in subcellular fractions from GSC11 (left) and GSC17 (right). Note that GAPDH mRNA is predominantly located in cytoplasm and MALAT1 RNA is predominantly located in nucleus. Results from one representative experiments are shown. Error bars: ±SD of triplicates.

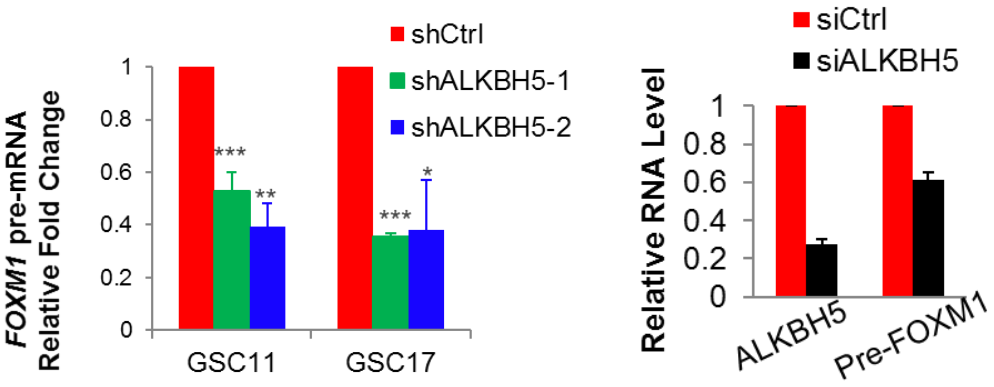

Figure 25. qPCR analysis for FOXM1 pre-mRNA in GSCs with or without ALKBH5 knockdown by shRNAs (left) or siRNAs (right). Error bars: ±SEM of triplicates.

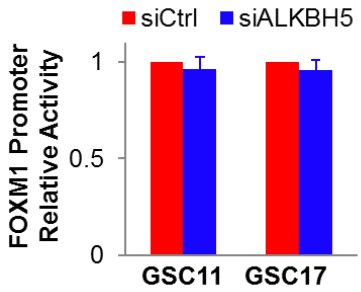

Figure 26. Analysis for activities of FOXM1 promoter firefly luciferase reporter in GSC17 cells treated with siRNAs for control or ALKBH5. A Renilla luciferase reporter driven by Actin promoter was used as a transfection efficiency control. The ratios between FOXM1 promoter reporter and Renilla control were determined 48 hr after siRNA treatment. Results from one representative experiments are shown. Error bars: ±SD of triplicates.

It was earlier proposed that ALKBH5 colocalizes with nuclear speckles and promotes proper assembly/modification of certain mRNA processing factors (12). Nuclear speckles are the sites where post-transcriptional splicing occurs and the storage/assembly/modification compartments that supply splicing factors to active transcription sites (138, 139). It is unknown, however, whether ALKBH5 can act on precursor mRNA. To address this, we separated nuclei from the cytoplasmic fraction of GSC11 and fractionated nuclei into a soluble nucleoplasmic fraction containing nuclear speckles and an insoluble fraction containing nascent RNAs and chromatin-associated components, such as active RNA Pol II (132, 138, 140). Western blotting for compartment-specific proteins α-tubulin, U1-70K, and histone H3 confirmed subfractionation of the organelle. We found that ALKBH5 is present in both nucleoplasmic and insoluble fractions. However, unlike the nuclear RNA binding protein HuR, the majority of ALKBH5 is enriched in the insoluble fraction in a transcription-dependent manner because the nuclear abundance was sharply decreased after Actinomycin D treatment determined by Western blotting (Figure 27). We also found *FOXM1* pre-mRNA is restricted to the insoluble chromatin-associated fractions (Figure 28), which can be explained by the widespread co-transcriptional splicing model in the human brain (141). Moreover, the native RNA immunoprecipitation (RIP) retrieved *FOXM1* pre-mRNA in ALKBH5-FLAG pull-down fraction, implicating the interaction *in vivo* (Figure 29). The observable association between mature *FOXM1* mRNA and ALKBH5 might occur during RNA export at ALKBH5-containing nuclear speckles or the co-transcriptional maturation of nascent transcripts. Altogether, our data indicate that ALKBH5 activity is tightly coupled with transcription. In agreement with this, it interacts with *FOXM1* nascent transcripts, which could be the substrate for ALKBH5.

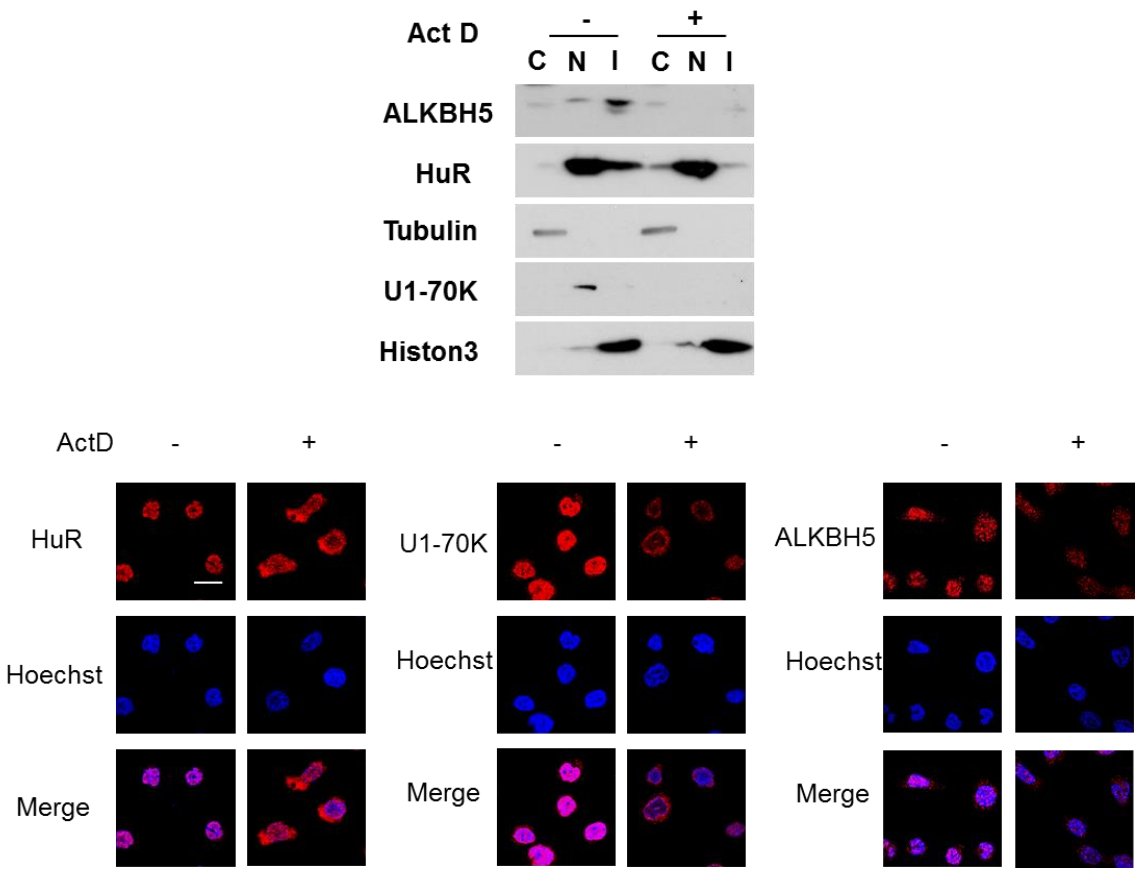

Figure 27. ALKBH5 distribution in subcellular fractions. GSC11 treated with or without 5μg/ml actinomycin D for 2 hours were fractionated into cytoplasmic (C), nucleoplasmic (N) and insoluble (I) fractions as described in the Methods. Western blotting (top panel) was performed with antibodies against ALKBH5, α-tubulin, U1-70K, HuR and histone 3. Representative IF images (bottom panel) of GSC17 treated with or without 5ug/ml actinomycin D for 2 hours and stained with antibodies against ALKBH5, U1-70K or HuR. Images taken by confocal microscope. Scale bar, 100 μm.

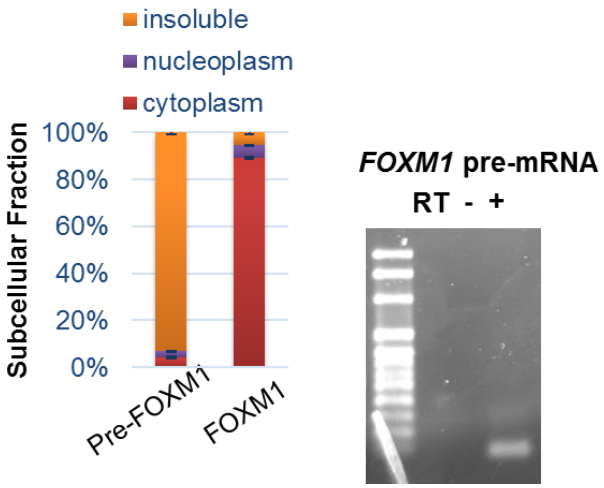

Figure 28. FOXM1 transcripts distribution in subcellular fractions was measured by qPCR. Agarose gel pictures showing PCR analysis of FOXM1 pre-mRNA in cDNA synthesized with or without reverse transcriptase and indicating no genomic DNA contamination in Figure 3H. *p<0.05, **p<0.01, ***p<0.001.

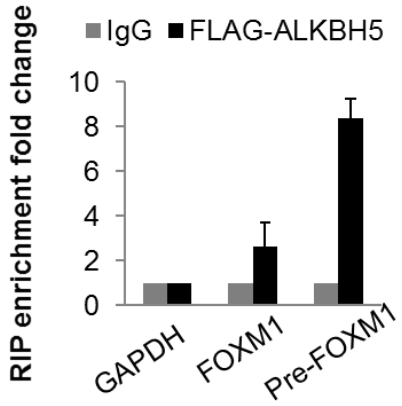

Figure 29. RIP analysis of transcripts from nuclear extracts of GSC17 cells expressing FLAG-ALKBH5. Interaction with FLAG-ALKBH5 was quantified by qPCR and normalized to GAPDH mRNA. Data in bar plots are represented as mean +SEM of three independent biological replicates.

FOXM1 3'UTR Mediates ALKBH5 Regulation

To ascertain FOXM1 as a substrate for RNA demethylase ALKBH5, we determined the *FOXM1* m^{6}A methylation levels following ALKBH5 knockdown by MeRIP-qPCR. Our analysis confirmed that the m^{6}A methylation is readily detectable on *FOXM1* pre-mRNA. Moreover, ALKBH5 knockdown resulted in an increase of m^{6}A levels *FOXM1* pre-mRNA in comparison with the control (Figure 30).

With the advent of the RNA cross-linking and immunoprecipitation (CLIP)-based techniques, tens of thousands of m^{6}A residues have been mapped in human transcriptome at single-nucleotide resolution (136, 137, 142). These studies together with initial effort to identify m^{6}A sites revealed the static topology of m^{6}A sites across different cellular systems (9), including many m^{6}A positions enriched in the last exons and 3'UTR. With access to m^{6}A database (143), we searched CLIP-identified m^{6}A sites at *FOXM1* transcripts, as well as the putative m^{6}A sites predicted by consensus sequence "DRACH" (where D denotes A, G or U, R denotes A or G and H denotes A, C or U) based on the m^{6}A-containing RNA fragments generated from published studies using MeRIP-seq (or m^{6}A-Seq, m^6 A-specific methylated RNA immunoprecipitation and sequencing). We found 16 m^{6}A sites distributed across the RNA body before last exon, 22 m^{6}A sites located at the last exon, including 7 sites at 3'UTR and 6 sites near stop codon within 150 nucleotides. No m^{6}A sites were found at 5'UTR. Next, to determine the potential m^{6}A sites affected by ALKBH5, we divided *FOXM1* into coding sequence and 3'UTR. Then we generated FLAG-tagged expression constructs containing the entire FOXM1 including coding sequence with 3'UTR (CDS-3'UTR) or the coding region alone (CDS). Upon ALKBH5 knockdown in the GSCs transfected with either of the above two constructs, FLAG-FOXM1 expression significantly decreased in the CDS-3'UTR transfected group but not in the CDS group (Figure 31), suggesting the critical

involvement of 3'UTR in ALKBH5-FOXM1 regulation and implying that the reversible m^{6}A incorporation could be splicing-independent and typical chromatin structure might be dispensable. This effect of *FOXM1* 3'UTR could be explained by two distinct models: a tandem cis-regulation model in which the 3'UTR functions as a sensor whereas *FOXM1* CDS m^{6}A sites are the effector; or alternatively, 3'UTR is sufficient to initiate the regulation regardless the m^{6}A status in coding sequence. To test these possibilities, *FOXM1* 3'UTR was fused downstream to the firefly luciferase. By using dual luciferase assays, we found ALKBH5 knockdown decreased activity of the luciferase construct containing *FOXM1* 3'UTR, thereby providing strong evidence supporting the second model (Figure 32).

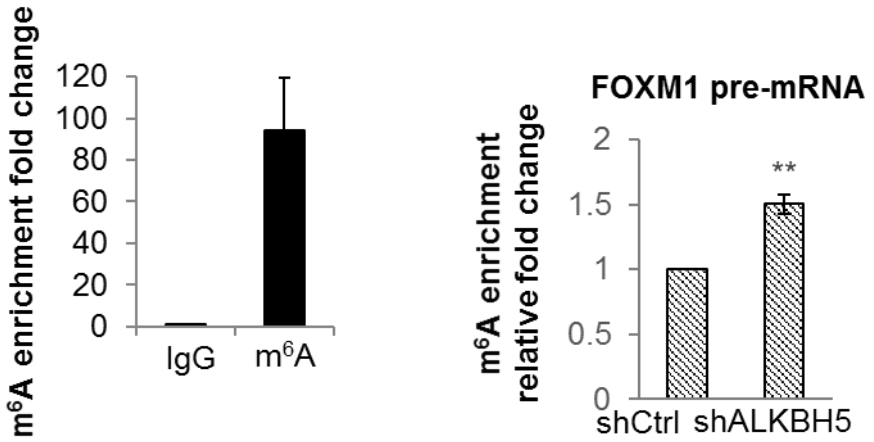

Figure 30. m^{6}A methylation of FOXM1 pre-mRNA in GSC17 cells determined by MeRIP-qPCR assay (left). Analysis of m^{6}A methylation levels of FOXM1 pre-mRNA in GSC11 cells with or without ALKBH5 knockdown by MeRIP-qPCR assay (right). Poly-A selected RNA bound to m6A antibodies was measured by real-time PCR and normalized to input. Data are represented as mean +SEM of three independent biological replicates.

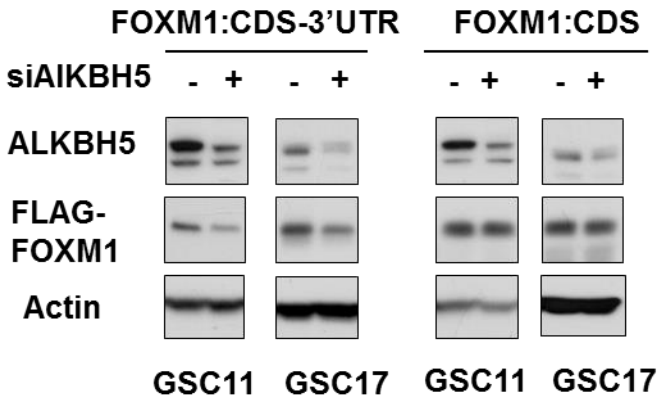

Figure 31. Western blotting of FLAG-FOXM1 in GSCs expressing FLAG-FOXM1 with 3'UTR (FOXM1 CDS-3'UTR) or without 3'UTR (FOXM1 CDS) and treated with siRNAs for control or ALKBH5.

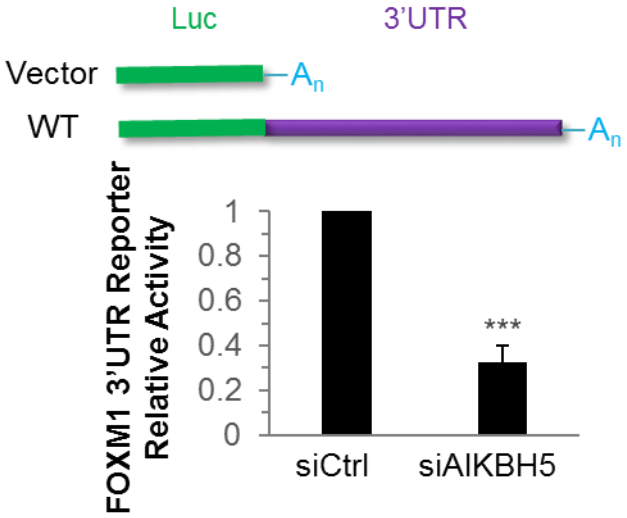

Figure 32. Analysis for activities of FOXM1 3'UTR firefly luciferase reporter in GSC17 cells treated with siRNAs for control or ALKBH5. A Renilla luciferase reporter driven by Actin promoter was used as a transfection efficiency control. The ratios between FOXM1 3'UTR reporter and Renilla control were determined 48 hr after siRNA treatment, and relative luciferase activity (fold) was normalized to that in cells transfected with the firefly luciferase vector control. Data in bar plots are represented as mean +SEM of three independent biological replicates.

ALKBH5 Promotes HuR Association with FOXM1 mRNA

The biological consequence of m^6A is achieved by RNA-binding proteins, such as the m^6A specific RNA-binding proteins ('readers') (10, 19, 20, 22, 142). The m^6A specific 'readers' include several YTH family proteins located in cytoplasmic (YTHDF1, YTHDF2) and nuclear (YTHDC1) compartments. YTHDF1 and YTHDF2 affect RNA translation and stability respectively (19, 21). YTHDC1 is reported to affect RNA splicing (22). YTHDF3 is another reader present in both cytoplasm and nucleus with unknown function (Figure 33). We were interested in the impact of the nuclear RNA-binding proteins on ALKBH5-FOXM1 regulation. However, we found that *FOXM1* expression remained unaffected by YTHDF3 knockdown (Figure 34).

In addition to m^6A readers, the nuclear RNA-binding protein HuR (ELAVL1) reportedly regulating both pre-mRNA splicing and expression (144, 145) has also been shown with positive or negative "indirect" (through other proteins or RNA structure changes) interaction with m^6A (14, 142). The consequences of HuR binding are complex: RNA to be stabilized or decayed depends on the RNA secondary structure and cofactor, such as AUF1 (146). To directly test the possible role of HuR, we first tested whether HuR could interact with *FOXM1* transcripts. The RIP-qPCR results revealed that in addition to the existence of interaction between HuR and *FOXM1* transcripts, the interaction was decreased following ALKBH5 knockdown (Figure 35). Accordingly, transient HuR knockdown suppressed expression of *FOXM1* (Figures 36), and reduced *FOXM1* 3'UTR luciferase activity (Figure 37).

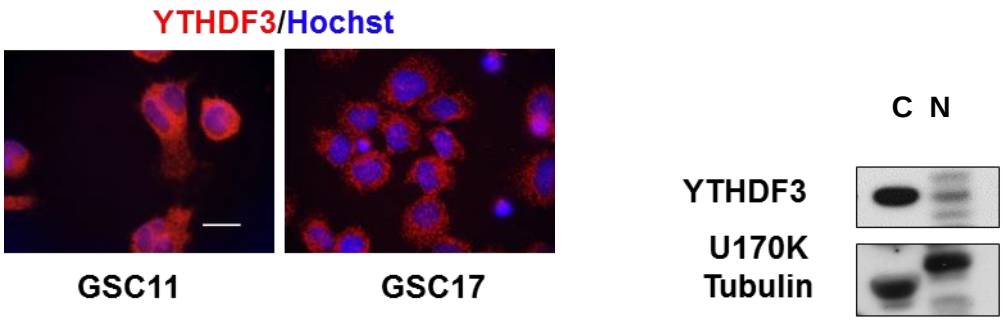

Figure 33. YTHDF3 localization. Representative IF images of GSC17 stained with antibodies against YTHDF3 (left). Scale bar, 100 μm. Western blotting of YTHDF3, α-tubulin, and U1-70K in cytoplasmic (C) and nuclear (N) fractions of GSC17 (Right).

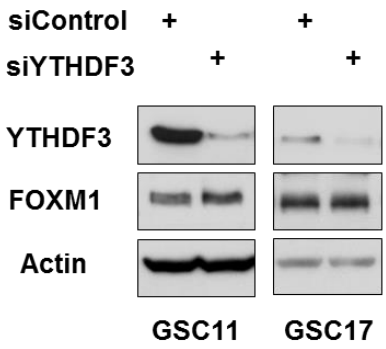

Figure 34. Western blotting of FOXM1 in GSCs treated with siRNAs for control or YTHDF3.

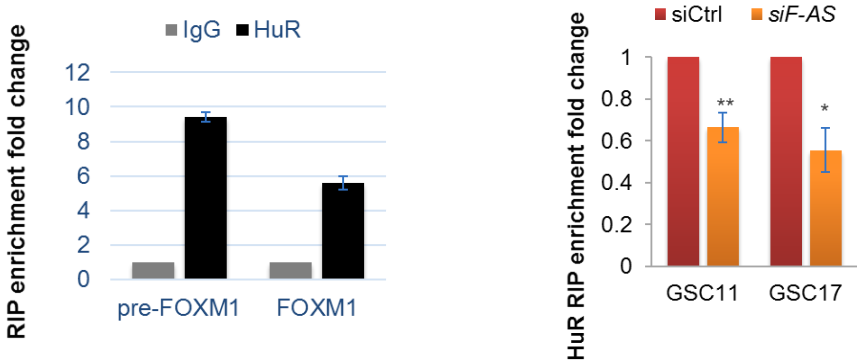

Figure 35. RIP analysis of the interaction of HuR with FOXM1 transcripts using total cell lysates of GSC17 (Left). RNA associated with HuR was measured by qPCR and normalized by GAPDH mRNA levels. Right, RIP analysis of the interaction of HuR with FOXM1 pre-mRNA using total cell lysates of GSCs with or without ALKBH5 knockdown. RNA associated with HuR was measured by qPCR. All data in bar plots are represented as mean + SEM of three independent experiments.

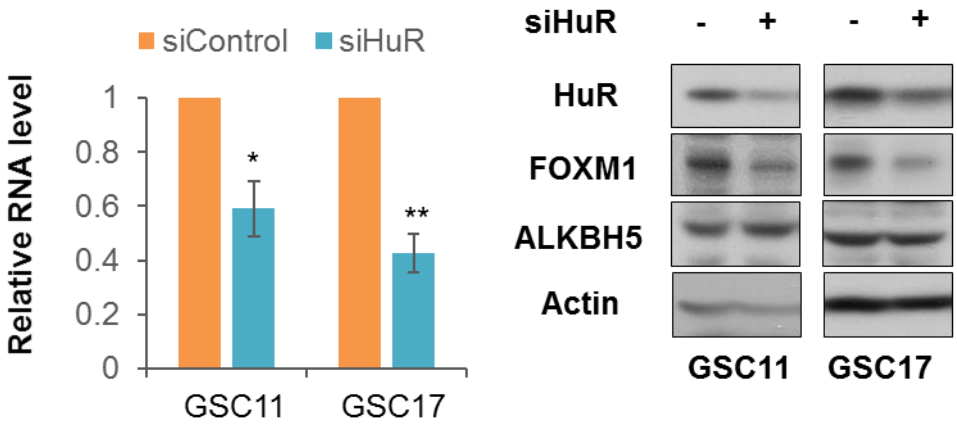

Figure 36. FOXM1 expression in GSCs treated with siRNAs for control or HuR. Left, qPCR analysis for FOXM1 RNA expression in GSCs treated with siRNAs for control or HuR. Right, Western blotting of FOXM1 in GSCs treated with siRNAs for control or HuR. All data in bar plots are represented as mean + SEM of three independent experiments.

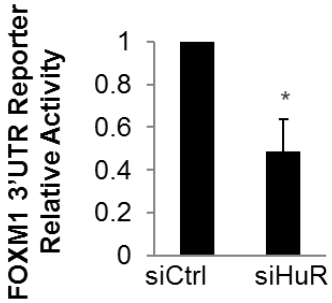

Figure 37. Analysis for activities of FOXM1 3'UTR firefly luciferase reporter in GSC17 cells treated with siRNAs for control or HuR. Data in bar plots are represented as mean + SEM of three independent experiments.

FOXM1-AS Is a Nuclear lncRNA That Facilitates the Interaction between ALKBH5 and *FOXM1* Nascent Transcripts

In spite of the similar m^{6}A distribution in different human cell lines (15, 31), recent studies showed that the levels of m^{6}A on specific genes are dynamic at different developmental states or in response to cellular physiology, probably with the help of regulating proteins or microRNAs (26, 31, 33, 147, 148). It is unclear whether removing the m^{6}A also involves gene- or cell- specific mechanisms. We explored the local elements that possibly contribute to the preferential regulation of *FOXM1* 3'UTR by ALKBH5. Intriguingly, we found a long non-coding RNA (lncRNA) *LOC100507424* located on chromosome 12 (chr12: 2945982-2968961, GRCh37/hg19) which is transcribed in the opposite direction to *FOXM1*, with 457 nucleotides complementary to the last exon of *FOXM1* mRNA (Figure 38). Antisense long non-coding RNA can act locally in nucleus or distally in cytoplasm to affect sense gene expression during normal tissue development or disease processes (149). We subsequently focused our attention on the *LOC100507424* (referred to hereafter as *FOXM1-AS*) for several reasons. First, *FOXM1-AS* may regulate *FOXM1* expression in *cis* based on sequence complementarity. Second, most glioma cells with higher levels of *FOXM1-AS* also express FOXM1 at higher levels determined by qPCR using the primers for the *FOXM1-AS* non-overlapping region, suggesting a concordant pattern of regulation (Figure 39). Third, the insoluble fraction enriching *FOXM1-AS* prompts us to investigate if it interacts with ALKBH5 and *FOXM1* RNA and is involved the ALKBH5-FOXM1 regulation (Figure 40).

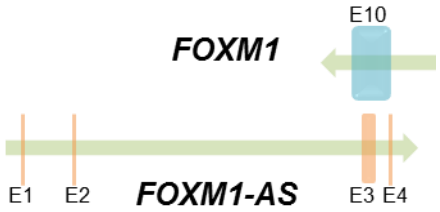

Figure 38. Physical map of FOXM1 and FOXM1-AS transcription units. Arrows show the opposite direction of transcription. Exons are marked and depicted as vertical bars.

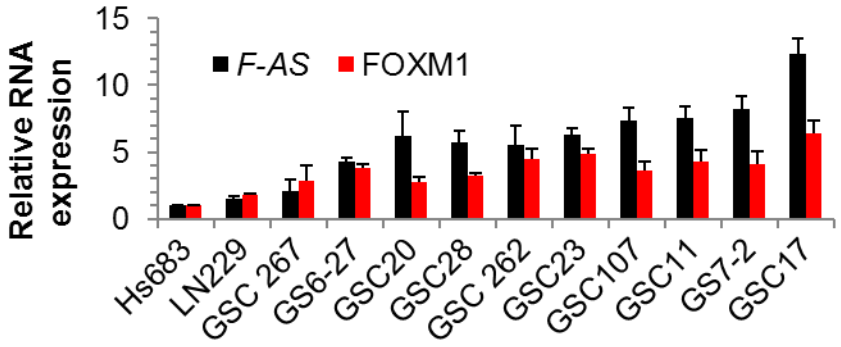

Figure 39. qPCR analysis for FOXM1 and FOXM1-AS (F-AS) RNA relative expression in glioma cells and GSCs. Error bars: + SEM, n=2.

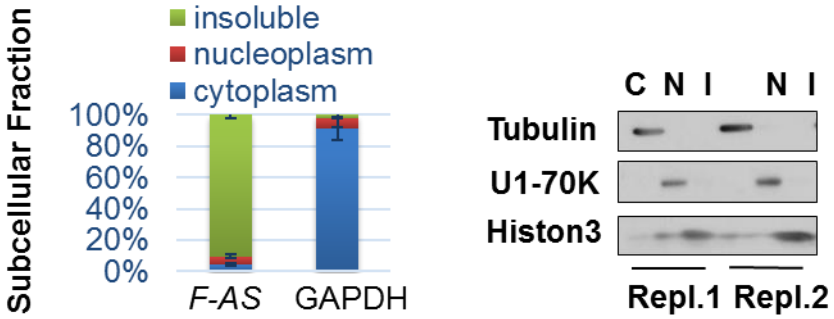

Figure 40. qPCR analysis for F-AS and GAPDH RNA distribution in subcellular fractions. GAPDH mRNA is predominantly located in cytoplasm and serves as a quality control for subcellular separation. Right, Western blotting of a-tubulin, U1-70K, and histone 3 in two independent experiments.

To test out hypothesis, the interaction between *FOXM1-AS* and ALKBH5 was assessed by native RIP which revealed a considerable enrichment of *FOXM1-AS* in ALKBH5-FLAG compared to mouse Immunoglobulin G (IgG) (Figure 41), and was further confirmed by RNA pull-down experiments which showed that the biotinylated RNA probes to capture *FOXM1-AS*, but not the antisense nucleotides to the probes, retrieved ALKBH5 proteins from the GSC nuclear extracts (Figure 41). Another abundant nuclear RNA binding protein, HuR, however, was not retrieved in this condition, suggesting the specific interaction with ALKBH5. On the other hand, we fixed RNA-RNA hybrids in GSCs with 4′-aminomethyltrioxalen (AMT), a psoralen-derivative crosslinker. Direct *in vivo* RNA-RNA interactions would be captured by AMT crosslink in RNA pull-down experiment since AMT penetrates intact cells and generates inter-strand crosslinks between uridine bases in RNA upon UV irradiation but does not react with proteins (150). We found that *FOXM1* pre-mRNA, but not mature RNA could be retrieved from the biotinylated *FOXM1-AS* RNA probes pull-down fractions of AMT-treated GSCs, whereas neither *FOXM1* pre-mRNA nor mature RNA was retrieved from the pull-down fractions of AMT-untreated cells or from the pull-down fractions using antisense probes (Figure 42). *In vitro* RNA re-association by base-pairing was negligible since RNA pull-down failed to enrich for *FOXM1* mature mRNA. These results suggest *FOXM1* nascent transcripts are the major associating partner with *FOXM1-AS in vivo*. Collectively, these data indicate *FOXM1-AS* interacts with both *FOXM1* nascent transcripts and ALKBH5. Having discovered that *FOXM1-AS* interacts with *FOXM1* transcripts and ALKBH5 protein, and knowing that ALKBH5 binds to *FOXM1* RNA, we asked whether the former was required for the latter. First, we screened five different siRNAs against *FOXM1-AS* with unique sequences at non-overlapping regions for their efficacy to ablate *FOXM1-AS* expression, and found that siRNA#2 and #3 are most

effective (Figure 43). Next, two shRNAs were constructed based on the sequences of siRNA#2 and #3. Notably, RNA recovery from RIP of ALKBH5-FLAG revealed a ~80% decrease of ALKBH5 associated *FOXM1* nascent transcripts when knocking down *FOXM1-AS* with *FOXM1-AS* shRNA*,* which implicates a positive role of *FOXM1-AS* in the association of ALKBH5 with *FOXM1* nascent transcripts (Figure 44). Consistently, *FOXM1-AS* knockdown increased the m^6A modification of *FOXM1* nascent transcripts (Figure 45). Furthermore, *FOXM1-AS* knockdown using pooled siRNA (siRNA#2 and #3) decreased *FOXM1* 3'UTR plasmid expression in a similar manner as ALKBH5 inhibition (Figure 46); reduced *FOXM1* 3'UTR luciferase activity (Figure 47); increased FLAG-YTHDC1 and *FOXM1* RNA association; and decreased HuR and *FOXM1* RNA association (Figure 48).

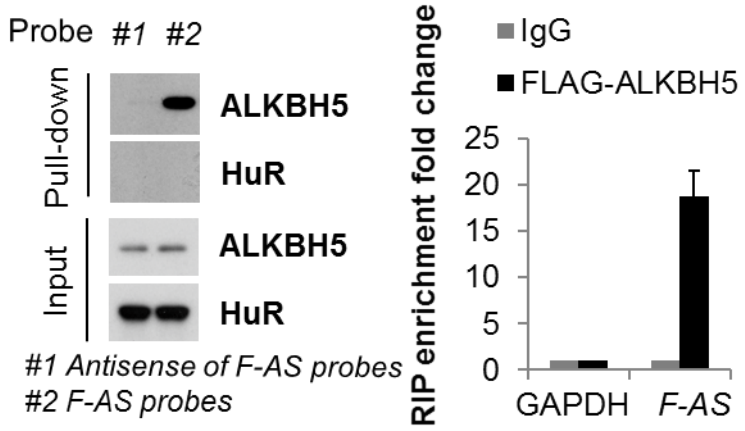

Figure 41. Analysis of the interaction between FOXM1-AS and ALKBH5 by RNA pull-down assay using biotinylated-probes to capture FOXM1-AS in nuclear extracts of GSC17 cells (D) and RIP assay using FLAG antibodies (E) in nuclear extracts of GSC17 cells expressing FLAG-ALKBH5. The RNA in the RNA-protein complex was then detected by qPCR and the proteins were detected by Western blotting. Antisense probes and HuR were served as negative controls. Inputs correspond to 5% nuclear extracts used for RNA pull-down. Error bars: + SEM, n=2.

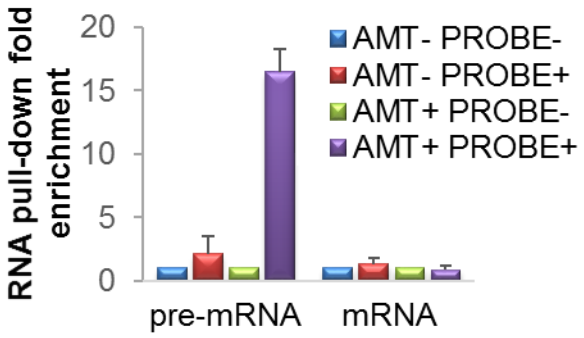

Figure 42. RNA pull-down of F-AS -associated RNA from GSC17. Biotinylated F-AS probes or antisense probes were incubated with AMT crosslinked or untreated RNA and collected with streptavidin beads. Interaction with F-AS was quantified by real-time PCR. All data in bar plots are represented as mean + SEM of three independent experiments.

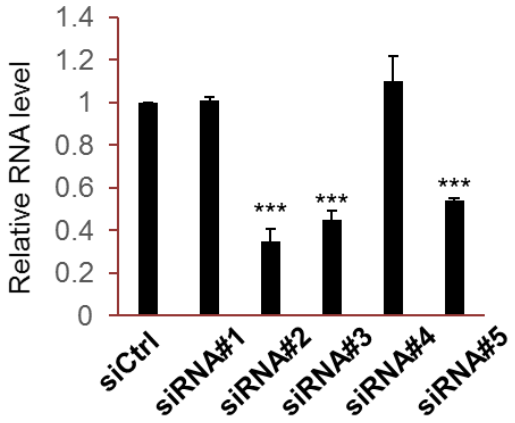

Figure 43. qPCR analysis for FOXM1-AS expression in GSC17 treated with siRNAs for control or FOXM1-AS. Error bars: ±SEM of triplicates. ***p<0.001.

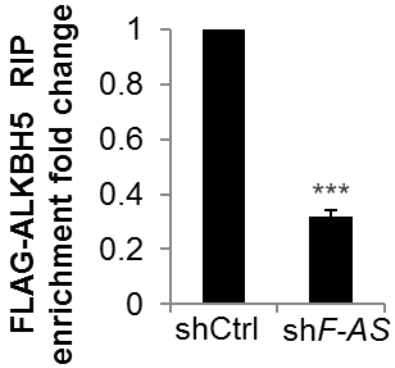

Figure 44. RIP analysis of the interaction of FOXM1 pre-mRNA with ALKBH5 in nuclear extracts of GSC17 cells expressing FLAG-ALKBH5 with or without FOXM1-AS knockdown. The relative amount of FOXM1 pre-mRNA bound with FLAG-ALKBH5 protein was measured by qPCR. All data in bar plots are represented as mean + SEM of three independent experiments.

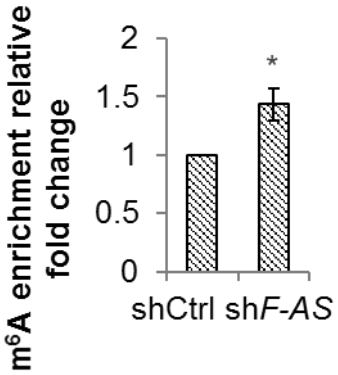

Figure 45. Analysis of m6A methylation levels of FOXM1 pre-mRNA in GSC17 cells with or without F-AS knockdown by MeRIP-qPCR assay. All data in bar plots are represented as mean + SEM of three independent experiments.

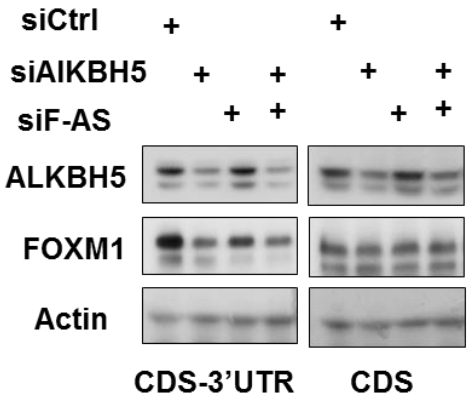

Figure 46. Western blotting of FOXM1 and ALKBH5 in GSC17 transfected with FOXM1 CDS plasmid or CDS-3'UTR plasmid followed by siRNA treatment for control, ALKBH5, F-AS.

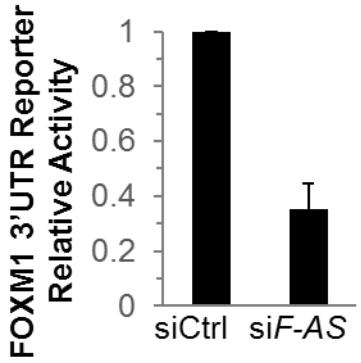

Figure 47. Analysis for activities of FOXM1 3'UTR firefly luciferase reporter in GSC17 cells treated with siRNAs for control or FOXM1-AS. The ratios between FOXM1 3'UTR reporter and Renilla control were determined 48 hr after siRNA treatment, and relative luciferase activity (fold) was normalized to that in cells transfected with the firefly luciferase control. Data in bar plots are represented as mean + SEM of three independent experiments.

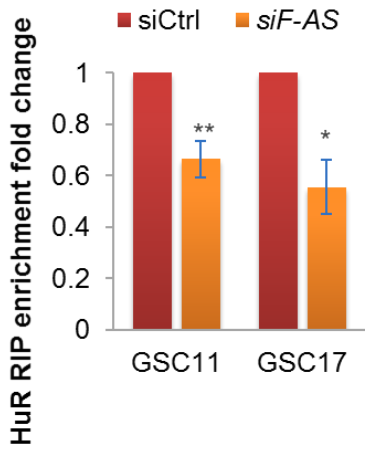

Figure 48. RIP analysis for the interaction of FOXM1 pre-mRNA with HuR in GSC17 and GSC11 cells with or without F-AS knockdown. FOXM1 pre-mRNA bound to HuR was measured by qPCR. Data in bar plots are represented as mean + SEM of three independent experiments.

Next, we sought to determine whether *FOXM1-AS* is biological functional in GBM. The observed upregulation of *FOXM1-AS* in the majority of GSCs suggests an important role in GSCs. Knockdown of *FOXM1-AS* led to a significant decrease in expression of *FOXM1* transcripts and protein (Figure 49). Moreover, sh*FOXM1-AS* substantially reduced GSC cell growth and BrdU incorporation (Figure 50). In addition, sh*FOXM1-AS* impaired tumorsphere formation and suppressed CSC maker expression, which was rescued by forced re-expression of *FOXM1-AS* (Figures 51-52). Thus, we conclude that *FOXM1-AS* stimulates *FOXM1* expression and contributes to GSC maintenance.

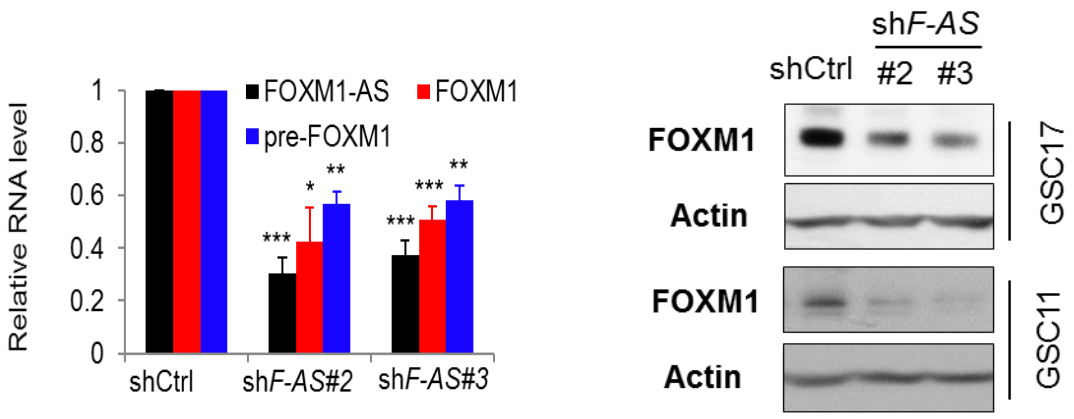

Figure 49. FOXM1 levels in GSC17 with or without F-AS knockdown. Left, qPCR analysis for FOXM1 transcript levels in GSC17 with or without F-AS knockdown. Right, Western blotting of FOXM1 in GSCs with or without FOXM1-AS knockdown. Data in bar plots are represented as mean + SEM of three independent experiments.

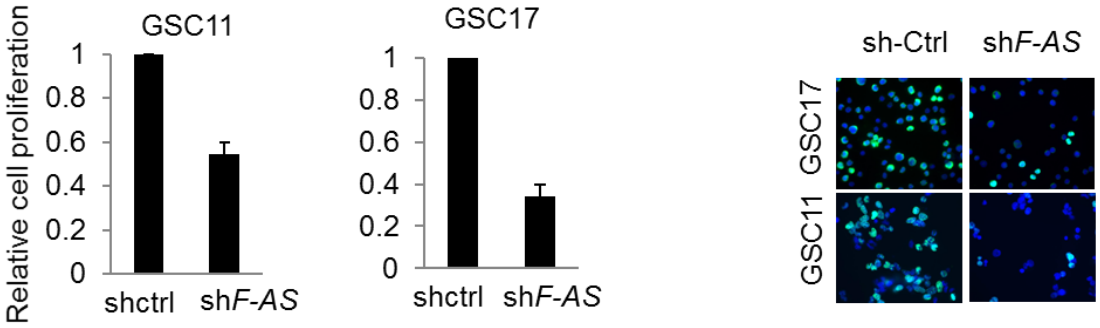

Figure 50. Proliferation of GSCs with or without FOXM1-AS knockdown determined by cell counting (Left). Right, Representative IF images of GSCs stained with antibodies against 5-Bromo-2'-deoxyuridine (BrdU). Data in bar plots are represented as mean + SEM of three independent experiments.

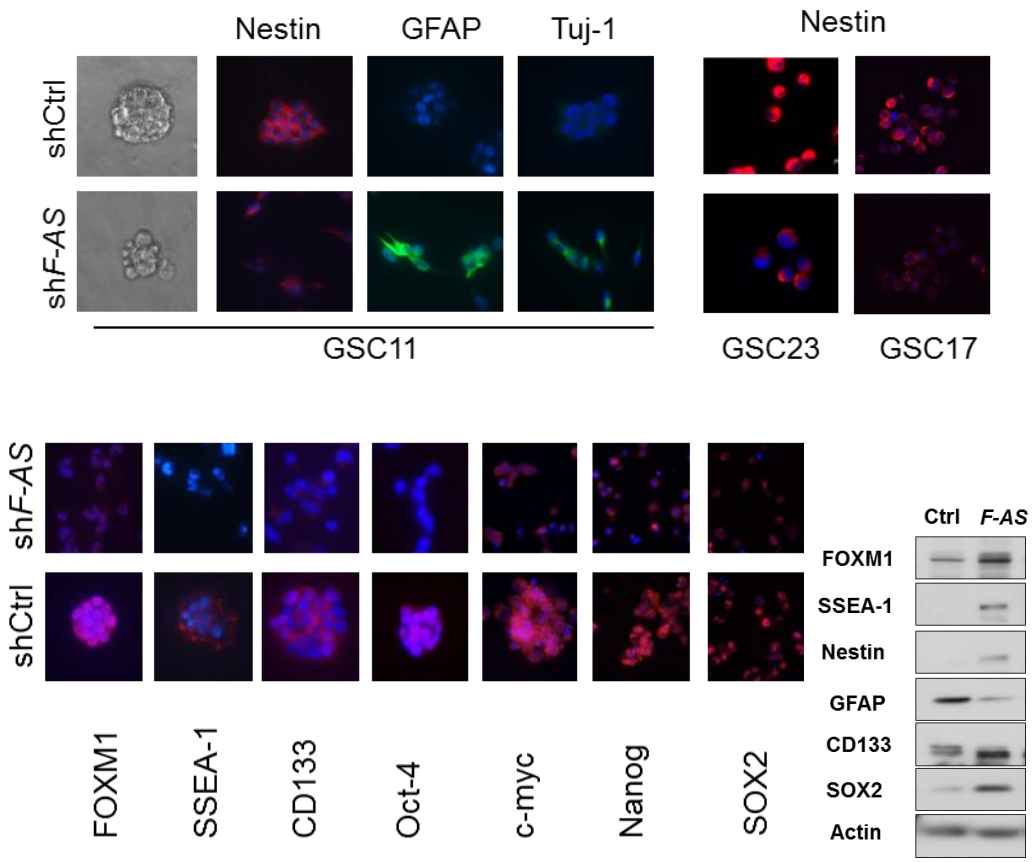

Figure 51. Fluorescence and bright-field micrographs of GSCs with or without F-AS knockdown. Cells were IF-stained with indicated antibodies. Western blotting showing expression of indicated proteins in GSC11 with FOXM1-AS knockdown then transduced with control or FOXM1-AS.

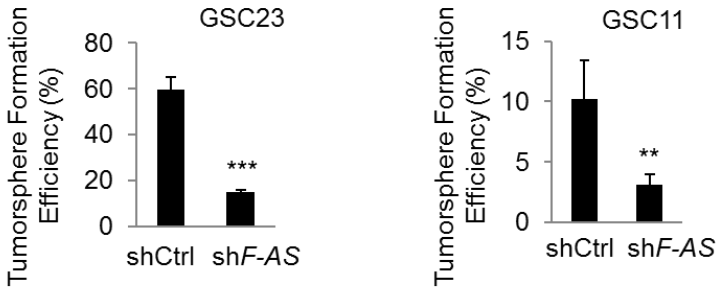

Figure 52. Tumorsphere formation efficiency of GSC11 with or without F-AS knockdown calculated by sphere number per 100 single cells after 7-day incubation in a 96-well plate. Data in bar plots are represented as mean + SEM of three independent experiments.

FOXM1 Reinstates Tumor Growth of GSCs with Depleted ALKBH5 or *FOXM1-AS*

To ascertain FOXM1 as a major contributor to the tumorigenic ALKBH5 function, we directly tested whether adding back FOXM1 could reverse the effects of ALKBH5 inhibition. Stable forced expression of FOXM1 CDS without 3'UTR robustly stimulated re-expression of proliferation related genes such as PLK1, AURKA, AURKB and CENPE (Figure 53). In contrast to the absence of tumor formation by ALKBH5 or *FOXM1-AS* knockdown, ectopic expression of FOXM1 largely abolished the tumor growth inhibition and these cells developed brain resembling human GBM as control (Figure 54). Immunohistochemical analysis confirmed expression of Sox2 and Ki67, a proliferation maker in these xenografts (Figure 55). These results confirmed that the downstream transcription factor FOXM1 plays master control roles of proliferation and self-renewal in ALKBH5-dependent GSCs.

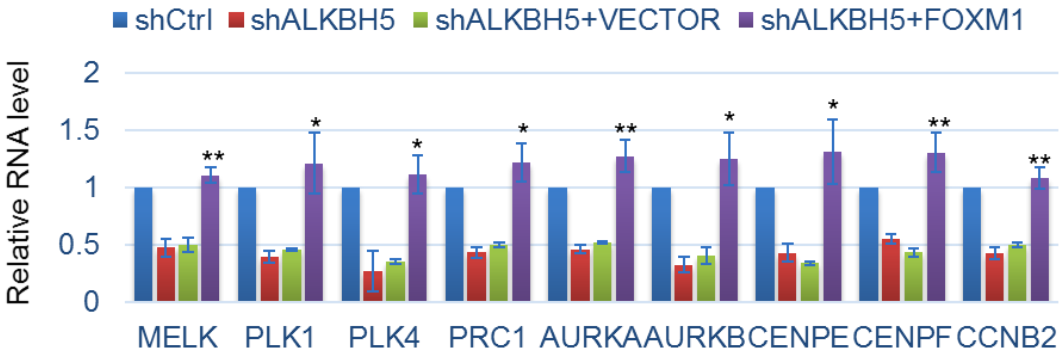

Figure 53. qPCR analysis for indicated mRNA levels in GSC11 with or without ALKBH5 knockdown and rescued by exogenous FOXM1. Error bars: ±SEM of triplicates. *p<0.05, **p<0.01, versus shALKBH5+Vector.

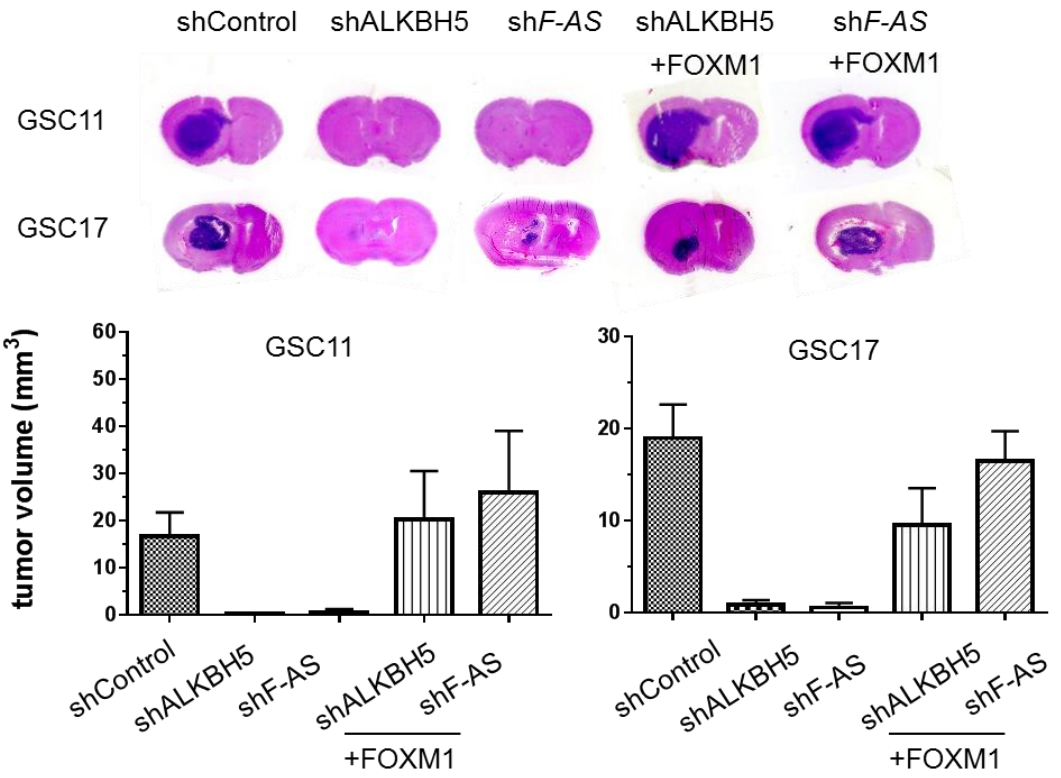

Figure 54. Representative images of hematoxylin- and eosin- analysis of tumor formation of indicated cells in mouse brains. Histograms show tumor volumes. Error bars: ±SEM, n=8.

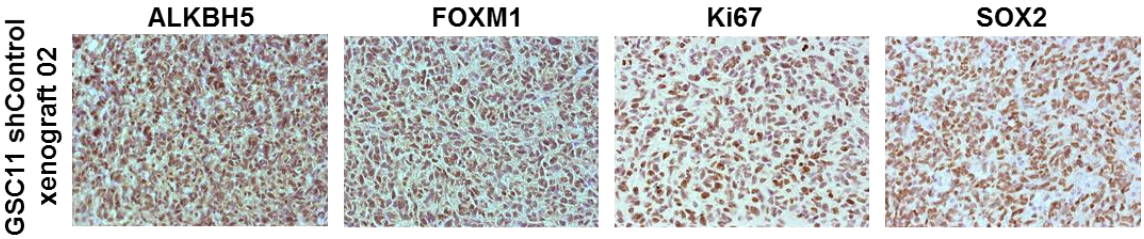

Figure 55. Representative images of IHC staining of indicated proteins in GSC11 xenografts.

Tabel 1. List of 206 genes with expression fold change in GSCs with shALKBH5

Transcript. ID	11shALKBH5 vs. shCtrl.Fold. Change	17shALKBH5 vs. shCtrl Fold Change	Fold Change	symbol
16658184	2.77	3.8	3.24	TPRG1L
16662648	-2.49	-3.17	-2.81	CDCA8
16667119	2.08	2.56	2.31	KIAA1107
16670387	-2.15	-4.22	-3.01	HIST2H3A; HIST2H3C; HIST2H3D
16673154	-3.21	-3.99	-3.58	NUF2
16677425	-2.86	-2.83	-2.85	CENPF
16679785	-2.04	-3.07	-2.5	OR2M1P
16681891	-3.63	-2.63	-3.09	
16685729	-2.02	-2.14	-2.08	BMP8B
16687385	-2.04	-3.96	-2.85	RP4-784A16.3
16688386	-2.2	-2.19	-2.2	DEPDC1
16691755	2.38	2.35	2.36	
16691883	-2.51	-2.22	-2.36	FAM72C; FAM72D
16692583	-2.22	-2.18	-2.2	FAM72D; FAM72C; RP11-38J22.1; FAM72B; FAM72A
16692616	-2.15	-4.22	-3.01	HIST2H3A; HIST2H3C; HIST2H3D
16692636	-2.37	-6.06	-3.79	HIST2H2AB
16692724	-2.06	-2.8	-2.4	ANP32E
16697544	-2.65	-3.76	-3.15	ASPM
16697695	-3.05	-4.07	-3.52	KIF14
16698023	-2.2	-4.39	-3.11	UBE2T
16698984	-2.16	-2.36	-2.26	NEK2
16700888	-2.02	-3.76	-2.76	NID1
16702571	-2.01	-4.51	-3.01	MCM10
16707221	-2.62	-2.84	-2.73	KIF20B
16707468	-2.51	-3.35	-2.9	KIF11
16707551	-2.71	-2.72	-2.72	CEP55

16717676	-2.09	-2.35	-2.22	RP11-108L7.15
16719515	-2.11	-3.04	-2.53	MKI67
16720728	-2.22	-2.13	-2.18	LOC100505570; AP006285.6
16722960	3.02	2.85	2.93	RNA5SP338
16748449	-2.5	-2.93	-2.7	PTMA; MIR1244-1; MIR1244-2; MIR1244-3; LOC728026; LOC100506248; PTMAP5
16753663	-2.37	-2.93	-2.63	
16755498	-2.06	-2.77	-2.39	TMPO
16755928	-2.2	-2.25	-2.23	PARPBP; C12orf48
16758336	-2.07	-2.11	-2.09	KNTC1
16760048	-2.07	-4.4	-3.02	FOXM1
16761116	-2.5	-2.93	-2.7	PTMA; MIR1244-1; MIR1244-2; MIR1244-3; LOC728026; LOC100506248; PTMAP5
16764894	-2.05	-2.13	-2.09	KRT6B
16765513	-2.07	-2.57	-2.31	CBX5
16765878	-2.06	-2.34	-2.2	RP11-973D8.4
16766318	-2.3	-2.66	-2.47	PRIM1
16775732	-2.18	-2.08	-2.13	SLITRK5
16777278	-2.43	-4	-3.12	SKA3
16779546	-2.2	-4.54	-3.16	DIAPH3
16782132	3.55	3.88	3.71	ABHD4
16783905	-2.11	-2.07	-2.09	LRR1
16784299	-2.03	-2.86	-2.41	CDKN3
16784381	2.28	3.75	2.92	LGALS3
16790360	2.63	3.77	3.15	SNORD9
16790362	2.62	2.78	2.7	SNORD8
16793225	-2.19	-4.12	-3	DLGAP5
16798132	2.24	3.99	2.99	SNORD116-1

16798146	2.04	3.79	2.78	SNORD116-5; SNORD116-7; SNORD116-3; SNORD116-8; SNORD116-9
16798150	2.04	3.79	2.78	SNORD116-5; SNORD116-7; SNORD116-3; SNORD116-8; SNORD116-9
16798164	2.18	3.56	2.79	SNORD116-14; SNRPN
16798206	2.28	3.29	2.74	SNORD116-20; SNORD116-19; SNORD116-17; SNORD116-21; SNORD116@; RP11-701H24.4
16798208	2.17	3.95	2.93	SNORD116-21; SNORD116-19; SNORD116-17; SNORD116-20; SNORD116@; RP11-701H24.4
16798212	2.06	3.52	2.7	SNORD116-23
16798216	2.17	3.29	2.67	SNORD116-24
16798228	2.13	4.66	3.15	SNORD116-26
16798236	2.16	3.26	2.65	SNORD116-29
16798242	2.33	4.33	3.18	SNORD116-30
16798252	2.39	3.61	2.94	
16798782	2.17	2.07	2.12	
16798801	-2.46	-3.3	-2.85	ARHGAP11B; LOC100288637
16798810	-2.32	-2.07	-2.19	
16798919	-2.07	-2.67	-2.35	ARHGAP11A
16799598	-2.62	-2.94	-2.78	CASC5
16799637	-2.51	-3.92	-3.13	RAD51
16799793	-2.32	-2.74	-2.52	NUSAP1
16801557	-2.49	-3.15	-2.8	CCNB2
16802519	-2.18	-3.58	-2.8	KIF23
16804557	-2.15	-2.1	-2.13	RNU7-195P

16804559	-2.54	-3.68	-3.05	FANCI
16804902	-2.39	-4.4	-3.25	BLM
16809511	2.39	4.25	3.19	FAM214A; KIAA1370
16809748	-2.04	-3.48	-2.67	MNS1
16810933	-2.09	-2.16	-2.13	TIPIN
16813342	-2.04	-3.51	-2.68	PRC1
16817017	-2.03	-5.32	-3.29	PLK1
16823046	2.1	2.93	2.48	SNORD60
16825561	3.49	5.63	4.43	SEZ6L2
16826970	2.25	2.46	2.35	SLC38A7
16828108	2.98	4.63	3.71	SNORD71
16828886	-2.04	-7.64	-3.95	GINS2
16829764	-2.31	-2.46	-2.38	GSG2
16836492	-2.27	-3.56	-2.84	PRR11
16838057	-2.19	-2.12	-2.15	
16840902	-2.07	-4.48	-3.04	AURKB
16842673	-2.1	-4.98	-3.23	SPAG5
16844312	-2.13	-4.04	-2.93	TOP2A
16848079	2.24	2.22	2.23	WIPI1
16850517	-2.61	-4.53	-3.44	NDC80
16852312	-2.43	-2.31	-2.37	SKA1
16854801	-2.22	-6.14	-3.69	MIR924
16855673	-2.15	-3.68	-2.82	BCL2
16859788	2.03	2.43	2.22	PGPEP1; FKBP8
16863534	-2.05	-3.97	-2.85	
16868838	-2.41	-5.1	-3.51	SPC24
16871586	2.18	2.15	2.16	CLIP3
16882975	-2.19	-5.32	-3.42	NCAPH
16885976	3.3	2.45	2.84	
16889627	2.76	2.07	2.39	SNORD70
16889958	2.33	2.08	2.2	ZDBF2

16897998	2.38	2.2	2.29	LOC339803; AC016747.3
16901197	2.01	2.14	2.07	SNORD89; RNF149
16901755	-2.2	-3.73	-2.87	BUB1
16901957	-2.54	-3.6	-3.02	CKAP2L
16903186	2.87	2.38	2.62	LRP1B
16908197	3.38	4.5	3.9	IGFBP5
16914315	-2.01	-3.73	-2.74	UBE2C
16914741	2.18	2.67	2.41	SNORD12C
16920548	-2.19	-2.64	-2.41	AURKA
16937505	-2.46	-5.39	-3.65	FANCD2
16939960	-2.62	-5.09	-3.65	KIF15
16941689	2.03	2.38	2.2	
16948021	-2.04	-3.04	-2.49	ECT2
16948572	2.74	2.24	2.48	KLHL24
16950173	-2.3	-3.05	-2.65	LOC101928670; FAM157A
16951485	-2.81	-3.09	-2.94	SGOL1
16957170	-2.55	-2.49	-2.52	KIAA1524
16965027	2.2	4.08	2.99	USP17L5
16966967	2.17	2.08	2.13	RNU6-652P
16970563	-2.59	-3.29	-2.92	PLK4
16971573	-2.67	-2.53	-2.6	MND1
16978568	-2.51	-3.21	-2.84	CENPE
16979389	-2.53	-2.71	-2.62	MAD2L1
16980918	2.23	2.16	2.2	CTSO
16981500	-2.22	-2.21	-2.21	
16981502	-2.5	-2.17	-2.33	RP11-798M19.3
16982024	-2.02	-2.87	-2.41	CENPU; MLF1IP
16985614	-2.91	-3.22	-3.06	CENPH
16986583	2.06	6.3	3.6	JMY
16988297	-2.5	-2.93	-2.7	PTMA; MIR1244-1; MIR1244-2; MIR1244-3; LOC728026;

				LOC100506248; PTMAP5
16989636	-2.13	-4.84	-3.21	KIF20A
16990678	2.38	3.11	2.72	STK32A
16991460	-2.02	-3.64	-2.71	KIF4B
16991859	-2.4	-2.15	-2.27	HMMR
16995024	2.32	2.04	2.17	MIR579
16996433	3.06	2.98	3.02	PLK2
16996545	-2.03	-2.86	-2.41	DEPDC1B
16996722	-2.33	-2.24	-2.28	CENPK
16997615	2.19	2.12	2.15	SERINC5
17005589	-2.55	-5.15	-3.62	HIST1H2AE
17005603	-2.59	-6.2	-4.01	HIST1H2BI
17005858	-2.35	-4.17	-3.13	HIST1H2AI; HIST1H2AK; HIST1H2AL; HIST1H2AM; HIST1H2AG; HIST1H2AH
17005871	2.31	6.47	3.87	HIST1H2BN
17007459	-2.4	-3.33	-2.83	KIFC1
17010552	-2.14	-2.38	-2.26	TTK
17010760	-2.7	-3.31	-2.99	NT5E
17010929	2.19	2.83	2.49	PNRC1
17013657	3.66	3.08	3.36	ULBP1
17013664	-2.82	-3.63	-3.2	PPP1R14C
17015637	-2.05	-2.05	-2.05	ELOVL2
17015817	-2.51	-2.06	-2.27	RNU6-645P
17016363	-4.78	-8.57	-6.4	HIST1H3B
17016369	-3.08	-7.15	-4.69	HIST1H2BB
17016379	2.94	2.63	2.78	HIST1H2BG; HIST1H2BF; HIST1H2BE; HIST1H2BI; HIST1H2BC
17016383	-2.12	-4.11	-2.96	HIST1H4D
17016393	-2.75	-6.3	-4.16	HIST1H1D

17016400	-2.22	-9.08	-4.48	HIST1H3F
17016403	-3.71	-7.74	-5.36	HIST1H3G
17016406	2.68	2.42	2.55	HIST1H4H
17016490	-2.67	-3.22	-2.93	HIST1H2AJ
17016499	-2.46	-13.79	-5.82	HIST1H1B
17016512	-2.06	-4.75	-3.13	HIST1H2AM
17024002	-2.18	-2.9	-2.51	MTFR2
17024980	-2.07	-3.45	-2.67	FBXO5
17038792	-2.4	-3.33	-2.83	KIFC1
17041352	-2.4	-3.33	-2.83	KIFC1
17048102	2.09	2.84	2.43	C7orf63
17050154	-2.01	-2.46	-2.22	PRKAR2B
17051943	2.55	3.8	3.11	TMEM140
17054325	-2.2	-3.02	-2.58	GPR146; RP11-449P15.1
17055095	-2.08	-2.17	-2.13	
17056105	-2.57	-2.84	-2.7	HOXA2
17061099	-2.03	-5.17	-3.24	RASA4B; RASA4
17064679	-2.03	-3.05	-2.49	XRCC2
17067102	-2.15	-3.14	-2.59	CDCA2
17067332	-2.1	-5.42	-3.37	ESCO2
17072225	-2.1	-2.18	-2.14	MTBP
17074342	2.14	2.07	2.11	LINC00965
17075776	-2.25	-5.17	-3.41	PBK
17079317	2.13	3.24	2.62	TP53INP1
17083197	4.07	2.41	3.13	VLDLR
17084904	-2.54	-2.7	-2.62	MELK
17087413	-2.06	-2.08	-2.07	GALNT12
17087716	-2.45	-2.1	-2.27	SMC2
17100771	3.34	2.16	2.68	
17103951	2.34	4.08	3.09	TSPYL2
17104049	3.51	13.72	6.94	SNORA11; MAGED2

17104519	-2.23	-6	-3.66	RNY4P23
17105401	-2.04	-3.95	-2.84	CENPI
17107676	-2.25	-2.91	-2.56	MAMLD1
17107855	-2.83	-2.34	-2.57	GABRQ
17108779	2.01	2.27	2.13	ARSD
17114220	-2.68	-2.65	-2.67	MBNL3
17115014	-3.57	-2.06	-2.71	GABRA3
17118664	2.1	2.24	2.17	SNORD45A; RABGGTB; SNORD45B; SNORD45C
17118948	2.12	2.06	2.09	IPW; SNORD107; PWARSN; SNORD116-4; SNORD116-22; SNORD115-7; SNORD115-13; SNORD115-26; SNORD116-28; LOC101930404; SNRPN; SNHG14
17119086	2.09	2.05	2.07	SNORD1C; SNORD1A; SNHG16
17119728	2.13	2.14	2.14	SNORD36B; RPL7A; SNORD36A; SNORD24
17121912	-2.33	-3.37	-2.8	LINC00669; RP11-244M2.1
17121916	-2.19	-4.43	-3.11	LINC00669; RP11-244M2.1
17122656	-2.97	-2.25	-2.58	LINC00152; MIR4435-1HG; LOC101930489
17122664	-3.24	-3.29	-3.27	LINC00152; LOC101930489; MIR4435-1HG
17122666	-2.33	-2.12	-2.22	LINC00152; MIR4435-1HG; LOC101930489
17123262	2.52	3.18	2.83	TRANK1
17125836	-2.02	-2.18	-2.1	FAM89A; MIR1182

Table 2. List of genes predicted to mediate the altered gene expression profile

Upstream Regulator	Exp Fold Change	Molecule Type	Predicted Activation State	Activation z-score	p-value of overlap
Vegf		group	Inhibited	-4.630	8.63E-13
RABL6		other	Inhibited	-4.123	1.37E-21
CCND1		transcription regulator	Inhibited	-2.828	1.69E-23
EP400		other	Inhibited	-2.621	3.23E-08
CD24		other	Inhibited	-2.449	1.94E-04
PTGER2		g-protein coupled receptor	Inhibited	-4.796	9.73E-28
MED1		transcription regulator	Inhibited	-2.390	1.01E-03
CSF2		cytokine	Inhibited	-5.098	2.35E-16
NKX2-3		transcription regulator	Inhibited	-2.000	8.49E-02
FOXM1	-3.020	transcription regulator	Inhibited	-3.065	1.41E-11
FOXO1		transcription regulator	Inhibited	-3.138	6.57E-06
S100A6		transporter	Inhibited	-2.646	2.23E-09
MITF		transcription regulator	Inhibited	-3.357	4.98E-10
YAP1		transcription regulator	Inhibited	-2.000	1.27E-05
HGF		growth factor	Inhibited	-4.640	1.98E-12
RARA		ligand-dependent nuclear receptor	Inhibited	-3.464	1.21E-06
TBX2		transcription regulator	Inhibited	-3.162	5.37E-10
ESR1		ligand-dependent nuclear receptor	Inhibited	-4.955	3.07E-08
MYC		transcription regulator	Inhibited	-2.923	2.57E-04
HCAR2		g-protein coupled receptor	Activated	2.000	9.52E-06
PTEN		phosphatase	Activated	2.394	9.64E-05
miR-291a-3p (and other miRNAs w/seed AAGUGCU)		mature microrna	Activated	2.000	5.49E-03
let-7		microrna	Activated	2.975	1.42E-06
NUPR1		transcription regulator	Activated	5.745	2.87E-22
CDKN2A		transcription regulator	Activated	3.383	1.30E-07
BNIP3L		other	Activated	3.317	4.44E-13
ATF3		transcription regulator	Activated	2.000	1.48E-03
TCF3		transcription regulator	Activated	3.051	1.07E-08
CTLA4		transmembrane receptor	Activated	2.000	1.07E-03
RBL2		other	Activated	2.583	7.91E-06
NLRP3		other	Activated	2.000	9.32E-04
SMARCB1		transcription regulator	Activated	2.363	2.31E-04
KDM5B		transcription regulator	Activated	3.157	9.42E-08
Irgm1		other	Activated	2.828	5.37E-10
TP53		transcription regulator	Activated	4.296	2.63E-12

CHAPTER 4: DISCUSSION

Summary

N^6-methyladenosine is the most abundant modification on mRNA but its functions in human diseases are poorly understood. Here we show that overexpression of m^{6}A demethylase ALKBH5 is required for FOXM1- mediated proliferation of GSCs, a subpopulation of therapeutic resistant glioblastoma cells, which contribute to the recurrence of the most lethal brain tumor. Demethylation of *FOXM1* nascent transcript by ALKBH5 is facilitated with a nuclear long noncoding *FOXM1* antisense transcript. This promotes *FOXM1* pre-mRNA to interact with HuR, thereby maintaining FOXM1 expression. The vulnerability of GSC to disruption in the ALKBH5-dependent gene expression supports a central role for m^{6}A in tumor development and provides a rationale for the therapeutic targeting of epitranscriptomic modulators.

ALKBH5 in GSCs

Acute loss of ALKBH5 affects RNA metabolism and increases mRNA export. *Alkbh5* knockout mice were viable but showed compromised spermatogenesis (12), suggesting that the general effects of ALKBH5 on RNA biology is not required for most tissue development thereby limiting ALKBH5 contribution to a subset of cells rather than systemic regulation of vertebrate development. Disease associated expression and function of ALKBH5 have remained unclear. We show that ALKBH5 function is at least important to some GSCs. Interestingly, GSCs are addicted to the overexpression of transferrin, transferrin receptor and ferritin. Depleting ferritin disrupted GSC mitotic progression (119). ALKBH5 belongs to the AlkB family of nonheme Fe(II)/α-ketoglutarate (α-KG)-dependent dioxygenases, whose activity is iron-dependent (12). ALKBH5 is not

GSC specific, yet GSCs rely on ALKBH5 expression and preferential iron trafficking. These molecular components of GSCs may be integrated synergistically as evidenced by the gene expression analysis from the ferritin study that also pointed out FOXM1 as the central molecular mediator. FOXM1 was proposed to act downstream from STAT3 in the ferritin-STAT3-FOXM1 feedback loop, which can be true for phosphorylated STAT3 expressing cells. However, pSTAT3 is mostly restricted to the mesenchymal GBM subtype and absent in proneural subtype (134). The generally observed FOXM1 decrease now may be partially explained by our findings: ferritin deficiency resulted in ALKBH5 inactivation in GSCs, consequently inhibiting FOXM1 expression.

During the preparation of manuscript, ALKBH5 was reported to mediate hypoxia-induced and HIF-dependent breast cancer stem cell (BCSC) phenotype (40). ALKBH5 deficiency impairs hypoxia-induced BCSC enrichment and tumor formation in *vivo*. These findings again emphasize the important tumorigenic role of ALKBH5 in cancer and also suggest the possibility of CSC-associated function in other cancer types. ALKBH5 is a direct target of HIF-1α (41), and might also be regulated by HIF-2α (40). GSCs are addicted to HIFs under both normoxic and hypoxic conditions (90, 151). To which extent ALKBH5 expression is stimulated by HIFs and other potential regulators in GSCs may be defined by future study.

Gene Expression Regulated by ALKBH5

No RNA stability and mRNA export are found to cause *FOXM1* downregulation in GSCs transduced with shALKBH5. These findings could be explained by several reasons: (1) the half-life of majority of mRNA is not subject to the change of ALKBH5 or m^6A. Whereas YTHDF2 knockdown led to a 30% prolonged average lifetimes of its mRNA targets (19), global loss of m^6A modification by methylation inhibitor did not exert

dramatic destabilization of the cytoplasmic mRNA (30), suggesting that only a few m^{6}A-marked transcripts are susceptible to destabilize upon loss of m^{6}A excluding *FOXM1*. (2) Besides technical limitation, the accelerated nuclear export of *FOXM1* mRNA in shALKBH5 cells is not able to be detected in the steady-state. (3) an alternative mechanism is that these functions of ALKBH5 can be compensated by other pathways in line with the observation that *Alkbh5* knockout mice were viable. A recent study suggested ALKBH5 might be associated with THOC7 (152), a putative component of the THO complex (153), which couples transcription with mRNA export (154) and cooperates with the nuclear RNA surveillance machinery (155). THO is reported to affect <20% of the transcriptome in *Drosophila*, but is required for export of heat-shock mRNAs under heat stress (153). The percentage of transcriptome regulated by ALKBH5 in nuclear export, however, is unknown, and probably *FOXM1* mRNA export is not restricted to ALKBH5 function. Although these findings do not directly illustrate the effect of ALKBH5 on gene expression, they imply a close relationship between ALKBH5 and pre-mRNA. The recent evidence of FTO regulating RNA splicing through m^{6}A change also suggests m^{6}A demethylase regulates pre-mRNA processing (24). Moreover, our direct evidence showing ALKBH5 interacts with *FOXM1* nascent transcripts in the RNA transcription or elongation dependent manner points out ALKBH5 may function on pre-mRNA. It would be important to know whether this mode of action could be extended to other transcripts in further elucidation of demethylation mechanism. m^{6}A can be attracted by m^{6}A readers or repelled by other RNA binding proteins in different complexes. Such events individually or coordinately determine the fate of m^{6}A modified mRNA. To date, only a few RNA binding proteins are on the list, including YTHDC1, HNRNPC, HNRNPA2B1, and HuR which are involved in pre-mRNA processing (27). Little is known about the amount of their overlapping targets and the detailed

mechanisms integrating RNA methylation and readers to execute complex cellular processes.

Given the microarray-based transcriptomic analysis, the effect of ALKBH5 on RNA translation was not examined. Considering several lines of evidence showing the m^6A relation to RNA translation (21, 25, 26), there can be direct or indirect effects of ALKBH5 on translation yet to be determined.

Role of LncRNA

Unlike the FOXM1 orthologs being expressed across eukaryotic tree of life, ALKBH5 arose with the advent of vertebrates, suggesting that ALKBH5-FOXM1 regulatory interaction may reflect a late-occurring process associated with certain cell identities or tumor development. We found a nuclear antisense lncRNA mediates the ALKBH5-FOXM1 interaction, which contributes to the target specificity in GSCs. *FOXM1-AS* locally promotes *FOXM1* mRNA expression by facilitating ALKBH5 interaction. This lncRNA preferentially binds to the nascent but not mature transcripts of *FOXM1* suggesting that additional factors such as RNA binding proteins may exist to facilitate this interaction or it is immobilized by other mechanism in the nucleus. Enhancement of HNRNPC binding to the lncRNA MALAT1 through an m^6A switch provides a model where m^6A modifications are functional to affect local structure and protein association (27). It remains unclear whether *FOXM1-AS* undergoes m^6A modification which might be required for its direct interaction with ALKBH5 or recruitment of other RNA binding proteins to bridge the association. Given that lncRNAs can function simultaneously at multiple steps to affect gene expression, *FOXM1-AS* might be able to act *in cis* or *in trans* to regulate *FOXM1* expression through other mechanisms, or even beyond its role in affecting *FOXM1.*

It is known that more than 70% of mammalian transcriptome have antisense transcription (156). These antisense transcripts are generally low in abundance and preferentially accumulate in the nucleus (157). Because the current view of methylation regulation is still preliminary, with many details remaining to be established, an open question would be whether other antisense lncRNAs exist giving rise to the specificity of mRNA methylation. A related question is how these lncRNAs associate with m^6A writers/erasers/readers.

CHAPTER 5: FUTURE DIRECTIONS

The studies of m^6A revive since the discovery of FTO as the first manmalian m^6A demethylase in 2011 (11). The function and mechanism of this modification is still largely unknown in most biological models. During the preparation of this manuscript, ALKBH5 (40) and METTL3 (23) were found to be associated with cancer stem cell phenotype in breast cancer and invasive growth of lung cancer, respectively, which implicates a crucial invovlement of m^6A in several stages of cancer development. This systematic study with mechanistic illustration opens up new avenues for effective treatment development and better understanding of disease mechanisms. Indeed, on the basis of this study and the other ALKBH5 study in breast cancer cells, pharmacological inhibitors of ALKBH5 have been under development, which represents an important step toward clinical application.

Meanwhile, the regulation of the methylation and demethylation reaction including enzyme activity, target recogniztion and specificity should be investigated within a variety of biological sources and conditions. For example, low-grade glioma and secondary GBM often harbor *IDH* mutation (158), which leads to the accumlation of 2-hydroxyglutarate (2–HG), an α-KG antagonist with potent inhibitory effect on α-KG-dependent dioxygenases, such as the lysine histone demethylases (KDM) and the ten-eleven translocation (TET) family of DNA hydroxylases (159). Whether ALKBH5 and FTO are inactivated in the *IDH*-mutated tumors remains to be determined. ALKBH5 activity also depends on iron, an essential metabolite for survival of GSC (119). The physiological range has not been defined for FTO and ALKBH5. It is unclear whether they require the iron equally as other enzymes and therefore, it is unkown whether a theraputic window exists for targeting iron trafficing alternatively.

The efficient methylation depends on the overall context of the consensus sequence (7) and *trans* factors such as microRNAs and transcription factors (147, 148). It is not surpring to find demethylation on certain RNA targets can be guided by long non-coding RNA. Antisense lncRNAs are more spesific in recognizing targets based on compematary sequence compared to microRNAs and transcription factors. These low abundant lncRNA may serve to fine tune the m^6A epitranscriptom and are associated with disease. The detailed mechanism of the regulation by lncRNA should be identified in future study.

Another important findings of this study is the GSC addiction to FOXM1-mediated proliferation, which is consistent with a series of previous studies (97, 119, 120). Although this pro-proliferation transcription factor has been known for two decades for its central role in tumor development, efficient pharmacological inhibitors is lacking in the market. However, according to recent research, FOXM1 protein is stablized by Wnt signaling in tumor cells (160), which enables rational Wnt inhibitor therapeutic strategies. FOXM1 is also stablized and activated by CDK4/6 in cancer cells and hence susceptible to CDK4/6 inhibition (135). CDK4/6 inhibitors have shown promising antitumor effectiveness in clinical trials in patients with breast cancer (161). These may provide clinical choices to treat GBM with more efficacy in combination with current therapy.

CHAPTER 6: BIBLIOGRAPHY

1. Iwanami, Y., and G. M. Brown. 1968. Methylated bases of transfer ribonucleic acid from HeLa and L cells. *Arch Biochem Biophys* 124: 472-482.
2. Iwanami, Y., and G. M. Brown. 1968. Methylated bases of ribosomal ribonucleic acid from HeLa cells. *Arch Biochem Biophys* 126: 8-15.
3. Desrosiers, R., K. Friderici, and F. Rottman. 1974. Identification of methylated nucleosides in messenger RNA from Novikoff hepatoma cells. *Proc Natl Acad Sci U S A* 71: 3971-3975.
4. Wei, C. M., A. Gershowitz, and B. Moss. 1976. 5'-Terminal and internal methylated nucleotide sequences in HeLa cell mRNA. *Biochemistry* 15: 397-401.
5. Wei, C. M., and B. Moss. 1977. Nucleotide sequences at the N6-methyladenosine sites of HeLa cell messenger ribonucleic acid. *Biochemistry* 16: 1672-1676.
6. Schibler, U., D. E. Kelley, and R. P. Perry. 1977. Comparison of methylated sequences in messenger RNA and heterogeneous nuclear RNA from mouse L cells. *J Mol Biol* 115: 695-714.
7. Narayan, P., R. L. Ludwiczak, E. C. Goodwin, and F. M. Rottman. 1994. Context effects on N6-adenosine methylation sites in prolactin mRNA. *Nucleic Acids Res* 22: 419-426.
8. Csepany, T., A. Lin, C. J. Baldick, Jr., and K. Beemon. 1990. Sequence specificity of mRNA N6-adenosine methyltransferase. *J Biol Chem* 265: 20117-20122.
9. Meyer, K. D., Y. Saletore, P. Zumbo, O. Elemento, C. E. Mason, and S. R. Jaffrey. 2012. Comprehensive analysis of mRNA methylation reveals enrichment in 3' UTRs and near stop codons. *Cell* 149: 1635-1646.

10. Dominissini, D., S. Moshitch-Moshkovitz, S. Schwartz, M. Salmon-Divon, L. Ungar, S. Osenberg, K. Cesarkas, J. Jacob-Hirsch, N. Amariglio, M. Kupiec, R. Sorek, and G. Rechavi. 2012. Topology of the human and mouse m6A RNA methylomes revealed by m6A-seq. *Nature* 485: 201-206.

11. Jia, G., Y. Fu, X. Zhao, Q. Dai, G. Zheng, Y. Yang, C. Yi, T. Lindahl, T. Pan, Y. G. Yang, and C. He. 2011. N6-methyladenosine in nuclear RNA is a major substrate of the obesity-associated FTO. *Nat Chem Biol* 7: 885-887.

12. Zheng, G., J. A. Dahl, Y. Niu, P. Fedorcsak, C. M. Huang, C. J. Li, C. B. Vagbo, Y. Shi, W. L. Wang, S. H. Song, Z. Lu, R. P. Bosmans, Q. Dai, Y. J. Hao, X. Yang, W. M. Zhao, W. M. Tong, X. J. Wang, F. Bogdan, K. Furu, Y. Fu, G. Jia, X. Zhao, J. Liu, H. E. Krokan, A. Klungland, Y. G. Yang, and C. He. 2013. ALKBH5 is a mammalian RNA demethylase that impacts RNA metabolism and mouse fertility. *Mol Cell* 49: 18-29.

13. Liu, J., Y. Yue, D. Han, X. Wang, Y. Fu, L. Zhang, G. Jia, M. Yu, Z. Lu, X. Deng, Q. Dai, W. Chen, and C. He. 2014. A METTL3-METTL14 complex mediates mammalian nuclear RNA N6-adenosine methylation. *Nat Chem Biol* 10: 93-95.

14. Wang, Y., Y. Li, J. I. Toth, M. D. Petroski, Z. Zhang, and J. C. Zhao. 2014. N6-methyladenosine modification destabilizes developmental regulators in embryonic stem cells. *Nat Cell Biol* 16: 191-198.

15. Schwartz, S., M. R. Mumbach, M. Jovanovic, T. Wang, K. Maciag, G. G. Bushkin, P. Mertins, D. Ter-Ovanesyan, N. Habib, D. Cacchiarelli, N. E. Sanjana, E. Freinkman, M. E. Pacold, R. Satija, T. S. Mikkelsen, N. Hacohen, F. Zhang, S. A. Carr, E. S. Lander, and A. Regev. 2014. Perturbation of m6A writers reveals two distinct classes of mRNA methylation at internal and 5' sites. *Cell Rep* 8: 284-296.

16. Bokar, J. A., M. E. Rath-Shambaugh, R. Ludwiczak, P. Narayan, and F. Rottman. 1994. Characterization and partial purification of mRNA N6-adenosine methyltransferase from HeLa cell nuclei. Internal mRNA methylation requires a multisubunit complex. *J Biol Chem* 269: 17697-17704.

17. Ping, X. L., B. F. Sun, L. Wang, W. Xiao, X. Yang, W. J. Wang, S. Adhikari, Y. Shi, Y. Lv, Y. S. Chen, X. Zhao, A. Li, Y. Yang, U. Dahal, X. M. Lou, X. Liu, J. Huang, W. P. Yuan, X. F. Zhu, T. Cheng, Y. L. Zhao, X. Wang, J. M. Rendtlew Danielsen, F. Liu, and Y. G. Yang. 2014. Mammalian WTAP is a regulatory subunit of the RNA N6-methyladenosine methyltransferase. *Cell Res* 24: 177-189.

18. Fu, Y., G. Jia, X. Pang, R. N. Wang, X. Wang, C. J. Li, S. Smemo, Q. Dai, K. A. Bailey, M. A. Nobrega, K. L. Han, Q. Cui, and C. He. 2013. FTO-mediated formation of N6-hydroxymethyladenosine and N6-formyladenosine in mammalian RNA. *Nat Commun* 4: 1798.

19. Wang, X., Z. Lu, A. Gomez, G. C. Hon, Y. Yue, D. Han, Y. Fu, M. Parisien, Q. Dai, G. Jia, B. Ren, T. Pan, and C. He. 2014. N6-methyladenosine-dependent regulation of messenger RNA stability. *Nature* 505: 117-120.

20. Xu, C., X. Wang, K. Liu, I. A. Roundtree, W. Tempel, Y. Li, Z. Lu, C. He, and J. Min. 2014. Structural basis for selective binding of m6A RNA by the YTHDC1 YTH domain. *Nat Chem Biol* 10: 927-929.

21. Wang, X., B. S. Zhao, I. A. Roundtree, Z. Lu, D. Han, H. Ma, X. Weng, K. Chen, H. Shi, and C. He. 2015. N(6)-methyladenosine Modulates Messenger RNA Translation Efficiency. *Cell* 161: 1388-1399.

22. Xiao, W., S. Adhikari, U. Dahal, Y. S. Chen, Y. J. Hao, B. F. Sun, H. Y. Sun, A. Li, X. L. Ping, W. Y. Lai, X. Wang, H. L. Ma, C. M. Huang, Y. Yang, N. Huang, G.

B. Jiang, H. L. Wang, Q. Zhou, X. J. Wang, Y. L. Zhao, and Y. G. Yang. 2016. Nuclear mA Reader YTHDC1 Regulates mRNA Splicing. *Mol Cell*.

23. Lin, S., J. Choe, P. Du, R. Triboulet, and R. I. Gregory. 2016. The m(6)A Methyltransferase METTL3 Promotes Translation in Human Cancer Cells. *Mol Cell* 62: 335-345.

24. Zhao, X., Y. Yang, B. F. Sun, Y. Shi, X. Yang, W. Xiao, Y. J. Hao, X. L. Ping, Y. S. Chen, W. J. Wang, K. X. Jin, X. Wang, C. M. Huang, Y. Fu, X. M. Ge, S. H. Song, H. S. Jeong, H. Yanagisawa, Y. Niu, G. F. Jia, W. Wu, W. M. Tong, A. Okamoto, C. He, J. M. Rendtlew Danielsen, X. J. Wang, and Y. G. Yang. 2014. FTO-dependent demethylation of N6-methyladenosine regulates mRNA splicing and is required for adipogenesis. *Cell Res* 24: 1403-1419.

25. Meyer, K. D., D. P. Patil, J. Zhou, A. Zinoviev, M. A. Skabkin, O. Elemento, T. V. Pestova, S. B. Qian, and S. R. Jaffrey. 2015. 5' UTR m(6)A Promotes Cap-Independent Translation. *Cell* 163: 999-1010.

26. Zhou, J., J. Wan, X. Gao, X. Zhang, S. R. Jaffrey, and S. B. Qian. 2015. Dynamic m(6)A mRNA methylation directs translational control of heat shock response. *Nature* 526: 591-594.

27. Liu, N., Q. Dai, G. Zheng, C. He, M. Parisien, and T. Pan. 2015. N(6)-methyladenosine-dependent RNA structural switches regulate RNA-protein interactions. *Nature* 518: 560-564.

28. Alarcon, C. R., H. Lee, H. Goodarzi, N. Halberg, and S. F. Tavazoie. 2015. N6-methyladenosine marks primary microRNAs for processing. *Nature* 519: 482-485.

29. Alarcon, C. R., H. Goodarzi, H. Lee, X. Liu, S. Tavazoie, and S. F. Tavazoie. 2015. HNRNPA2B1 Is a Mediator of m(6)A-Dependent Nuclear RNA Processing Events. *Cell* 162: 1299-1308.

30. Camper, S. A., R. J. Albers, J. K. Coward, and F. M. Rottman. 1984. Effect of undermethylation on mRNA cytoplasmic appearance and half-life. *Mol Cell Biol* 4: 538-543.

31. Batista, P. J., B. Molinie, J. Wang, K. Qu, J. Zhang, L. Li, D. M. Bouley, E. Lujan, B. Haddad, K. Daneshvar, A. C. Carter, R. A. Flynn, C. Zhou, K. S. Lim, P. Dedon, M. Wernig, A. C. Mullen, Y. Xing, C. C. Giallourakis, and H. Y. Chang. 2014. m(6)A RNA modification controls cell fate transition in mammalian embryonic stem cells. *Cell Stem Cell* 15: 707-719.

32. Geula, S., S. Moshitch-Moshkovitz, D. Dominissini, A. A. Mansour, N. Kol, M. Salmon-Divon, V. Hershkovitz, E. Peer, N. Mor, Y. S. Manor, M. S. Ben-Haim, E. Eyal, S. Yunger, Y. Pinto, D. A. Jaitin, S. Viukov, Y. Rais, V. Krupalnik, E. Chomsky, M. Zerbib, I. Maza, Y. Rechavi, R. Massarwa, S. Hanna, I. Amit, E. Y. Levanon, N. Amariglio, N. Stern-Ginossar, N. Novershtern, G. Rechavi, and J. H. Hanna. 2015. Stem cells. m6A mRNA methylation facilitates resolution of naive pluripotency toward differentiation. *Science* 347: 1002-1006.

33. Fustin, J. M., M. Doi, Y. Yamaguchi, H. Hida, S. Nishimura, M. Yoshida, T. Isagawa, M. S. Morioka, H. Kakeya, I. Manabe, and H. Okamura. 2013. RNA-methylation-dependent RNA processing controls the speed of the circadian clock. *Cell* 155: 793-806.

34. Frayling, T. M., N. J. Timpson, M. N. Weedon, E. Zeggini, R. M. Freathy, C. M. Lindgren, J. R. Perry, K. S. Elliott, H. Lango, N. W. Rayner, B. Shields, L. W. Harries, J. C. Barrett, S. Ellard, C. J. Groves, B. Knight, A. M. Patch, A. R. Ness,

S. Ebrahim, D. A. Lawlor, S. M. Ring, Y. Ben-Shlomo, M. R. Jarvelin, U. Sovio, A. J. Bennett, D. Melzer, L. Ferrucci, R. J. Loos, I. Barroso, N. J. Wareham, F. Karpe, K. R. Owen, L. R. Cardon, M. Walker, G. A. Hitman, C. N. Palmer, A. S. Doney, A. D. Morris, G. D. Smith, A. T. Hattersley, and M. I. McCarthy. 2007. A common variant in the FTO gene is associated with body mass index and predisposes to childhood and adult obesity. *Science* 316: 889-894.

35. Dina, C., D. Meyre, S. Gallina, E. Durand, A. Korner, P. Jacobson, L. M. Carlsson, W. Kiess, V. Vatin, C. Lecoeur, J. Delplanque, E. Vaillant, F. Pattou, J. Ruiz, J. Weill, C. Levy-Marchal, F. Horber, N. Potoczna, S. Hercberg, C. Le Stunff, P. Bougneres, P. Kovacs, M. Marre, B. Balkau, S. Cauchi, J. C. Chevre, and P. Froguel. 2007. Variation in FTO contributes to childhood obesity and severe adult obesity. *Nat Genet* 39: 724-726.

36. Fischer, J., L. Koch, C. Emmerling, J. Vierkotten, T. Peters, J. C. Bruning, and U. Ruther. 2009. Inactivation of the Fto gene protects from obesity. *Nature* 458: 894-898.

37. Church, C., L. Moir, F. McMurray, C. Girard, G. T. Banks, L. Teboul, S. Wells, J. C. Bruning, P. M. Nolan, F. M. Ashcroft, and R. D. Cox. 2010. Overexpression of Fto leads to increased food intake and results in obesity. *Nat Genet* 42: 1086-1092.

38. Smemo, S., J. J. Tena, K. H. Kim, E. R. Gamazon, N. J. Sakabe, C. Gomez-Marin, I. Aneas, F. L. Credidio, D. R. Sobreira, N. F. Wasserman, J. H. Lee, V. Puviindran, D. Tam, M. Shen, J. E. Son, N. A. Vakili, H. K. Sung, S. Naranjo, R. D. Acemel, M. Manzanares, A. Nagy, N. J. Cox, C. C. Hui, J. L. Gomez-Skarmeta, and M. A. Nobrega. 2014. Obesity-associated variants within FTO form long-range functional connections with IRX3. *Nature* 507: 371-375.

39. Claussnitzer, M., S. N. Dankel, K. H. Kim, G. Quon, W. Meuleman, C. Haugen, V. Glunk, I. S. Sousa, J. L. Beaudry, V. Puviindran, N. A. Abdennur, J. Liu, P. A. Svensson, Y. H. Hsu, D. J. Drucker, G. Mellgren, C. C. Hui, H. Hauner, and M. Kellis. 2015. FTO Obesity Variant Circuitry and Adipocyte Browning in Humans. *N Engl J Med* 373: 895-907.

40. Zhang, C., D. Samanta, H. Lu, J. W. Bullen, H. Zhang, I. Chen, X. He, and G. L. Semenza. 2016. Hypoxia induces the breast cancer stem cell phenotype by HIF-dependent and ALKBH5-mediated m6A-demethylation of NANOG mRNA. *Proc Natl Acad Sci U S A*.

41. Thalhammer, A., Z. Bencokova, R. Poole, C. Loenarz, J. Adam, L. O'Flaherty, J. Schodel, D. Mole, K. Giaslakiotis, C. J. Schofield, E. M. Hammond, P. J. Ratcliffe, and P. J. Pollard. 2011. Human AlkB homologue 5 is a nuclear 2-oxoglutarate dependent oxygenase and a direct target of hypoxia-inducible factor 1alpha (HIF-1alpha). *PLoS One* 6: e16210.

42. Heddleston, J. M., Z. Li, J. D. Lathia, S. Bao, A. B. Hjelmeland, and J. N. Rich. 2010. Hypoxia inducible factors in cancer stem cells. *Br J Cancer* 102: 789-795.

43. Goodenberger, M. L., and R. B. Jenkins. 2012. Genetics of adult glioma. *Cancer Genet* 205: 613-621.

44. Louis, D. N., H. Ohgaki, O. D. Wiestler, W. K. Cavenee, P. C. Burger, A. Jouvet, B. W. Scheithauer, and P. Kleihues. 2007. The 2007 WHO classification of tumours of the central nervous system. *Acta Neuropathol* 114: 97-109.

45. Ostrom, Q. T., H. Gittleman, J. Fulop, M. Liu, R. Blanda, C. Kromer, Y. Wolinsky, C. Kruchko, and J. S. Barnholtz-Sloan. 2015. CBTRUS Statistical Report: Primary Brain and Central Nervous System Tumors Diagnosed in the United States in 2008-2012. *Neuro Oncol* 17 Suppl 4: iv1-iv62.

46. Biernat, W., H. Huang, H. Yokoo, P. Kleihues, and H. Ohgaki. 2004. Predominant expression of mutant EGFR (EGFRvIII) is rare in primary glioblastomas. *Brain Pathol* 14: 131-136.

47. Ohgaki, H., and P. Kleihues. 2005. Population-based studies on incidence, survival rates, and genetic alterations in astrocytic and oligodendroglial gliomas. *J Neuropathol Exp Neurol* 64: 479-489.

48. Verhaak, R. G., K. A. Hoadley, E. Purdom, V. Wang, Y. Qi, M. D. Wilkerson, C. R. Miller, L. Ding, T. Golub, J. P. Mesirov, G. Alexe, M. Lawrence, M. O'Kelly, P. Tamayo, B. A. Weir, S. Gabriel, W. Winckler, S. Gupta, L. Jakkula, H. S. Feiler, J. G. Hodgson, C. D. James, J. N. Sarkaria, C. Brennan, A. Kahn, P. T. Spellman, R. K. Wilson, T. P. Speed, J. W. Gray, M. Meyerson, G. Getz, C. M. Perou, D. N. Hayes, and N. Cancer Genome Atlas Research. 2010. Integrated genomic analysis identifies clinically relevant subtypes of glioblastoma characterized by abnormalities in PDGFRA, IDH1, EGFR, and NF1. *Cancer Cell* 17: 98-110.

49. Purow, B. W., and D. Schiff. 2010. Glioblastoma genetics: in rapid flux. *Discov Med* 9: 125-131.

50. Cancer Genome Atlas Research, N. 2008. Comprehensive genomic characterization defines human glioblastoma genes and core pathways. *Nature* 455: 1061-1068.

51. Blume-Jensen, P., and T. Hunter. 2001. Oncogenic kinase signalling. *Nature* 411: 355-365.

52. Nishikawa, R., X. D. Ji, R. C. Harmon, C. S. Lazar, G. N. Gill, W. K. Cavenee, and H. J. Huang. 1994. A mutant epidermal growth factor receptor common in

human glioma confers enhanced tumorigenicity. *Proc Natl Acad Sci U S A* 91: 7727-7731.

53. Ekstrand, A. J., C. D. James, W. K. Cavenee, B. Seliger, R. F. Pettersson, and V. P. Collins. 1991. Genes for epidermal growth factor receptor, transforming growth factor alpha, and epidermal growth factor and their expression in human gliomas in vivo. *Cancer Res* 51: 2164-2172.

54. Nishikawa, R., T. Sugiyama, Y. Narita, F. Furnari, W. K. Cavenee, and M. Matsutani. 2004. Immunohistochemical analysis of the mutant epidermal growth factor, deltaEGFR, in glioblastoma. *Brain Tumor Pathol* 21: 53-56.

55. Mao, H., D. G. Lebrun, J. Yang, V. F. Zhu, and M. Li. 2012. Deregulated signaling pathways in glioblastoma multiforme: molecular mechanisms and therapeutic targets. *Cancer Invest* 30: 48-56.

56. Inda, M. M., R. Bonavia, A. Mukasa, Y. Narita, D. W. Sah, S. Vandenberg, C. Brennan, T. G. Johns, R. Bachoo, P. Hadwiger, P. Tan, R. A. Depinho, W. Cavenee, and F. Furnari. 2010. Tumor heterogeneity is an active process maintained by a mutant EGFR-induced cytokine circuit in glioblastoma. *Genes Dev* 24: 1731-1745.

57. Fan, Q. W., C. K. Cheng, W. C. Gustafson, E. Charron, P. Zipper, R. A. Wong, J. Chen, J. Lau, C. Knobbe-Thomsen, M. Weller, N. Jura, G. Reifenberger, K. M. Shokat, and W. A. Weiss. 2013. EGFR phosphorylates tumor-derived EGFRvIII driving STAT3/5 and progression in glioblastoma. *Cancer Cell* 24: 438-449.

58. Huang, P. H., A. Mukasa, R. Bonavia, R. A. Flynn, Z. E. Brewer, W. K. Cavenee, F. B. Furnari, and F. M. White. 2007. Quantitative analysis of EGFRvIII cellular signaling networks reveals a combinatorial therapeutic strategy for glioblastoma. *Proc Natl Acad Sci U S A* 104: 12867-12872.

59. Jo, M., D. B. Stolz, J. E. Esplen, K. Dorko, G. K. Michalopoulos, and S. C. Strom. 2000. Cross-talk between epidermal growth factor receptor and c-Met signal pathways in transformed cells. *J Biol Chem* 275: 8806-8811.

60. Reznik, T. E., Y. Sang, Y. Ma, R. Abounader, E. M. Rosen, S. Xia, and J. Laterra. 2008. Transcription-dependent epidermal growth factor receptor activation by hepatocyte growth factor. *Mol Cancer Res* 6: 139-150.

61. Clarke, I. D., and P. B. Dirks. 2003. A human brain tumor-derived PDGFR-alpha deletion mutant is transforming. *Oncogene* 22: 722-733.

62. Kumabe, T., Y. Sohma, T. Kayama, T. Yoshimoto, and T. Yamamoto. 1992. Amplification of alpha-platelet-derived growth factor receptor gene lacking an exon coding for a portion of the extracellular region in a primary brain tumor of glial origin. *Oncogene* 7: 627-633.

63. Ozawa, T., C. W. Brennan, L. Wang, M. Squatrito, T. Sasayama, M. Nakada, J. T. Huse, A. Pedraza, S. Utsuki, Y. Yasui, A. Tandon, E. I. Fomchenko, H. Oka, R. L. Levine, K. Fujii, M. Ladanyi, and E. C. Holland. 2010. PDGFRA gene rearrangements are frequent genetic events in PDGFRA-amplified glioblastomas. *Genes Dev* 24: 2205-2218.

64. Nazarenko, I., S. M. Hede, X. He, A. Hedren, J. Thompson, M. S. Lindstrom, and M. Nister. 2012. PDGF and PDGF receptors in glioma. *Ups J Med Sci* 117: 99-112.

65. Carnero, A., C. Blanco-Aparicio, O. Renner, W. Link, and J. F. Leal. 2008. The PTEN/PI3K/AKT signalling pathway in cancer, therapeutic implications. *Curr Cancer Drug Targets* 8: 187-198.

66. Yuan, T. L., and L. C. Cantley. 2008. PI3K pathway alterations in cancer: variations on a theme. *Oncogene* 27: 5497-5510.

67. Teng, D. H., R. Hu, H. Lin, T. Davis, D. Iliev, C. Frye, B. Swedlund, K. L. Hansen, V. L. Vinson, K. L. Gumpper, L. Ellis, A. El-Naggar, M. Frazier, S. Jasser, L. A. Langford, J. Lee, G. B. Mills, M. A. Pershouse, R. E. Pollack, C. Tornos, P. Troncoso, W. K. Yung, G. Fujii, A. Berson, P. A. Steck, and et al. 1997. MMAC1/PTEN mutations in primary tumor specimens and tumor cell lines. *Cancer Res* 57: 5221-5225.

68. Tohma, Y., C. Gratas, W. Biernat, A. Peraud, M. Fukuda, Y. Yonekawa, P. Kleihues, and H. Ohgaki. 1998. PTEN (MMAC1) mutations are frequent in primary glioblastomas (de novo) but not in secondary glioblastomas. *J Neuropathol Exp Neurol* 57: 684-689.

69. Wang, S. I., J. Puc, J. Li, J. N. Bruce, P. Cairns, D. Sidransky, and R. Parsons. 1997. Somatic mutations of PTEN in glioblastoma multiforme. *Cancer Res* 57: 4183-4186.

70. Vivanco, I., D. Rohle, M. Versele, A. Iwanami, D. Kuga, B. Oldrini, K. Tanaka, J. Dang, S. Kubek, N. Palaskas, T. Hsueh, M. Evans, D. Mulholland, D. Wolle, S. Rajasekaran, A. Rajasekaran, L. M. Liau, T. F. Cloughesy, I. Dikic, C. Brennan, H. Wu, P. S. Mischel, T. Perera, and I. K. Mellinghoff. 2010. The phosphatase and tensin homolog regulates epidermal growth factor receptor (EGFR) inhibitor response by targeting EGFR for degradation. *Proc Natl Acad Sci U S A* 107: 6459-6464.

71. Wang, X., L. C. Trotman, T. Koppie, A. Alimonti, Z. Chen, Z. Gao, J. Wang, H. Erdjument-Bromage, P. Tempst, C. Cordon-Cardo, P. P. Pandolfi, and X. Jiang. 2007. NEDD4-1 is a proto-oncogenic ubiquitin ligase for PTEN. *Cell* 128: 129-139.

72. Dai, B., R. O. Pieper, D. Li, P. Wei, M. Liu, S. Y. Woo, K. D. Aldape, R. Sawaya, K. Xie, and S. Huang. 2010. FoxM1B regulates NEDD4-1 expression, leading to cellular transformation and full malignant phenotype in immortalized human astrocytes. *Cancer Res* 70: 2951-2961.

73. Hay, N., and N. Sonenberg. 2004. Upstream and downstream of mTOR. *Genes Dev* 18: 1926-1945.

74. Roberts, P. J., and C. J. Der. 2007. Targeting the Raf-MEK-ERK mitogen-activated protein kinase cascade for the treatment of cancer. *Oncogene* 26: 3291-3310.

75. Dasgupta, B., W. Li, A. Perry, and D. H. Gutmann. 2005. Glioma formation in neurofibromatosis 1 reflects preferential activation of K-RAS in astrocytes. *Cancer Res* 65: 236-245.

76. McGillicuddy, L. T., J. A. Fromm, P. E. Hollstein, S. Kubek, R. Beroukhim, T. De Raedt, B. W. Johnson, S. M. Williams, P. Nghiemphu, L. M. Liau, T. F. Cloughesy, P. S. Mischel, A. Parret, J. Seiler, G. Moldenhauer, K. Scheffzek, A. O. Stemmer-Rachamimov, C. L. Sawyers, C. Brennan, L. Messiaen, I. K. Mellinghoff, and K. Cichowski. 2009. Proteasomal and genetic inactivation of the NF1 tumor suppressor in gliomagenesis. *Cancer Cell* 16: 44-54.

77. Reifenberger, G., L. Liu, K. Ichimura, E. E. Schmidt, and V. P. Collins. 1993. Amplification and overexpression of the MDM2 gene in a subset of human malignant gliomas without p53 mutations. *Cancer Res* 53: 2736-2739.

78. Ruas, M., and G. Peters. 1998. The p16INK4a/CDKN2A tumor suppressor and its relatives. *Biochim Biophys Acta* 1378: F115-177.

79. Kamijo, T., F. Zindy, M. F. Roussel, D. E. Quelle, J. R. Downing, R. A. Ashmun, G. Grosveld, and C. J. Sherr. 1997. Tumor suppression at the mouse INK4a

locus mediated by the alternative reading frame product p19ARF. *Cell* 91: 649-659.

80. Zhang, Y., Y. Xiong, and W. G. Yarbrough. 1998. ARF promotes MDM2 degradation and stabilizes p53: ARF-INK4a locus deletion impairs both the Rb and p53 tumor suppression pathways. *Cell* 92: 725-734.

81. Kamijo, T., J. D. Weber, G. Zambetti, F. Zindy, M. F. Roussel, and C. J. Sherr. 1998. Functional and physical interactions of the ARF tumor suppressor with p53 and Mdm2. *Proc Natl Acad Sci U S A* 95: 8292-8297.

82. Clarke, M. F., J. E. Dick, P. B. Dirks, C. J. Eaves, C. H. Jamieson, D. L. Jones, J. Visvader, I. L. Weissman, and G. M. Wahl. 2006. Cancer stem cells--perspectives on current status and future directions: AACR Workshop on cancer stem cells. *Cancer Res* 66: 9339-9344.

83. Singh, S. K., C. Hawkins, I. D. Clarke, J. A. Squire, J. Bayani, T. Hide, R. M. Henkelman, M. D. Cusimano, and P. B. Dirks. 2004. Identification of human brain tumour initiating cells. *Nature* 432: 396-401.

84. Lee, J., S. Kotliarova, Y. Kotliarov, A. Li, Q. Su, N. M. Donin, S. Pastorino, B. W. Purow, N. Christopher, W. Zhang, J. K. Park, and H. A. Fine. 2006. Tumor stem cells derived from glioblastomas cultured in bFGF and EGF more closely mirror the phenotype and genotype of primary tumors than do serum-cultured cell lines. *Cancer Cell* 9: 391-403.

85. Lathia, J. D., S. C. Mack, E. E. Mulkearns-Hubert, C. L. Valentim, and J. N. Rich. 2015. Cancer stem cells in glioblastoma. *Genes Dev* 29: 1203-1217.

86. Suva, M. L., E. Rheinbay, S. M. Gillespie, A. P. Patel, H. Wakimoto, S. D. Rabkin, N. Riggi, A. S. Chi, D. P. Cahill, B. V. Nahed, W. T. Curry, R. L. Martuza, M. N. Rivera, N. Rossetti, S. Kasif, S. Beik, S. Kadri, I. Tirosh, I. Wortman, A. K.

Shalek, O. Rozenblatt-Rosen, A. Regev, D. N. Louis, and B. E. Bernstein. 2014. Reconstructing and reprogramming the tumor-propagating potential of glioblastoma stem-like cells. *Cell* 157: 580-594.

87. Gallo, M., J. Ho, F. J. Coutinho, R. Vanner, L. Lee, R. Head, E. K. Ling, I. D. Clarke, and P. B. Dirks. 2013. A tumorigenic MLL-homeobox network in human glioblastoma stem cells. *Cancer Res* 73: 417-427.

88. Gallo, M., F. J. Coutinho, R. J. Vanner, T. Gayden, S. C. Mack, A. Murison, M. Remke, R. Li, N. Takayama, K. Desai, L. Lee, X. Lan, N. I. Park, D. Barsyte-Lovejoy, D. Smil, D. Sturm, M. M. Kushida, R. Head, M. D. Cusimano, M. Bernstein, I. D. Clarke, J. E. Dick, S. M. Pfister, J. N. Rich, C. H. Arrowsmith, M. D. Taylor, N. Jabado, D. P. Bazett-Jones, M. Lupien, and P. B. Dirks. 2015. MLL5 Orchestrates a Cancer Self-Renewal State by Repressing the Histone Variant H3.3 and Globally Reorganizing Chromatin. *Cancer Cell* 28: 715-729.

89. Kim, E., M. Kim, D. H. Woo, Y. Shin, J. Shin, N. Chang, Y. T. Oh, H. Kim, J. Rheey, I. Nakano, C. Lee, K. M. Joo, J. N. Rich, D. H. Nam, and J. Lee. 2013. Phosphorylation of EZH2 activates STAT3 signaling via STAT3 methylation and promotes tumorigenicity of glioblastoma stem-like cells. *Cancer Cell* 23: 839-852.

90. Li, Z., S. Bao, Q. Wu, H. Wang, C. Eyler, S. Sathornsumetee, Q. Shi, Y. Cao, J. Lathia, R. E. McLendon, A. B. Hjelmeland, and J. N. Rich. 2009. Hypoxia-inducible factors regulate tumorigenic capacity of glioma stem cells. *Cancer Cell* 15: 501-513.

91. Flavahan, W. A., Q. Wu, M. Hitomi, N. Rahim, Y. Kim, A. E. Sloan, R. J. Weil, I. Nakano, J. N. Sarkaria, B. W. Stringer, B. W. Day, M. Li, J. D. Lathia, J. N. Rich, and A. B. Hjelmeland. 2013. Brain tumor initiating cells adapt to restricted nutrition through preferential glucose uptake. *Nat Neurosci* 16: 1373-1382.

92. Xie, Q., Q. Wu, C. M. Horbinski, W. A. Flavahan, K. Yang, W. Zhou, S. M. Dombrowski, Z. Huang, X. Fang, Y. Shi, A. N. Ferguson, D. F. Kashatus, S. Bao, and J. N. Rich. 2015. Mitochondrial control by DRP1 in brain tumor initiating cells. *Nat Neurosci* 18: 501-510.

93. Ricci-Vitiani, L., R. Pallini, M. Biffoni, M. Todaro, G. Invernici, T. Cenci, G. Maira, E. A. Parati, G. Stassi, L. M. Larocca, and R. De Maria. 2010. Tumour vascularization via endothelial differentiation of glioblastoma stem-like cells. *Nature* 468: 824-828.

94. Wang, R., K. Chadalavada, J. Wilshire, U. Kowalik, K. E. Hovinga, A. Geber, B. Fligelman, M. Leversha, C. Brennan, and V. Tabar. 2010. Glioblastoma stem-like cells give rise to tumour endothelium. *Nature* 468: 829-833.

95. Cheng, L., Z. Huang, W. Zhou, Q. Wu, S. Donnola, J. K. Liu, X. Fang, A. E. Sloan, Y. Mao, J. D. Lathia, W. Min, R. E. McLendon, J. N. Rich, and S. Bao. 2013. Glioblastoma stem cells generate vascular pericytes to support vessel function and tumor growth. *Cell* 153: 139-152.

96. Zheng, H., H. Ying, R. Wiedemeyer, H. Yan, S. N. Quayle, E. V. Ivanova, J. H. Paik, H. Zhang, Y. Xiao, S. R. Perry, J. Hu, A. Vinjamoori, B. Gan, E. Sahin, M. G. Chheda, C. Brennan, Y. A. Wang, W. C. Hahn, L. Chin, and R. A. DePinho. 2010. PLAGL2 regulates Wnt signaling to impede differentiation in neural stem cells and gliomas. *Cancer Cell* 17: 497-509.

97. Zhang, N., P. Wei, A. Gong, W. T. Chiu, H. T. Lee, H. Colman, H. Huang, J. Xue, M. Liu, Y. Wang, R. Sawaya, K. Xie, W. K. Yung, R. H. Medema, X. He, and S. Huang. 2011. FoxM1 promotes beta-catenin nuclear localization and controls Wnt target-gene expression and glioma tumorigenesis. *Cancer Cell* 20: 427-442.

98. Kim, Y., E. Kim, Q. Wu, O. Guryanova, M. Hitomi, J. D. Lathia, D. Serwanski, A. E. Sloan, R. J. Weil, J. Lee, A. Nishiyama, S. Bao, A. B. Hjelmeland, and J. N. Rich. 2012. Platelet-derived growth factor receptors differentially inform intertumoral and intratumoral heterogeneity. *Genes Dev* 26: 1247-1262.

99. Gong, A. H., P. Wei, S. Zhang, J. Yao, Y. Yuan, A. D. Zhou, F. F. Lang, A. B. Heimberger, G. Rao, and S. Huang. 2015. FoxM1 Drives a Feed-Forward STAT3-Activation Signaling Loop That Promotes the Self-Renewal and Tumorigenicity of Glioblastoma Stem-like Cells. *Cancer research* 75: 2337-2348.

100. Bao, S., Q. Wu, R. E. McLendon, Y. Hao, Q. Shi, A. B. Hjelmeland, M. W. Dewhirst, D. D. Bigner, and J. N. Rich. 2006. Glioma stem cells promote radioresistance by preferential activation of the DNA damage response. *Nature* 444: 756-760.

101. Chen, J., Y. Li, T. S. Yu, R. M. McKay, D. K. Burns, S. G. Kernie, and L. F. Parada. 2012. A restricted cell population propagates glioblastoma growth after chemotherapy. *Nature* 488: 522-526.

102. Laoukili, J., M. Stahl, and R. H. Medema. 2007. FoxM1: at the crossroads of ageing and cancer. *Biochim Biophys Acta* 1775: 92-102.

103. Ye, H., T. F. Kelly, U. Samadani, L. Lim, S. Rubio, D. G. Overdier, K. A. Roebuck, and R. H. Costa. 1997. Hepatocyte nuclear factor 3/fork head homolog 11 is expressed in proliferating epithelial and mesenchymal cells of embryonic and adult tissues. *Mol Cell Biol* 17: 1626-1641.

104. Li, Y., S. Zhang, and S. Huang. 2012. FoxM1: a potential drug target for glioma. *Future oncology* 8: 223-226.

105. Wang, I. C., Y. J. Chen, D. Hughes, V. Petrovic, M. L. Major, H. J. Park, Y. Tan, T. Ackerson, and R. H. Costa. 2005. Forkhead box M1 regulates the

transcriptional network of genes essential for mitotic progression and genes encoding the SCF (Skp2-Cks1) ubiquitin ligase. *Mol Cell Biol* 25: 10875-10894.

106. Laoukili, J., M. R. Kooistra, A. Bras, J. Kauw, R. M. Kerkhoven, A. Morrison, H. Clevers, and R. H. Medema. 2005. FoxM1 is required for execution of the mitotic programme and chromosome stability. *Nat Cell Biol* 7: 126-136.

107. Wonsey, D. R., and M. T. Follettie. 2005. Loss of the forkhead transcription factor FoxM1 causes centrosome amplification and mitotic catastrophe. *Cancer Res* 65: 5181-5189.

108. Wierstra, I., and J. Alves. 2007. FOXM1, a typical proliferation-associated transcription factor. *Biol Chem* 388: 1257-1274.

109. Liu, M., B. Dai, S. H. Kang, K. Ban, F. J. Huang, F. F. Lang, K. D. Aldape, T. X. Xie, C. E. Pelloski, K. Xie, R. Sawaya, and S. Huang. 2006. FoxM1B is overexpressed in human glioblastomas and critically regulates the tumorigenicity of glioma cells. *Cancer research* 66: 3593-3602.

110. Dai, B., S. H. Kang, W. Gong, M. Liu, K. D. Aldape, R. Sawaya, and S. Huang. 2007. Aberrant FoxM1B expression increases matrix metalloproteinase-2 transcription and enhances the invasion of glioma cells. *Oncogene* 26: 6212-6219.

111. Zhang, Y., N. Zhang, B. Dai, M. Liu, R. Sawaya, K. Xie, and S. Huang. 2008. FoxM1B transcriptionally regulates vascular endothelial growth factor expression and promotes the angiogenesis and growth of glioma cells. *Cancer Res* 68: 8733-8742.

112. Dai, B., A. Gong, Z. Jing, K. D. Aldape, S. H. Kang, R. Sawaya, and S. Huang. 2013. Forkhead box M1 is regulated by heat shock factor 1 and promotes glioma cells survival under heat shock stress. *J Biol Chem* 288: 1634-1642.

113. Zhang, N., X. Wu, L. Yang, F. Xiao, H. Zhang, A. Zhou, Z. Huang, and S. Huang. 2012. FoxM1 inhibition sensitizes resistant glioblastoma cells to temozolomide by downregulating the expression of DNA-repair gene Rad51. *Clin Cancer Res* 18: 5961-5971.

114. Xue, J., A. Zhou, C. Tan, Y. Wu, H. T. Lee, W. Li, K. Xie, and S. Huang. 2015. Forkhead Box M1 Is Essential for Nuclear Localization of Glioma-associated Oncogene Homolog 1 in Glioblastoma Multiforme Cells by Promoting Importin-7 Expression. *J Biol Chem* 290: 18662-18670.

115. Clement, V., P. Sanchez, N. de Tribolet, I. Radovanovic, and A. Ruiz i Altaba. 2007. HEDGEHOG-GLI1 signaling regulates human glioma growth, cancer stem cell self-renewal, and tumorigenicity. *Curr Biol* 17: 165-172.

116. Cao, Y., J. D. Lathia, C. E. Eyler, Q. Wu, Z. Li, H. Wang, R. E. McLendon, A. B. Hjelmeland, and J. N. Rich. 2010. Erythropoietin Receptor Signaling Through STAT3 Is Required For Glioma Stem Cell Maintenance. *Genes Cancer* 1: 50-61.

117. Wang, H., J. D. Lathia, Q. Wu, J. Wang, Z. Li, J. M. Heddleston, C. E. Eyler, J. Elderbroom, J. Gallagher, J. Schuschu, J. MacSwords, Y. Cao, R. E. McLendon, X. F. Wang, A. B. Hjelmeland, and J. N. Rich. 2009. Targeting interleukin 6 signaling suppresses glioma stem cell survival and tumor growth. *Stem Cells* 27: 2393-2404.

118. Sherry, M. M., A. Reeves, J. K. Wu, and B. H. Cochran. 2009. STAT3 is required for proliferation and maintenance of multipotency in glioblastoma stem cells. *Stem Cells* 27: 2383-2392.

119. Schonberg, D. L., T. E. Miller, Q. Wu, W. A. Flavahan, N. K. Das, J. S. Hale, C. G. Hubert, S. C. Mack, A. M. Jarrar, R. T. Karl, A. M. Rosager, A. M. Nixon, P. J. Tesar, P. Hamerlik, B. W. Kristensen, C. Horbinski, J. R. Connor, P. L. Fox, J. D.

Lathia, and J. N. Rich. 2015. Preferential Iron Trafficking Characterizes Glioblastoma Stem-like Cells. *Cancer Cell* 28: 441-455.

120. Joshi, K., Y. Banasavadi-Siddegowda, X. Mo, S. H. Kim, P. Mao, C. Kig, D. Nardini, R. W. Sobol, L. M. Chow, H. I. Kornblum, R. Waclaw, M. Beullens, and I. Nakano. 2013. MELK-dependent FOXM1 phosphorylation is essential for proliferation of glioma stem cells. *Stem Cells* 31: 1051-1063.

121. Kim, S. H., K. Joshi, R. Ezhilarasan, T. R. Myers, J. Siu, C. Gu, M. Nakano-Okuno, D. Taylor, M. Minata, E. P. Sulman, J. Lee, K. P. Bhat, A. E. Salcini, and I. Nakano. 2015. EZH2 protects glioma stem cells from radiation-induced cell death in a MELK/FOXM1-dependent manner. *Stem cell reports* 4: 226-238.

122. Wang, Z., S. Zhang, T. L. Siu, and S. Huang. 2015. Glioblastoma multiforme formation and EMT: role of FoxM1 transcription factor. *Curr Pharm Des* 21: 1268-1271.

123. Carroll, S. M., P. Narayan, and F. M. Rottman. 1990. N6-methyladenosine residues in an intron-specific region of prolactin pre-mRNA. *Mol Cell Biol* 10: 4456-4465.

124. Chen, R., M. C. Nishimura, S. M. Bumbaca, S. Kharbanda, W. F. Forrest, I. M. Kasman, J. M. Greve, R. H. Soriano, L. L. Gilmour, C. S. Rivers, Z. Modrusan, S. Nacu, S. Guerrero, K. A. Edgar, J. J. Wallin, K. Lamszus, M. Westphal, S. Heim, C. D. James, S. R. VandenBerg, J. F. Costello, S. Moorefield, C. J. Cowdrey, M. Prados, and H. S. Phillips. 2010. A hierarchy of self-renewing tumor-initiating cell types in glioblastoma. *Cancer Cell* 17: 362-375.

125. Chong, Y. K., E. Sandanaraj, L. W. Koh, M. Thangaveloo, M. S. Tan, G. R. Koh, T. B. Toh, G. G. Lim, J. D. Holbrook, O. L. Kon, M. Nadarajah, I. Ng, W. H. Ng, N. S. Tan, K. L. Lim, C. Tang, and B. T. Ang. 2016. ST3GAL1-Associated

Transcriptomic Program in Glioblastoma Tumor Growth, Invasion, and Prognosis. *J Natl Cancer Inst* 108.

126. Hodgson, J. G., R. F. Yeh, A. Ray, N. J. Wang, I. Smirnov, M. Yu, S. Hariono, J. Silber, H. S. Feiler, J. W. Gray, P. T. Spellman, S. R. Vandenberg, M. S. Berger, and C. D. James. 2009. Comparative analyses of gene copy number and mRNA expression in glioblastoma multiforme tumors and xenografts. *Neuro-oncology* 11: 477-487.

127. Bai, H., A. S. Harmanci, E. Z. Erson-Omay, J. Li, S. Coskun, M. Simon, B. Krischek, K. Ozduman, S. B. Omay, E. A. Sorensen, S. Turcan, M. Bakirciglu, G. Carrion-Grant, P. B. Murray, V. E. Clark, A. G. Ercan-Sencicek, J. Knight, L. Sencar, S. Altinok, L. D. Kaulen, B. Gulez, M. Timmer, J. Schramm, K. Mishra-Gorur, O. Henegariu, J. Moliterno, A. Louvi, T. A. Chan, S. L. Tannheimer, M. N. Pamir, A. O. Vortmeyer, K. Bilguvar, K. Yasuno, and M. Gunel. 2016. Integrated genomic characterization of IDH1-mutant glioma malignant progression. *Nat Genet* 48: 59-66.

128. Lee, Y., K. H. Kim, D. G. Kim, H. J. Cho, Y. Kim, J. Rheey, K. Shin, Y. J. Seo, Y. S. Choi, J. I. Lee, J. Lee, K. M. Joo, and D. H. Nam. 2015. FoxM1 Promotes Stemness and Radio-Resistance of Glioblastoma by Regulating the Master Stem Cell Regulator Sox2. *PLoS One* 10: e0137703.

129. Noushmehr, H., D. J. Weisenberger, K. Diefes, H. S. Phillips, K. Pujara, B. P. Berman, F. Pan, C. E. Pelloski, E. P. Sulman, K. P. Bhat, R. G. Verhaak, K. A. Hoadley, D. N. Hayes, C. M. Perou, H. K. Schmidt, L. Ding, R. K. Wilson, D. Van Den Berg, H. Shen, H. Bengtsson, P. Neuvial, L. M. Cope, J. Buckley, J. G. Herman, S. B. Baylin, P. W. Laird, K. Aldape, and N. Cancer Genome Atlas

Research. 2010. Identification of a CpG island methylator phenotype that defines a distinct subgroup of glioma. *Cancer Cell* 17: 510-522.

130. Sonoda, Y., T. Ozawa, Y. Hirose, K. D. Aldape, M. McMahon, M. S. Berger, and R. O. Pieper. 2001. Formation of intracranial tumors by genetically modified human astrocytes defines four pathways critical in the development of human anaplastic astrocytoma. *Cancer Res* 61: 4956-4960.

131. Tsai, M. C., O. Manor, Y. Wan, N. Mosammaparast, J. K. Wang, F. Lan, Y. Shi, E. Segal, and H. Y. Chang. 2010. Long noncoding RNA as modular scaffold of histone modification complexes. *Science* 329: 689-693.

132. Wuarin, J., and U. Schibler. 1994. Physical isolation of nascent RNA chains transcribed by RNA polymerase II: evidence for cotranscriptional splicing. *Mol Cell Biol* 14: 7219-7225.

133. Brennan, C. W., R. G. Verhaak, A. McKenna, B. Campos, H. Noushmehr, S. R. Salama, S. Zheng, D. Chakravarty, J. Z. Sanborn, S. H. Berman, R. Beroukhim, B. Bernard, C. J. Wu, G. Genovese, I. Shmulevich, J. Barnholtz-Sloan, L. Zou, R. Vegesna, S. A. Shukla, G. Ciriello, W. K. Yung, W. Zhang, C. Sougnez, T. Mikkelsen, K. Aldape, D. D. Bigner, E. G. Van Meir, M. Prados, A. Sloan, K. L. Black, J. Eschbacher, G. Finocchiaro, W. Friedman, D. W. Andrews, A. Guha, M. Iacocca, B. P. O'Neill, G. Foltz, J. Myers, D. J. Weisenberger, R. Penny, R. Kucherlapati, C. M. Perou, D. N. Hayes, R. Gibbs, M. Marra, G. B. Mills, E. Lander, P. Spellman, R. Wilson, C. Sander, J. Weinstein, M. Meyerson, S. Gabriel, P. W. Laird, D. Haussler, G. Getz, L. Chin, and T. R. Network. 2013. The somatic genomic landscape of glioblastoma. *Cell* 155: 462-477.

134. Bhat, K. P., V. Balasubramaniyan, B. Vaillant, R. Ezhilarasan, K. Hummelink, F. Hollingsworth, K. Wani, L. Heathcock, J. D. James, L. D. Goodman, S. Conroy,

L. Long, N. Lelic, S. Wang, J. Gumin, D. Raj, Y. Kodama, A. Raghunathan, A. Olar, K. Joshi, C. E. Pelloski, A. Heimberger, S. H. Kim, D. P. Cahill, G. Rao, W. F. Den Dunnen, H. W. Boddeke, H. S. Phillips, I. Nakano, F. F. Lang, H. Colman, E. P. Sulman, and K. Aldape. 2013. Mesenchymal differentiation mediated by NF-kappaB promotes radiation resistance in glioblastoma. *Cancer Cell* 24: 331-346.

135. Anders, L., N. Ke, P. Hydbring, Y. J. Choi, H. R. Widlund, J. M. Chick, H. Zhai, M. Vidal, S. P. Gygi, P. Braun, and P. Sicinski. 2011. A systematic screen for CDK4/6 substrates links FOXM1 phosphorylation to senescence suppression in cancer cells. *Cancer Cell* 20: 620-634.

136. Linder, B., A. V. Grozhik, A. O. Olarerin-George, C. Meydan, C. E. Mason, and S. R. Jaffrey. 2015. Single-nucleotide-resolution mapping of m6A and m6Am throughout the transcriptome. *Nat Methods* 12: 767-772.

137. Ke, S., E. A. Alemu, C. Mertens, E. C. Gantman, J. J. Fak, A. Mele, B. Haripal, I. Zucker-Scharff, M. J. Moore, C. Y. Park, C. B. Vagbo, A. Kussnierczyk, A. Klungland, J. E. Darnell, Jr., and R. B. Darnell. 2015. A majority of m6A residues are in the last exons, allowing the potential for 3' UTR regulation. *Genes Dev* 29: 2037-2053.

138. Girard, C., C. L. Will, J. Peng, E. M. Makarov, B. Kastner, I. Lemm, H. Urlaub, K. Hartmuth, and R. Luhrmann. 2012. Post-transcriptional spliceosomes are retained in nuclear speckles until splicing completion. *Nature communications* 3: 994.

139. Spector, D. L., and A. I. Lamond. 2011. Nuclear speckles. *Cold Spring Harb Perspect Biol* 3.

140. Bhatt, D. M., A. Pandya-Jones, A. J. Tong, I. Barozzi, M. M. Lissner, G. Natoli, D. L. Black, and S. T. Smale. 2012. Transcript dynamics of proinflammatory genes revealed by sequence analysis of subcellular RNA fractions. *Cell* 150: 279-290.

141. Ameur, A., A. Zaghlool, J. Halvardson, A. Wetterbom, U. Gyllensten, L. Cavelier, and L. Feuk. 2011. Total RNA sequencing reveals nascent transcription and widespread co-transcriptional splicing in the human brain. *Nat Struct Mol Biol* 18: 1435-1440.

142. Chen, K., Z. Lu, X. Wang, Y. Fu, G. Z. Luo, N. Liu, D. Han, D. Dominissini, Q. Dai, T. Pan, and C. He. 2015. High-resolution N(6) -methyladenosine (m(6) A) map using photo-crosslinking-assisted m(6) A sequencing. *Angew Chem Int Ed Engl* 54: 1587-1590.

143. Sun, W. J., J. H. Li, S. Liu, J. Wu, H. Zhou, L. H. Qu, and J. H. Yang. 2015. RMBase: a resource for decoding the landscape of RNA modifications from high-throughput sequencing data. *Nucleic Acids Res*.

144. Mukherjee, N., D. L. Corcoran, J. D. Nusbaum, D. W. Reid, S. Georgiev, M. Hafner, M. Ascano, Jr., T. Tuschl, U. Ohler, and J. D. Keene. 2011. Integrative regulatory mapping indicates that the RNA-binding protein HuR couples pre-mRNA processing and mRNA stability. *Mol Cell* 43: 327-339.

145. Lebedeva, S., M. Jens, K. Theil, B. Schwanhausser, M. Selbach, M. Landthaler, and N. Rajewsky. 2011. Transcriptome-wide analysis of regulatory interactions of the RNA-binding protein HuR. *Mol Cell* 43: 340-352.

146. Chang, N., J. Yi, G. Guo, X. Liu, Y. Shang, T. Tong, Q. Cui, M. Zhan, M. Gorospe, and W. Wang. 2010. HuR uses AUF1 as a cofactor to promote p16INK4 mRNA decay. *Mol Cell Biol* 30: 3875-3886.

147. Aguilo, F., F. Zhang, A. Sancho, M. Fidalgo, S. Di Cecilia, A. Vashisht, D. F. Lee, C. H. Chen, M. Rengasamy, B. Andino, F. Jahouh, A. Roman, S. R. Krig, R. Wang, W. Zhang, J. A. Wohlschlegel, J. Wang, and M. J. Walsh. 2015. Coordination of m(6)A mRNA Methylation and Gene Transcription by ZFP217 Regulates Pluripotency and Reprogramming. *Cell Stem Cell* 17: 689-704.

148. Chen, T., Y. J. Hao, Y. Zhang, M. M. Li, M. Wang, W. Han, Y. Wu, Y. Lv, J. Hao, L. Wang, A. Li, Y. Yang, K. X. Jin, X. Zhao, Y. Li, X. L. Ping, W. Y. Lai, L. G. Wu, G. Jiang, H. L. Wang, L. Sang, X. J. Wang, Y. G. Yang, and Q. Zhou. 2015. m(6)A RNA methylation is regulated by microRNAs and promotes reprogramming to pluripotency. *Cell Stem Cell* 16: 289-301.

149. Faghihi, M. A., and C. Wahlestedt. 2009. Regulatory roles of natural antisense transcripts. *Nat Rev Mol Cell Biol* 10: 637-643.

150. Calvet, J. P., and T. Pederson. 1979. Heterogeneous nuclear RNA double-stranded regions probed in living HeLa cells by crosslinking with the psoralen derivative aminomethyltrioxsalen. *Proc Natl Acad Sci U S A* 76: 755-759.

151. Qiang, L., T. Wu, H. W. Zhang, N. Lu, R. Hu, Y. J. Wang, L. Zhao, F. H. Chen, X. T. Wang, Q. D. You, and Q. L. Guo. 2012. HIF-1alpha is critical for hypoxia-mediated maintenance of glioblastoma stem cells by activating Notch signaling pathway. *Cell Death Differ* 19: 284-294.

152. Hein, M. Y., N. C. Hubner, I. Poser, J. Cox, N. Nagaraj, Y. Toyoda, I. A. Gak, I. Weisswange, J. Mansfeld, F. Buchholz, A. A. Hyman, and M. Mann. 2015. A human interactome in three quantitative dimensions organized by stoichiometries and abundances. *Cell* 163: 712-723.

153. Rehwinkel, J., A. Herold, K. Gari, T. Kocher, M. Rode, F. L. Ciccarelli, M. Wilm, and E. Izaurralde. 2004. Genome-wide analysis of mRNAs regulated by the THO complex in Drosophila melanogaster. *Nat Struct Mol Biol* 11: 558-566.

154. Strasser, K., S. Masuda, P. Mason, J. Pfannstiel, M. Oppizzi, S. Rodriguez-Navarro, A. G. Rondon, A. Aguilera, K. Struhl, R. Reed, and E. Hurt. 2002. TREX is a conserved complex coupling transcription with messenger RNA export. *Nature* 417: 304-308.

155. Larochelle, M., J. F. Lemay, and F. Bachand. 2012. The THO complex cooperates with the nuclear RNA surveillance machinery to control small nucleolar RNA expression. *Nucleic Acids Res* 40: 10240-10253.

156. Katayama, S., Y. Tomaru, T. Kasukawa, K. Waki, M. Nakanishi, M. Nakamura, H. Nishida, C. C. Yap, M. Suzuki, J. Kawai, H. Suzuki, P. Carninci, Y. Hayashizaki, C. Wells, M. Frith, T. Ravasi, K. C. Pang, J. Hallinan, J. Mattick, D. A. Hume, L. Lipovich, S. Batalov, P. G. Engstrom, Y. Mizuno, M. A. Faghihi, A. Sandelin, A. M. Chalk, S. Mottagui-Tabar, Z. Liang, B. Lenhard, C. Wahlestedt, R. G. E. R. Group, G. Genome Science, and F. Consortium. 2005. Antisense transcription in the mammalian transcriptome. *Science* 309: 1564-1566.

157. Pelechano, V., and L. M. Steinmetz. 2013. Gene regulation by antisense transcription. *Nat Rev Genet* 14: 880-893.

158. Yan, H., D. W. Parsons, G. Jin, R. McLendon, B. A. Rasheed, W. Yuan, I. Kos, I. Batinic-Haberle, S. Jones, G. J. Riggins, H. Friedman, A. Friedman, D. Reardon, J. Herndon, K. W. Kinzler, V. E. Velculescu, B. Vogelstein, and D. D. Bigner. 2009. IDH1 and IDH2 mutations in gliomas. *N Engl J Med* 360: 765-773.

159. Yang, H., D. Ye, K. L. Guan, and Y. Xiong. 2012. IDH1 and IDH2 mutations in tumorigenesis: mechanistic insights and clinical perspectives. *Clin Cancer Res* 18: 5562-5571.

160. Chen, Y., Y. Li, J. Xue, A. Gong, G. Yu, A. Zhou, K. Lin, S. Zhang, N. Zhang, C. J. Gottardi, and S. Huang. 2016. Wnt-induced deubiquitination FoxM1 ensures nucleus beta-catenin transactivation. *EMBO J* 35: 668-684.

161. O'Leary, B., R. S. Finn, and N. C. Turner. 2016. Treating cancer with selective CDK4/6 inhibitors. *Nat Rev Clin Oncol* 13: 417-430.

Vita

Sicong Zhang (張思聰) was born in Shanghai, China on February 4, 1989, the son of Jianxin Zhang and Juhui Qu. After completing his work at Jianping High School, Shanghai, China in 2007, he entered Fudan University in Shanghai, China. He received the degree of Bachelor of Science with a major in Biological Sciences in July, 2011. In September of 2011, he entered The University of Texas Graduate School of Biomedical Sciences at Houston.